CHAPTER 6

ROBUSTNESS AND MULTIVARIABLE FREQUENCY-DOMAIN TECHNIQUES

6.1 INTRODUCTION

Modeling Errors and Stability Robustness

In the design of aircraft control systems it is important to realize that the rigid-body equations that are the basis for design in Chapters 4 and 5 are only an approximation to the nonlinear aircraft dynamics. An aircraft has flexible modes that are important at high frequencies; we neglected these in our rigid-body design model. These *unmodeled high-frequency dynamics* can act to destabilize a control system that may have quite suitable behavior in terms only of the rigid-body model.

Moreover, as the aircraft changes its equilibrium flight condition, the linearized rigid-body model describing its perturbed behavior changes. This *parameter variation* is a low-frequency effect that can also act to destabilize the system. To compensate for this variation, one may determine suitable controller gains for linearized models at several design equilibrium points over a flight envelope. Then, these design gains may be scheduled in computer lookup tables for suitable controller performance over the whole envelope. For gain scheduling to work, it is essential for the controller gains at each design equilibrium point to guarantee stability for actual flight conditions near that equilibrium point. Thus, it is important to design controllers that have *stability robustness,* which is the ability to provide stability in spite of modeling errors due to high-frequency unmodeled dynamics and plant parameter variations.

Disturbances and Performance Robustness

It is often important to account for disturbances such as wind gusts and sensor measurement noise. Disturbances can often act to cause unsatisfactory performance in a

Aircraft Control and Simulation: Dynamics, Controls Design, and Autonomous Systems, Third Edition.
Brian L. Stevens, Frank L. Lewis, Eric N. Johnson.

system that has been designed without taking them into account. Thus, it is important to design controllers that have *performance robustness,* which is the ability to guarantee acceptable performance (in terms of percent overshoot, settling time, etc.) even though the system may be subject to disturbances.

Classical Robust Design

In classical control, robustness may be designed into the system from the beginning by providing sufficient gain and phase margin to counteract the effects of inaccurate modeling or disturbances. In terms of the Bode magnitude plot, it is known that the loop gain should be high at low frequencies for performance robustness but low at high frequencies, where unmodeled dynamics may be present, for stability robustness. The concept of bandwidth is important in this connection, as is the concept of the sensitivity function.

Classical control design techniques are generally in the frequency domain, so they afford a convenient approach to robust design for single-input/single-output (SISO) systems. However, it is well known that the individual gain margins, phase margins, and sensitivities of all the SISO transfer functions in a multivariable or multiloop system have little to do with its overall robustness. Thus, there have been problems in extending classical robust design notions to multi-input/multi-output (MIMO) systems.

Modern Robust Design

Modern control techniques provide a direct way to design multiloop controllers for MIMO systems by closing all the loops simultaneously. Performance is guaranteed in terms of minimizing a quadratic performance index (PI) which, with a sensible problem formulation, generally implies closed-loop stability as well. However, all our work in Chapter 5 assumed that the aircraft model is exactly known and that there are no disturbances. In fact, this is rarely the case.

In this chapter we show that the classical frequency-domain robustness measures are easily extended to MIMO systems in a rigorous fashion by using the notion of the *singular value*. In Section 6.2 we develop the *multivariable loop gain and sensitivity* and describe the *multivariable Bode magnitude plot*. In terms of this plot, we present bounds that *guarantee* both robust stability and robust performance for multivariable systems, deriving notions that are entirely analogous to those in classical control.

In Section 6.3 we give a design technique for robust multivariable controllers using modern output feedback theory, showing how robustness may be guaranteed. The approach is a straightforward extension of classical techniques. To yield both suitable time-domain performance and robustness, an iterative approach is described that is simple and direct using the software described in Appendix B. We illustrate by designing a pitch-rate control system that has good performance despite the presence of flexible modes and wind gusts.

A popular modern approach to the design of robust controllers is *linear quadratic Gaussian/loop transfer recovery* (LQG/LTR). This approach has been used extensively by Honeywell in the design of advanced multivariable aircraft control

systems. LQG/LTR relies on the *separation principle,* which involves designing a full-state-variable feedback (as in Section 5.7) and then an *observer* to provide the state estimates for feedback purposes. The result is a dynamic compensator that is similar to those resulting from classical control approaches. The importance of the separation principle is that compensators can be designed for *multivariable systems* in a straightforward manner by solving matrix equations. In Section 6.4 we discuss observers and the Kalman filter. In Section 6.5 we cover LQG/LTR design.

A recent approach to modern robust design is H-infinity design (Francis et al., 1984; Doyle et al., 1989; Kaminer et al., 1990). However, using H-infinity design it is difficult to obtain a controller with a desired structure. For this reason, as well as due to space limitations, we will not cover H-infinity design.

6.2 MULTIVARIABLE FREQUENCY-DOMAIN ANALYSIS

We will deal with system uncertainties, as in classical control, using robust design techniques which are conveniently examined in the frequency domain. To this point, our work in modern control has been in the time domain, since the LQ performance index is a time-domain criterion.

One problem that arises immediately for MIMO systems is that of extending the SISO Bode magnitude plot. We are not interested in making several individual SISO frequency plots for various combinations of the inputs and outputs in the MIMO system and examining gain and phase margins. Such approaches have been tried and may not always yield much insight into the true behavior of the MIMO system. This is due to the coupling that generally exists between *all* inputs and *all* outputs of a MIMO system.

Thus, in this section we introduce the *multivariable loop gain and sensitivity* and the *multivariable Bode magnitude plot,* which will be nothing but the plot versus frequency of the *singular values* of the transfer function matrix. This basic tool allows much of the rich experience of classical control theory to be applied to MIMO systems. Thus, we will discover that for robust performance the minimum singular value of the loop gain should be large at low frequencies, where disturbances are present. On the other hand, for robust stability the maximum singular value of the loop gain should be small at high frequencies, where there are significant modeling inaccuracies. We will also see that to guarantee stability despite parameter variations in the linearized model due to operating point changes, the maximum singular value should be below an upper limit.

Sensitivity and Cosensitivity

Figure 6.2-1 shows a standard feedback system of the sort that we have seen several times in our work to date. The plant is $G(s)$, and $K(s)$ is the feedback/feedforward compensator which can be designed by any of the techniques we have covered. The plant output is $z(t) \in \mathbf{R}^q$, the plant control input is $u(t) \in \mathbf{R}^m$, and the reference input is $r(t) \in \mathbf{R}^q$.

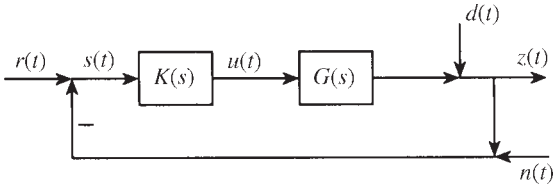

Figure 6.2-1 Standard feedback configuration.

We have mentioned in Section 5.4 that perfect tracking may not be achieved unless the number m of control inputs $u(t)$ is greater than or equal to the number q of performance outputs $z(t)$ (Kwakernaak and Sivan, 1972). Therefore, we will assume that $m = q$ so that the plant $G(s)$ and compensator $K(s)$ are square. This is only a consequence of sensible design, not a restriction on the sorts of plants that may be considered.

We have added a few items to the figure to characterize uncertainties. The signal $d(t)$ represents a *disturbance* acting on the system of the sort appearing in classical control. This could represent, for instance, wind gusts. The *sensor measurement noise* or errors are represented by $n(t)$. Both of these signals are generally vectors of dimension q. Typically, the disturbances occur at low frequencies, say below some ω_d, while the measurement noise $n(t)$ has its predominant effect at high frequencies, say above some value ω_n. Typical Bode plots for the magnitudes of these terms appear in Figure 6.2-2 for the case that $d(t)$ and $n(t)$ are scalars. The reference input is generally also a low-frequency signal (e.g., the unit step).

The tracking error is

$$e(t) \equiv r(t) - z(t) \tag{6.2-1}$$

Due to the presence of $n(t)$, $e(t)$ may not be symbolized in Figure 6.2-1. The signal $s(t)$ is in fact given by

$$s(t) = r(t) - z(t) - n(t) = e(t) - n(t) \tag{6.2-2}$$

Let us perform a frequency-domain analysis on the system to see the effects of the uncertainties on system performance. In terms of Laplace transforms we may write

$$Z(s) = G(s)K(s)S(s) + D(s) \tag{6.2-3}$$

$$S(s) = R(s) - Z(s) - N(s) \tag{6.2-4}$$

$$E(s) = R(s) - Z(s) \tag{6.2-5}$$

Now we may solve for $Z(s)$ and $E(s)$, obtaining the closed-loop transfer function relations (see the problems at the end of the chapter)

$$Z(s) = (I + GK)^{-1}GK(R - N) + (I + GK)^{-1}D \tag{6.2-6}$$

$$E(s) = [I - (I + GK)^{-1}GK]R + (I + GK)^{-1}GKN - (I + GK)^{-1}D \tag{6.2-7}$$

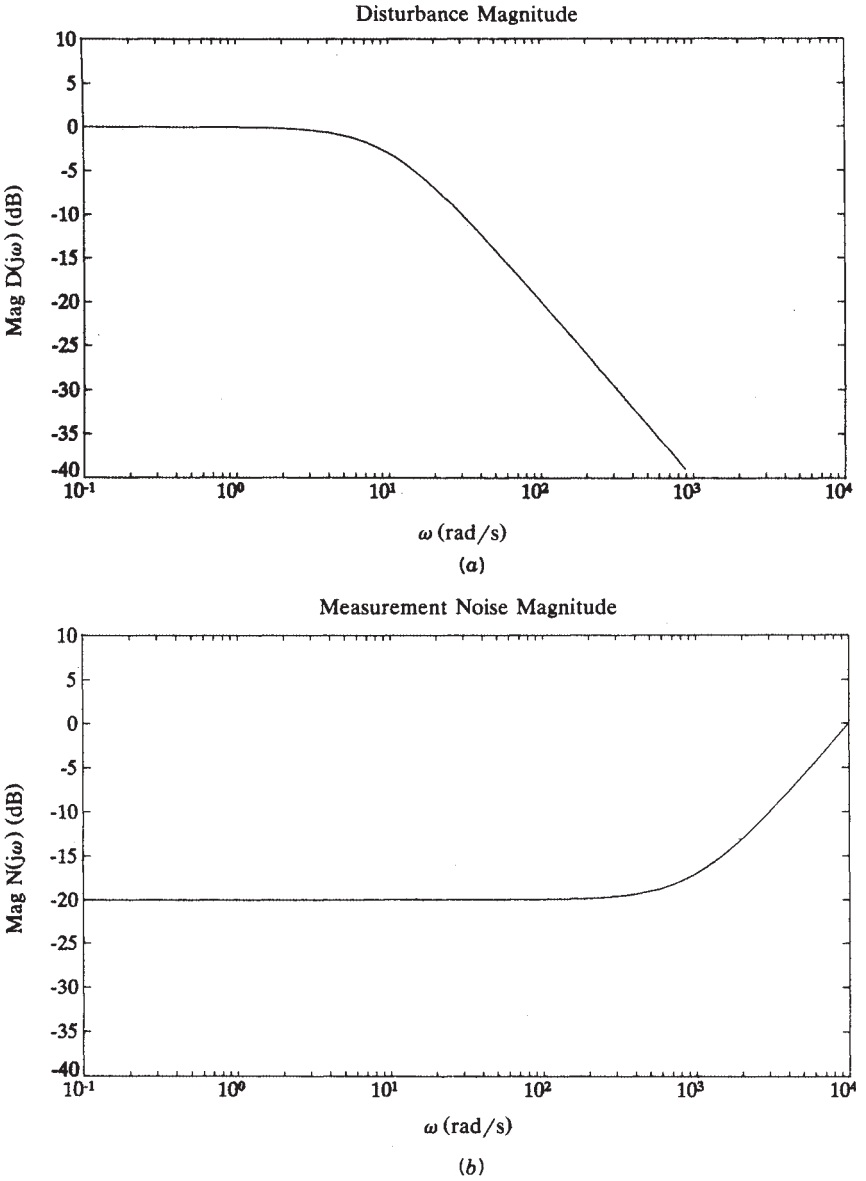

Figure 6.2-2 Typical Bode plots for the uncertain signals in the system: (*a*) disturbance magnitude; (*b*) measurement noise magnitude.

It is important to note that, unlike the case for SISO systems, care must be taken to perform the matrix operations in the correct order (for instance, $GK \neq KG$). The multiplications by matrix inverses must also be performed in the correct order.

We can put these equations into a more convenient form. According to the matrix inversion lemma, (6.2-7) may be written as

$$E(s) = (I + GK)^{-1}(R - D) + (I + GK)^{-1}GKN \tag{6.2-8}$$

Moreover, since GK is square and invertible, we can write

$$\begin{aligned}(I + GK)^{-1}GK &= [(GK)^{-1}(I + GK)]^{-1} = [(GK)^{-1} + I]^{-1} \\ &= [(I + GK)(GK)^{-1}]^{-1} = GK(I + GK)^{-1}\end{aligned} \tag{6.2-9}$$

Therefore, we may finally write $Z(s)$ and $E(s)$ as

$$Z(s) = GK\,(I + GK)^{-1}(R - N) + (I + GK)^{-1}D \tag{6.2-10}$$

$$E(s) = (I + GK)^{-1} + (R - D) + GK\,(I + GK)^{-1}N \tag{6.2-11}$$

To simplify things a bit, define the *system sensitivity*

$$S(s) = (I + GK)^{-1} \tag{6.2-12}$$

and

$$T(s) = GK(I + GK)^{-1} = (I + GK)^{-1}GK \tag{6.2-13}$$

Since

$$S(s) + T(s) = (I + GK)\,(I + GK)^{-1} = I \tag{6.2-14}$$

we call $T(s)$ the *complementary sensitivity,* or in short, the *cosensitivity*. Note that the *return difference*

$$L(s) = I + GK \tag{6.2-15}$$

is the inverse of the sensitivity. The *loop gain* is given by $G(s)K(s)$.

These expressions extend the classical notions of loop gain, return difference, and sensitivity to multivariable systems. They are generally square transfer function matrices of dimension $q \times q$. In terms of these new quantities, we have

$$Z(s) = T(s)\,(R(s) - N(s)) + S(s)D(s) \tag{6.2-16}$$

$$E(s) = S(s)\,(R(S) - D(s)) + T(s)N(s) \tag{6.2-17}$$

According to the second equation, to ensure small tracking errors, we must have $S(j\omega)$ small at those frequencies ω where the reference input $r(t)$ and disturbance $d(t)$ are large. This will yield good *disturbance rejection*. On the other hand, for

satisfactory *sensor noise rejection,* we should have $T(j\omega)$ small at those frequencies ω where $n(t)$ is large.

Unfortunately, a glance at (6.2-14) reveals that $S(j\omega)$ and $T(j\omega)$ cannot simultaneously be small at any one frequency ω. According to Figure 6.2-2, we should like to have $S(j\omega)$ small at low frequencies, where $r(t)$ and $d(t)$ dominate, and $T(j\omega)$ small at high frequencies, where $n(t)$ dominates.

These are nothing but the multivariable generalizations of the well-known SISO classical notion that a large loop gain $GK(j\omega)$ is required at low frequencies for satisfactory performance and small errors, but a small loop gain is required at high frequencies where sensor noises are present.

Multivariable Bode Plot

These notions are not difficult to understand on a heuristic level. Unfortunately, it is not so straightforward to determine a clear measure for the "smallness" of $S(j\omega)$ and $T(j\omega)$. These are both square matrices of dimension $q \times q$, with q the number of performance outputs $z(t)$ and reference inputs $r(t)$. They are complex functions of the frequency. Clearly, the classical notion of the Bode magnitude plot, which is defined only for *scalar* complex functions of ω, must be extended to the MIMO case.

Some work was done early on using the frequency-dependent eigenvalues of a square complex matrix as a measure of smallness (Rosenbrock, 1974; MacFarlane, 1970; MacFarlane and Kouvaritakis, 1977). However, note that the matrix

$$M = \begin{bmatrix} 0.1 & 100 \\ 0 & 0.1 \end{bmatrix} \tag{6.2-18}$$

has large and small components, but its eigenvalues are both at 0.1.

A better measure of the magnitude of square matrices is the *singular value (SV)* (Strang, 1980). Given any matrix M we may write its *singular value decomposition (SVD)* as

$$M = U\Sigma V^*, \tag{6.2-19}$$

with * denoting complex conjugate transpose, U and V square unitary matrices (i.e., $V^{-1} = V^*$, the complex conjugate transpose of V), and

$$\Sigma = \begin{bmatrix} \sigma_1 & & & & & & \\ & \sigma_2 & & & & & \\ & & \ddots & & & & \\ & & & \sigma_r & & & \\ & & & & 0 & & \\ & & & & & \ddots & \\ & & & & & & 0 \end{bmatrix}, \tag{6.2-20}$$

with $r = \text{rank}\,(M)$. The singular values are the σ_i, which are ordered so that $\sigma_1 \geq \sigma_2 \geq \cdots \geq \sigma_r$. The SVD may loosely be thought of as the extension to general matrices

(which may be nonsquare or complex) of the Jordan form. If M is a function of $j\omega$, so are U, σ_i, and V.

Since $MM^* = U\Sigma V^* V\Sigma^T U^* = U\Sigma^2 U^*$, it follows that the singular values of M are simply the (positive) square roots of the nonzero eigenvalues of MM^*. A similar proof shows that the nonzero eigenvalues of MM^* and those of M^*M are the same.

We note that the M given above has two singular values, $\sigma_1 = 100.0001$ and $\sigma_2 = 0.0001$. Thus, this measure indicates that M has a large and a small component. Indeed, note that

$$\begin{bmatrix} 0.1 & 100 \\ 0 & 0.1 \end{bmatrix} \begin{bmatrix} -1 \\ 0.001 \end{bmatrix} = \begin{bmatrix} 0 \\ 0.0001 \end{bmatrix} \tag{6.2-21}$$

while

$$\begin{bmatrix} 0.1 & 100 \\ 0 & 0.1 \end{bmatrix} \begin{bmatrix} 0.001 \\ 1 \end{bmatrix} = \begin{bmatrix} 100.0001 \\ 0.1 \end{bmatrix} \tag{6.2-22}$$

Thus, the singular value σ_2 has the *input direction*

$$\begin{bmatrix} -1 \\ 0.001 \end{bmatrix}$$

associated with it for which the output contains the value σ_2. On the other hand, the singular value σ_1 has an associated input direction of

$$\begin{bmatrix} 0.001 \\ 1 \end{bmatrix}$$

for which the output contains the value σ_1.

There are many nice properties of the singular value that make it a suitable choice for defining the magnitude of matrix functions. Among these is the fact that the maximum singular value is an *induced matrix norm,* and norms have several useful attributes. The use of the SVs in the context of modern control was explored by Doyle and Stein (1981) and Safonov et al. (1981).

A major factor is that there are many good software packages that have good routines for computing the singular value [e.g., subroutine LSVDF in IMSL (1980) or Moler et al. (1987)]. Thus, plots like those we will present may easily be obtained by writing only a computer program to drive the available subroutines. Indeed, since the SVD uses unitary matrices, its computation is numerically stable. An efficient technique for obtaining the SVs of a complex matrix as a function of frequency ω is given by Laub (1981).

We note that a complete picture of the behavior of a complex matrix versus ω must take into account the magnitudes of the SVs as well as the *multivariable phase,* which may also be obtained from the SVD (Postlethwaite et al., 1981). Thus, complete MIMO generalizations of the Bode magnitude *and* phase plots are available. However, the theory relating to the phase portion of the plot is more difficult to use in a practical design technique, although a MIMO generalization of the Bode gain-phase relation is available (Doyle and Stein, 1981). Therefore, we will only employ plots of the SVs versus frequency, which correspond to the Bode magnitude plot for MIMO systems.

The magnitude of a square transfer function matrix $H(j\omega)$ at any frequency ω depends on the direction of the input excitation. Inputs in a certain direction in the input space will excite only the SV(s) associated with that direction. However, for any input, the magnitude of the transfer function $H(j\omega)$ at any given frequency ω may be bounded above by its *maximum singular value,* denoted $\overline{\sigma}(H(j\omega))$ and below by its *minimum singular value,* denoted $\underline{\sigma}(H(j\omega))$. Therefore, all our results, as well as the plots we will give, need take into account only these two bounding values of "magnitude."

Example 6.2-1: MIMO Bode Magnitude Plots Here, we consider a simple non-aircraft system to make some points about the SV plots. Consider the multivariable system

$$\dot{x} = \begin{bmatrix} -1 & -1 & 0 & 0 \\ 1 & -1 & 0 & 0 \\ 0 & 0 & -2 & 6 \\ 0 & 0 & -6 & -2 \end{bmatrix} x + \begin{bmatrix} 1 & 0 \\ 0 & 0 \\ 0 & 1 \\ 0 & 0 \end{bmatrix} u = Ax + Bu \tag{1}$$

$$z = \begin{bmatrix} 1 & 0 & 0 & 0 \\ 0 & 0 & 1 & 0 \end{bmatrix} x = Hx, \tag{2}$$

which as a 2×2 MIMO transfer function of

$$H(s) = H(sI - A)^{-1}B = \frac{M(s)}{\Delta(s)}, \tag{3}$$

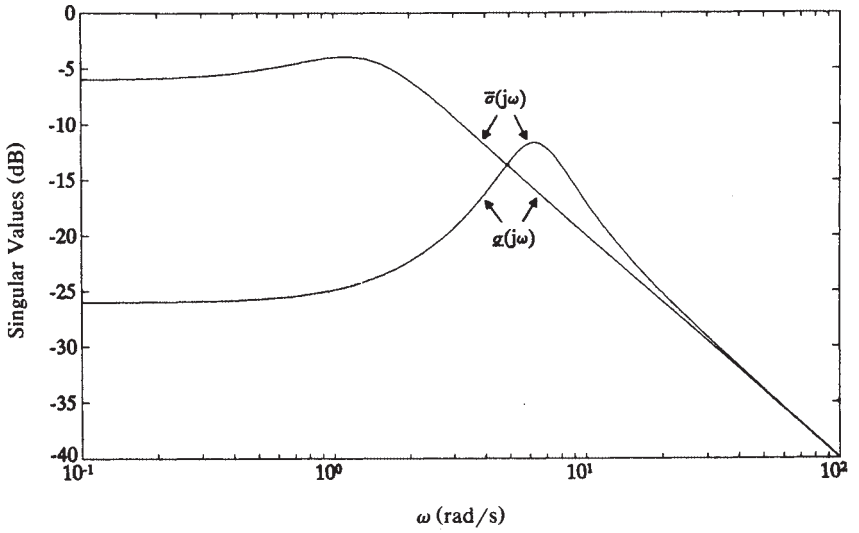

Figure 6.2-3 MIMO Bode magnitude plot of SVs versus frequency.

with

$$\Delta(s) = s^4 + 6s^3 + 50s^2 + 88s + 80$$

$$M(s) = \begin{bmatrix} 1 & 0 \\ 0 & 1 \end{bmatrix} s^3 + \begin{bmatrix} 5 & 0 \\ 0 & 4 \end{bmatrix} s^2 + \begin{bmatrix} 44 & 0 \\ 0 & 6 \end{bmatrix} s + \begin{bmatrix} 40 & 0 \\ 0 & 4 \end{bmatrix} \tag{4}$$

By writing a driver program that calls standard software (e.g., subroutine LSVDF in IMSL, 1980) to evaluate the SVs at closely spaced values of frequency ω, we may obtain the SV plots versus frequency shown in Figure 6.2-3. We call this the *multivariable Bode magnitude plot* for the MIMO transfer function $H(s)$.

Since $H(s)$ is 2×2, it has two SVs. Note that although each SV is continuous, the maximum and minimum SVs are not. This is due to the fact that the SVs can cross over each other, as the figure illustrates. ■

Example 6.2-2: Singular-Value Plots for F-16 Lateral Dynamics. To illustrate the difference between the SV plots and the individual SISO Bode plots of a multivariable system, let us consider the F-16 lateral dynamics of Examples 5.3-1 and 5.5-4. In the latter example, we designed a wing leveler. For convenience, refer to the figure there showing the control system structure. Using the system matrices A and B in that example, which include an integrator in the ϕ channel as well as actuator dynamics and a washout filter, take as the control inputs $u = [u_a \;\; u_r]^{\mathrm{T}}$, with u_a the aileron servo input and u_r the rudder servo input. Select as outputs $z = [\epsilon \;\; r_w]^{\mathrm{T}}$, with ϵ the integrator output in the ϕ channel and r_w the washed-out yaw rate.

The individual SISO transfer functions in this two-input/two-output open-loop system are

$$H_{11} = \frac{\epsilon}{u_a} = \frac{14.8}{s(s + 0.0163)(s + 3.615)(s + 20.2)} \tag{1}$$

$$H_{12} = \frac{r_w}{u_a} = \frac{-36.9s(s + 2.237)\;\; [(s + 0.55)^2 + 2.49^2]}{(s + 0.0163)(s + 1)(s + 3.165)(s + 20.2)\;\; [s + 0.4225)^2 + 3.063^2]} \tag{2}$$

$$H_{21} = \frac{\epsilon}{u_r} = \frac{-2.65(s + 2.573)(s - 2.283)}{s(s + 0.0163)(s + 3.615)(s + 20.2)\;\; [(s + 0.4225)^2 + 3.063^2]} \tag{3}$$

$$H_{22} = \frac{r_w}{u_r} = \frac{-0.718s\;\; [(s + 0.139)^2 + 0.446^2]}{(s + 0.0163)(s + 1)(s + 20.2)\;\; [s + 0.4225)^2 + 3.063^2]} \tag{4}$$

The standard Bode magnitude plots for these SISO transfer functions are shown in Figure 6.2-4. Clearly visible are the resonance due to the dutch roll mode as well as the integrator in the upper ϕ channel in the figure in Example 5.5-4.

On the other hand, shown in Figure 6.2-5 are the SVs of this multivariable system. Note that it is not immediately evident how they relate to the SISO plots in Figure 6.2-4. In the next section we will see that bounds for guaranteed robustness are given for MIMO systems in terms of the minimum SV being large at low

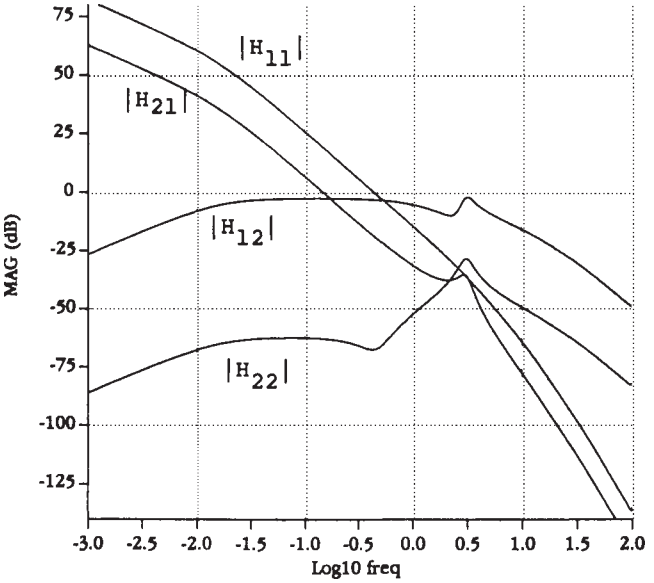

Figure 6.2-4 SISO Bode magnitude plots for F-16 lateral dynamics.

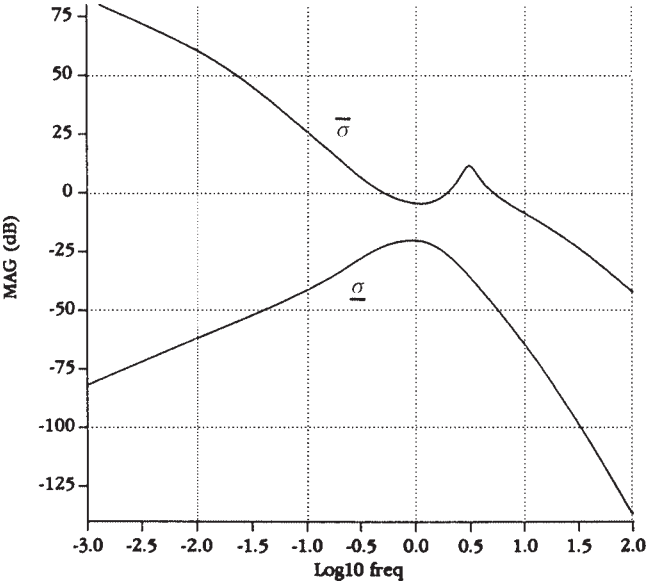

Figure 6.2-5 Singular values for F-16 lateral dynamics.

frequencies (for performance robustness) and the maximum SV being small at high frequencies (for stability robustness). The lack of any clear correspondence between Figures 6.2-4 and 6.2-5 shows that these bounds cannot be expressed in terms of the individual SISO Bode plots. ■

Frequency-Domain Performance Specifications

We have seen how to make a multivariable Bode magnitude plot of a square transfer function matrix. It is now necessary to discuss *performance specifications* in the frequency domain in order to determine what a "desirable" Bode plot means in the MIMO case. The important point is that the low-frequency requirements are generally in terms of the *minimum* SV being *large,* while the high-frequency requirements are in terms of the *maximum* SV being *small*.

First, let us point out that the classical notion of *bandwidth* holds in the MIMO case. This is the frequency ω_c for which the loop gain $GK(j\omega)$ passes through a value of 1, or 0 dB. If the bandwidth should be limited due to high-frequency noise considerations, the *largest* SV should satisfy $\overline{\sigma}(GK(j\omega)) = 1$ at the specified cutoff frequency ω_c.

L_2 Operator Gain To relate frequency-domain behavior to time-domain behavior, we may take into account the following considerations (Morari and Zafiriou, 1989). Define the L_2 norm of a vector time function $s(t)$ by

$$||s||_2 = \left[\int_0^\infty s^{\mathrm{T}}(t)\, s(t)dt\right]^{1/2} \tag{6.2-23}$$

This is related to the total energy in $s(t)$ and should be compared to the LQ performance index.

A linear time-invariant system has input $u(t)$ and output $z(t)$ related by the convolution integral

$$z(t) = \int_{-\infty}^{\infty} h(t-\tau)u(\tau)d\tau, \tag{6.2-24}$$

with $h(t)$ the impulse response. The L_2 *operator gain,* denoted $||H||_2$, of such a system is defined as the smallest value of γ such that

$$||z||_2 \le \gamma ||u||_2 \tag{6.2-25}$$

This is just the operator norm induced by the L_2 vector norm. An important result is that the L_2 operator gain is given by

$$||H||_2 = \max_{\omega}[\overline{\sigma}(H(j\omega))], \tag{6.2-26}$$

with $H(s)$ the system transfer function. That is, $||H||_2$ is nothing but the *maximum value* over ω of the maximum SV of $H(j\omega)$. Thus, $||H||_2$ is an *H-infinity norm* in the frequency domain.

This result gives increased importance to $\overline{\sigma}(H(j\omega))$, for if we are interested in keeping $z(t)$ small over a range of frequencies, we should take care that $\overline{\sigma}(H(j\omega))$ is small over that range.

It is now necessary to see how this result may be used in deriving frequency-domain performance specifications. Some facts we will use in this discussion are

$$\underline{\sigma}(GK) - 1 \leq \underline{\sigma}(I + GK) \leq \underline{\sigma}(GK) + 1 \tag{6.2-27}$$

$$\overline{\sigma}(M) = \frac{1}{\underline{\sigma}(M^{-1})}, \tag{6.2-28}$$

$$\overline{\sigma}(AB) \leq \overline{\sigma}(A)\overline{\sigma}(B) \tag{6.2-29}$$

for any matrices A, B, GK, M, with M nonsingular.

Before we begin a discussion of performance specifications, let us note the following. If $S(j\omega)$ is small, as desired at low frequencies, then

$$\overline{\sigma}(S) = \overline{\sigma}[(I + GK)^{-1}] = \frac{1}{\underline{\sigma}(I + GK)} \approx \frac{1}{\underline{\sigma}(GK)} \tag{6.2-30}$$

That is, a large value of $\underline{\sigma}(GK)$ guarantees a small value of $\overline{\sigma}(s)$.

On the other hand, if $T(j\omega)$ is small, as is desired at high frequencies, then

$$\overline{\sigma}(T) = \overline{\sigma}[GK(I + GK)^{-1}] \approx \overline{\sigma}(GK) \tag{6.2-31}$$

That is, a small value of $\overline{\sigma}(GK)$ guarantees a small value of $\overline{\sigma}(T)$.

This means that specifications that $S(j\omega)$ be small at low frequencies and $T(j\omega)$ be small at high frequencies may equally well be formulated in terms of $\underline{\sigma}(GK)$ being large at low frequencies and $\overline{\sigma}(GK)$ being small at high frequencies. Thus, all of our performance specifications will be in terms of the *minimum and maximum SVs of the loop gain* $GK(j\omega)$. The practical significance of this is that we need only compute the SVs of $GK(j\omega)$, not those of $S(j\omega)$ and $T(j\omega)$. These notions are symbolized in Figure 6.2-6, where it should be recalled that $S + T = I$.

Now, we will first consider low-frequency specifications on the SV plot and then high-frequency specifications. According to our discussion relating to (6.2-17), the former will involve the reference input $r(t)$ and disturbances $d(t)$, while the latter will involve the sensor noise $n(t)$.

Low-Frequency Specifications For low frequencies let us suppose that the sensor noise $n(t)$ is zero so that (6.2-17) becomes

$$E(s) = S(s)(R(s) - D(s)) \tag{6.2-32}$$

Thus, to keep $||e(t)||_2$ small, it is only necessary to ensure that the L_2 operator norm $||S||_2$ is small at all frequencies where $R(j\omega)$ and $D(j\omega)$ are appreciable. This may be achieved by ensuring that, at such frequencies, $\overline{\sigma}(S(j\omega))$ is small. As we have just seen, this may be guaranteed if we select

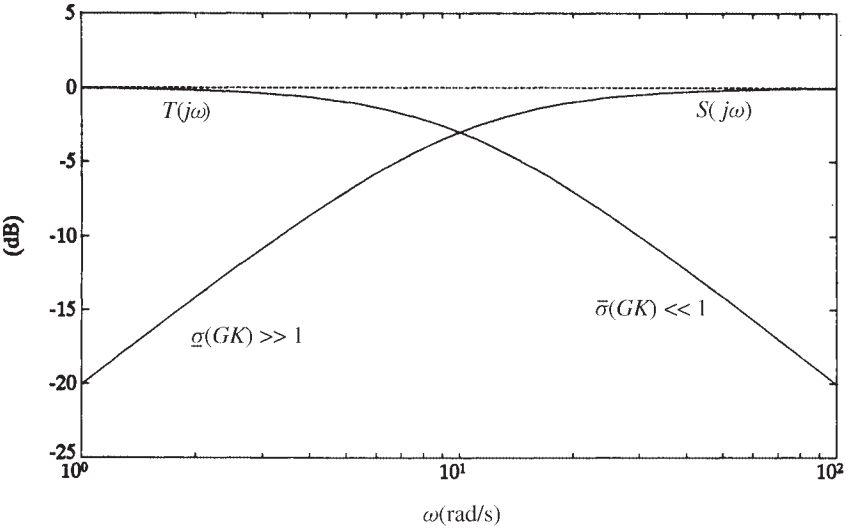

Figure 6.2-6 Magnitude specifications on $S(jw)$, $T(jw)$, and $GK(jw0)$.

$$\underline{\sigma}(GK(j\omega)) \gg 1 \qquad \text{for } \omega \leq \omega_d, \tag{6.2-33}$$

where $D(s)$ and $R(s)$ are appreciable for $\omega \leq \omega_d$.

Thus, exactly as in the classical case (Franklin et al., 1986), we are able to specify a low-frequency performance bound that guarantees *performance robustness,* that is, good performance in the face of low-frequency disturbances. For instance, to ensure that disturbances are attenuated by a factor of 0.01, we should ensure $\underline{\sigma}(GK(j\omega))$ is greater than 40 dB at low frequencies $\omega \leq \omega_d$.

At this point it is worth examining Figure 6.2-9 below, which illustrates the frequency-domain performance specifications we are beginning to derive. Another low-frequency performance bound may be derived from steady-state error considerations. Thus, suppose that $d(t) = 0$ and the reference input is a unit step of magnitude r so that $R(s) = r/s$. Then, according to (6.2-32) and the final-value theorem (Franklin et al., 1986), the steady-state error e_∞ is given by

$$e_\infty = \lim_{s \to 0} sE(s) = rS(0) \tag{6.2-34}$$

To ensure that the largest component of e_∞ is less than a prescribed small acceptable value δ_∞, we should therefore select

$$\underline{\sigma}(GK(0)) > \frac{r}{\delta_\infty} \tag{6.2-35}$$

The ultimate objective of all our concerns is to manufacture a compensator $K(s)$ in Figure 6.2-1 that gives desirable performance. Let us now mention two low-frequency

considerations that are important in the initial stages of the design of the compensator $K(s)$.

To make the steady-state error in response to a unit step at $r(t)$ exactly equal to zero, we may ensure that there is an integrator *in each path* of the system $G(s)$ so that it is of type 1 (Franklin et al., 1986). Thus, suppose that the system to be controlled is given by

$$\begin{aligned} \dot{x} &= Ax + Bv \\ z &= Hx \end{aligned} \tag{6.2-36}$$

To add an integrator to each control path, we may augment the dynamics so that

$$\frac{d}{dt}\begin{bmatrix} x \\ \epsilon \end{bmatrix} = \begin{bmatrix} A & B \\ 0 & 0 \end{bmatrix}\begin{bmatrix} x \\ \epsilon \end{bmatrix} + \begin{bmatrix} 0 \\ I \end{bmatrix} u, \tag{6.2-37}$$

with ϵ the integrator outputs (see Figure 6.2-7). The system $G(s)$ in Figure 6.2-1 should now be taken as (6.2-37), which contains the integrators as a precompensator.

Although augmenting each control path with an integrator results in zero steady-state error, in some applications this may result in an unnecessarily complicated compensator. Note that the steady-state error may be made as small as desired without integrators by selecting $K(s)$ so that (6.2-35) holds.

A final concern about the low-frequency behavior of $G(s)$ needs to be addressed. It is desirable in many situations to have $\underline{\sigma}(GK)$ and $\overline{\sigma}(GK)$ close to the same value. Then the speed of the responses will be nearly the same in all channels of the system. This is called the issue of *balancing the SVs at low frequency*. The SVs of $G(s)$ in Figure 6.2-1 may be balanced at low frequencies, as follows.

Suppose that the plant has the state-variable description (6.2-36), and let us add a square constant precompensator gain matrix P, so that

$$v = Pu \tag{6.2-38}$$

is the relation between the control input $u(t)$ in Figure 6.2-1 and the actual plant input $v(t)$. The transfer function of the plant plus precompensator is now

$$G(s) = H(sI - A)^{-1}BP \tag{6.2-39}$$

As s goes to zero, this approaches

$$G(0) = H(-A)^{-1}BP,$$

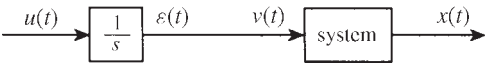

Figure 6.2-7 Plant augmented with integrators.

as long as A has no poles at the origin. Therefore, we may ensure that $G(0)$ has all SVs equal to a prescribed value of γ by selecting

$$P = \gamma[H(-A)^{-1}B]^{-1}, \tag{6.2-40}$$

for then $G(0) = \gamma I$.

The transfer function of (6.2-36) is

$$H(s) = H(sI - A)^{-1}B, \tag{6.2-41}$$

whence we see that the required value of the precompensator gain is

$$P = \gamma H^{-1}(0) \tag{6.2-42}$$

This is nothing but the (scaled) recriprocal dc gain.

Example 6.2-3: Precompensator for Balancing and Zero Steady-State Error Let us design a precompensator for the system in Example 6.2-1 using the notions just discussed. Substituting the values of A, B, and H in (6.2-40) with $\gamma = 1$ yields

$$P = [H(-A)^{-1}B]^{-1} = \begin{bmatrix} 2 & 0 \\ 0 & 20 \end{bmatrix} \tag{1}$$

To ensure zero-steady-state error as well as equal SVs at low frequencies, we may incorporate integrators in each input channel along with the gain matrix P by writing the augmented system

$$\frac{d}{dt}\begin{bmatrix} x \\ \epsilon \end{bmatrix} = \begin{bmatrix} A & B \\ 0 & 0 \end{bmatrix}\begin{bmatrix} x \\ \epsilon \end{bmatrix} + \begin{bmatrix} 0 \\ P \end{bmatrix} u \tag{2}$$

The SV plots for this plant plus precompensator appear in Figure 6.2-8. At low frequencies there is now a slope of -20 dB/decade as well as equality of $\underline{\sigma}$ and $\overline{\sigma}$. Thus, the augmented system is both balanced and of type 1. Compare Figure 6.2-8 to the SV plot of the uncompensated system in Figure 6.2-3. The remaining step is the selection of the feedback gain matrix for the augmented plant (2) so that the desired performance is achieved. ■

High-Frequency Specifications We now turn to a discussion of high-frequency performance specifications. The sensor noise is generally appreciable at frequencies above some known value ω_n (see Figure 6.2-2). Thus, according to (6.2-17), to keep the tracking error norm $||e||_2$ small in the face of measurement noise, we should ensure that the operator norm $||T||_2$ is small at high frequencies above this value. By (6.2-31) this may be guaranteed if

$$\overline{\sigma}(GK(j\omega)) \ll 1 \quad \text{for } \omega \geq \omega_n \tag{6.2-43}$$

(see Figure 6.2-9). For instance, to ensure that sensor noise is attenuated by a factor of 0.1, we should guarantee that $\overline{\sigma}(GK(j\omega)) < -20$ dB for $\omega \geq \omega_n$.

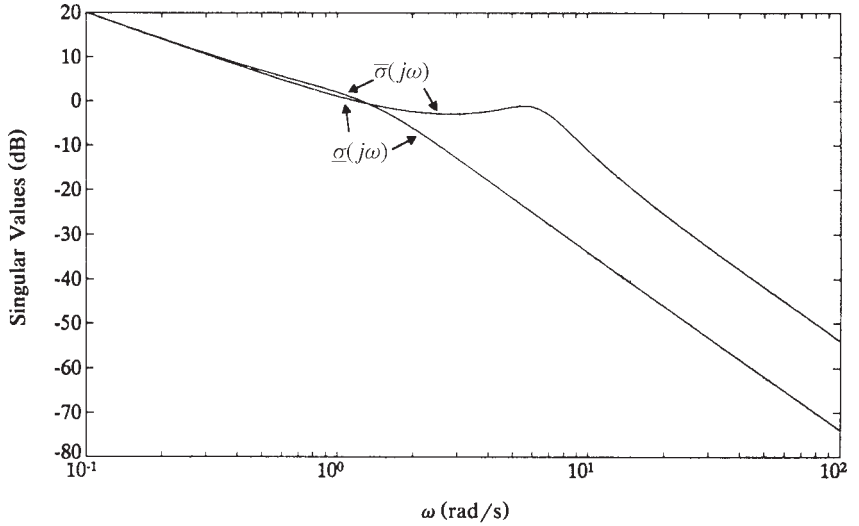

Figure 6.2-8 MIMO Bode magnitude plot for augmented plant.

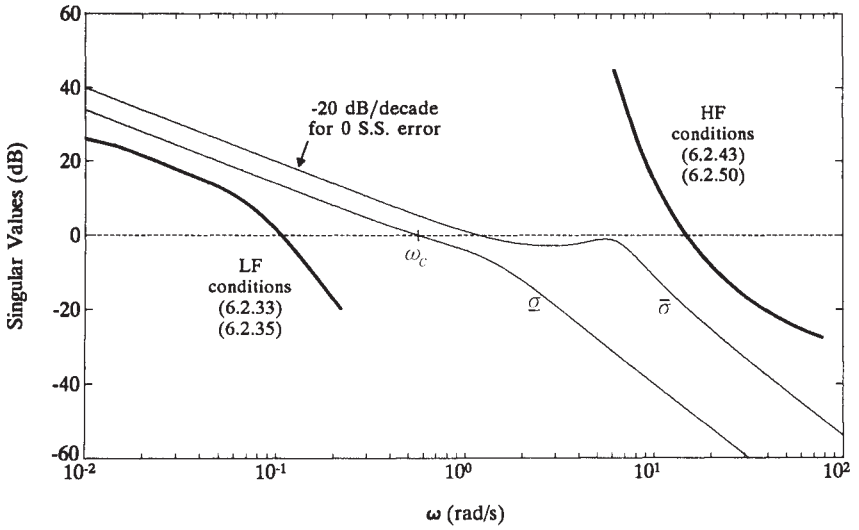

Figure 6.2-9 Frequency-domain performance specifications.

One final high-frequency robustness consideration needs to be mentioned. It is unusual for the plant model to be exactly known. There are two basic sorts of modeling inaccuracies that concern us in aircraft controls. The first is plant parameter variation due to changes in the linearization equilibrium point of the nonlinear model. This is a low-frequency phenomenon and will be discussed in the next subsection.

The second sort of inaccuracy is due to unmodeled high-frequency dynamics; this we discuss here.

We are assuming a rigid-body aircraft model for the purpose of control design and in so doing are neglecting flexible and vibrational modes at high frequencies. Thus, although our design may guarantee closed-loop stability for the *assumed mathematical model* $G(s)$, stability is not assured for the *actual* plant $G'(s)$ with flexible modes. To guarantee *stability robustness* in the face of plant parameter uncertainty, we may proceed as follows.

The model uncertainties may be of two types. The actual plant model G' and the assumed plant model G may differ by *additive uncertainties* so that

$$G'(j\omega) = G(j\omega) + \Delta G(j\omega), \tag{6.2-44}$$

where the unknown discrepancy satisfies a known bound

$$\overline{\sigma}(\Delta G(j\omega)) < a(\omega), \tag{6.2-45}$$

with $a(\omega)$ known for all ω.

On the other hand, the actual plant model $G'(s)$ and the assumed plant model $G(s)$ may differ by *multiplicative uncertainties* so that

$$G'(j\omega) = [I + M(j\omega)]G(j\omega), \tag{6.2-46}$$

where the unknown discrepancy satisfies a known bound

$$\overline{\sigma}(M(j\omega)) < M(\omega), \tag{6.2-47}$$

with $m(\omega)$ known for all ω. We will show several ways of finding the bound $m(\omega)$. In Example 6.2-4 we show how to construct a reduced-order model for the system, which may then be used for control design. There $m(\omega)$ is determined from the neglected dynamics. In Example 6.3-1 we show how $m(\omega)$ may be determined in terms of the aircraft's neglected flexible modes. In the next subsection we show how to determine $m(\omega)$ in terms of plant parameter variations in the linearized model due to operating point changes.

Since we may write (6.2-44) as

$$G'(j\omega) = [I + \Delta G(j\omega)G^{-1}(j\omega)]G(j\omega) \equiv [I + M(j\omega)]G(j\omega), \tag{6.2-48}$$

we will confine ourselves to a discussion of multiplicative uncertainties, following Doyle and Stein (1981).

Suppose that we have designed a compensator $K(s)$ so that the closed-loop system in Figure 6.2-1 is stable. We should now like to derive a frequency-domain condition that guarantees the stability of the *actual* closed-loop system, which contains not $G(s)$,

but $G'(s)$, satisfying (6.2-46)/(6.2-47). For this, the multivariable Nyquist condition (Rosenbrock, 1974) may be used.

Thus, it is required that the encirclement count of the map $|I + G'K|$ be equal to the negative number of unstable open-loop poles of $G'K$. By assumption, this number is the same as that of GK. Thus, the number of encirclements of $|I + G'K|$ must remain unchanged for all G' allowed by (6.2-47). This is assured if and only if $|I + G'K|$ remains nonzero as G is warped continuously toward G', or equivalently,

$$0 < \underline{\sigma}[I + [I + \epsilon M(s)]G(s)K(s)]$$

for all $0 \leq \epsilon \leq 1$, all $M(s)$ satisfying (6.2-47) and all s on the standard Nyquist contour.

Since G' vanishes on the infinite radius segment of the Nyquist contour, and assuming for simplicity that no indentations are required along the $j\omega$ -axis portion, this reduces to the following equivalent conditions:

$$0 < \underline{\sigma}[I + G(j\omega)K(j\omega) + \epsilon M(j\omega)G(j\omega)K(j\omega)]$$

for all $0 \leq \epsilon \leq 1, 0 \leq \omega < \infty$, all M,

$$\begin{aligned}
&\text{iff} \quad 0 < \underline{\sigma}[\{I + \epsilon MGK(I + GK)^{-1}\}\ (I + GK)] \\
&\text{iff} \quad 0 < \underline{\sigma}[I + MGK(I + GK)^{-1}] \\
&\text{all} \quad 0 \leq \omega < \infty, \text{ and all } M, \\
&\text{iff} \quad \overline{\sigma}[GK(I + GK)^{-1}] < \frac{1}{m(\omega)}
\end{aligned} \tag{6.2-49}$$

for all $0 \leq \omega < \infty$. Thus, stability robustness translates into a requirement that the cosensitivity $T(j\omega)$ be bounded above by the reciprocal of the multiplicative modeling discrepancy bound $m(\omega)$.

In the case of high-frequency unmodeled dynamics, $1/m(\omega)$ is small at high ω, so that according to (6.2-31), we may simplify (6.2-49) by writing it in terms of the loop gain as

$$\overline{\sigma}(GK(j\omega)) < \frac{1}{m(\omega)} \tag{6.2-50}$$

for all ω such that $m(\omega) \gg 1$.

This bound for stability robustness is illustrated in Figure 6.2-9.

An example will be useful at this point.

Example 6.2-4: Model Reduction and Stability Robustness In some situations we have a high-order aircraft model that is inconvenient to use for controller design. Examples occur in engine control and spacecraft control. In such situations, it is possible to compute a reduced-order model of the system which may then be used for controller design. Here we will show a convenient technique for model reduction as

well as an illustration of the stability robustness bound $m(\omega)$. The technique described here is from Athans et al. (1986).

(a) *Model Reduction by Partial Fraction Expansion*. Suppose that the actual plant is described by

$$\dot{x} = Ax + Bu \tag{1a}$$

$$z = Hx, \tag{1b}$$

with $x \in \mathbf{R}^n$. If A is simple with eigenvalues γ_i, right eigenvectors u_i, and left eigenvectors v_i so that

$$Au_i = \lambda_i u_i, \quad v_i^{\mathrm{T}} A = \lambda_i v_i^{\mathrm{T}}, \tag{2}$$

then the transfer function

$$G'(s) = H(sI - A)^{-1}B \tag{3}$$

may be written as the partial fraction expansion (Section 5.2)

$$G'(s) = \sum_{i=1}^{n} \frac{R_i}{s - \lambda_i}, \tag{4}$$

with residue matrices given by

$$R_i = Hu_i v_i^{\mathrm{T}} B \tag{5}$$

If the value of n is large, it may be desirable to find a *reduced-order approximation* to (1) for which a simplified compensator $K(s)$ in Figure 6.2-1 may be designed. Then, if the approximation is a good one, the compensator $K(s)$ should work well when used on the actual plant $G'(s)$.

To find a reduced-order approximation $G(s)$ to the plant, we may proceed as follows. Decide which of the eigenvalues λ_i in (4) are to be retained in $G(s)$. This may be done using engineering judgment, by omitting high-frequency modes, by omitting terms in (4) that have small residues, and so on. Let the r eigenvalues to be retained in $G(s)$ be $\lambda_i, \lambda_2, \ldots, \lambda_r$.

Define the matrix

$$Q = \operatorname{diag}\{Q_i\}, \tag{6}$$

where Q is an $r \times r$ matrix and the blocks Q_i are defined as

$$Q_i = \begin{cases} 1, & \text{for each real eigenvalue retained} \\ \begin{bmatrix} \frac{1}{2} & -\frac{j}{2} \\ \frac{1}{2} & \frac{j}{2} \end{bmatrix}, & \text{for each complex pair retained} \end{cases} \tag{7}$$

Compute the matrices

$$V \equiv Q^{-1} \begin{bmatrix} v_i^{\mathrm{T}} \\ \vdots \\ v_r^{\mathrm{T}} \end{bmatrix} \tag{8}$$

$$U \equiv \begin{bmatrix} u_1 & \cdots & u_r \end{bmatrix} Q \tag{9}$$

In terms of these constructions, the reduced-order system is nothing but a projection of (1) onto a space of dimension r with state defined by

$$w = Vx \tag{10}$$

The system matrices in the reduced-order approximate system

$$\dot{w} = Fw + Gu \tag{11a}$$

$$z = Jw + Du \tag{11b}$$

are given by

$$\begin{aligned} F &= VAU \\ G &= VB \\ J &= HU, \end{aligned} \tag{12}$$

with the direct-feed matrix given in terms of the residues of the neglected eigenvalues as

$$D = \sum_{i=r+1}^{n} - \frac{R_i}{\lambda_i} \tag{13}$$

The motivation for selecting such a D-matrix is as follows. The transfer function

$$G(s) = J(sI - F)^{-1}G + D$$

of the reduced system (11) is given as (verify!)

$$G(s) = \sum_{i=1}^{r} \frac{R_i}{s - \lambda_i} + \sum_{i=r+1}^{n} - \frac{R_i}{\lambda_i} \tag{14}$$

Evaluating $G(j\omega)$ and $G'(j\omega)$ at $\omega = 0$, it is seen that they are equal to dc. Thus, the modeling errors induced by taking $G(s)$ instead of the actual $G'(s)$ occur at higher frequencies. Indeed, they depend on the frequencies of the neglected eigenvalues of (1).

To determine the $M(s)$ in (6.2-46) that is induced by the order reduction, note that

$$G' = (I + M)G \tag{15}$$

so that

$$M = (G' - G)G^{-1} \tag{16}$$

or

$$M(s) = \left[\sum_{i=r+1}^{n} \frac{R_i}{\lambda_i} \frac{s}{s - \lambda_i}\right] G^{-1}(s) \tag{17}$$

Then the high-frequency robustness bound is given in terms of

$$m(j\omega) = \overline{\sigma}(M(j\omega)) \tag{18}$$

Note that $M(j\omega)$ tends to zero as ω becomes small, reflecting our perfect certainty of the actual plant at dc.

(b) *An Example*. Let us use an example to illustrate the model reduction procedure and show also how to compute the upper bound $m(\omega)$ in (6.2-46)/(6.2-47) on the high-frequency modeling errors thereby induced. To make it easy to see what is going on, we will take a Jordan form system.

Let there be prescribed the MIMO system

$$\dot{x} = \begin{bmatrix} -1 & 0 & 0 \\ 0 & -2 & 0 \\ 0 & 0 & -10 \end{bmatrix} x + \begin{bmatrix} 1 & 0 \\ 0 & 1 \\ 2 & 0 \end{bmatrix} u = Ax + Bu \tag{19a}$$

$$z = \begin{bmatrix} 1 & 0 & 0 \\ 0 & 1 & 1 \end{bmatrix} x = Cx \tag{19b}$$

The eigenvectors are given by $u_i = e_i$, $v_i = e_i$, $i = 1, 2, 3$, with e_i the ith column of the 3×3 identity matrix. Thus, the transfer function is given by the partial fraction expansion

$$G'(s) = \frac{R_1}{s+1} + \frac{R_2}{s+2} + \frac{R_3}{s+10}, \tag{20}$$

with

$$R_1 = \begin{bmatrix} 1 & 0 \\ 0 & 0 \end{bmatrix}, \qquad R_2 = \begin{bmatrix} 0 & 0 \\ 0 & 1 \end{bmatrix}, \qquad R_3 = \begin{bmatrix} 0 & 0 \\ 2 & 0 \end{bmatrix} \tag{21}$$

To find the reduced-order system that retains the poles at $\lambda = -1$ and $\lambda = -2$, define

$$Q = \begin{bmatrix} 1 & 0 \\ 0 & 1 \end{bmatrix}, \qquad V = \begin{bmatrix} 1 & 0 & 0 \\ 0 & 1 & 0 \end{bmatrix}, \qquad U = \begin{bmatrix} 1 & 0 \\ 0 & 1 \\ 0 & 0 \end{bmatrix} \tag{22}$$

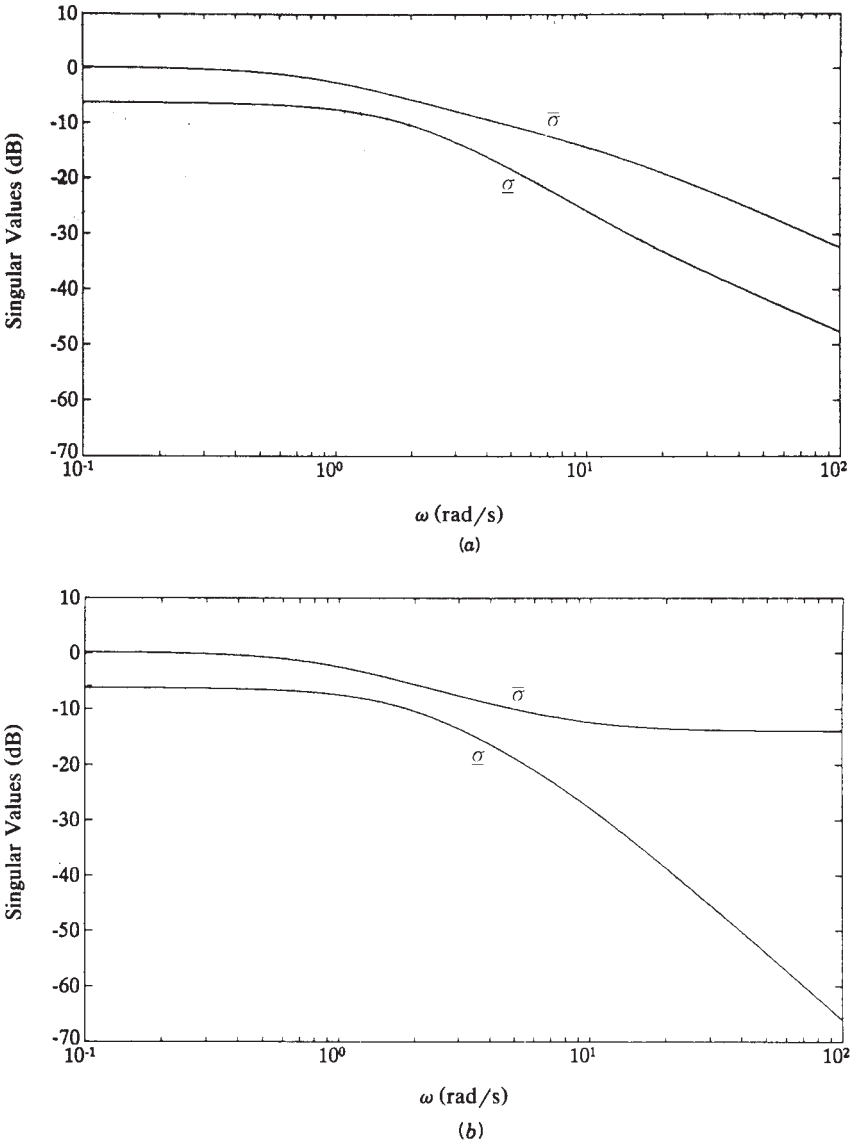

Figure 6.2-10 MIMO Bode magnitude plots of SVs: (*a*) actual plant; (*b*) reduced-order approximation.

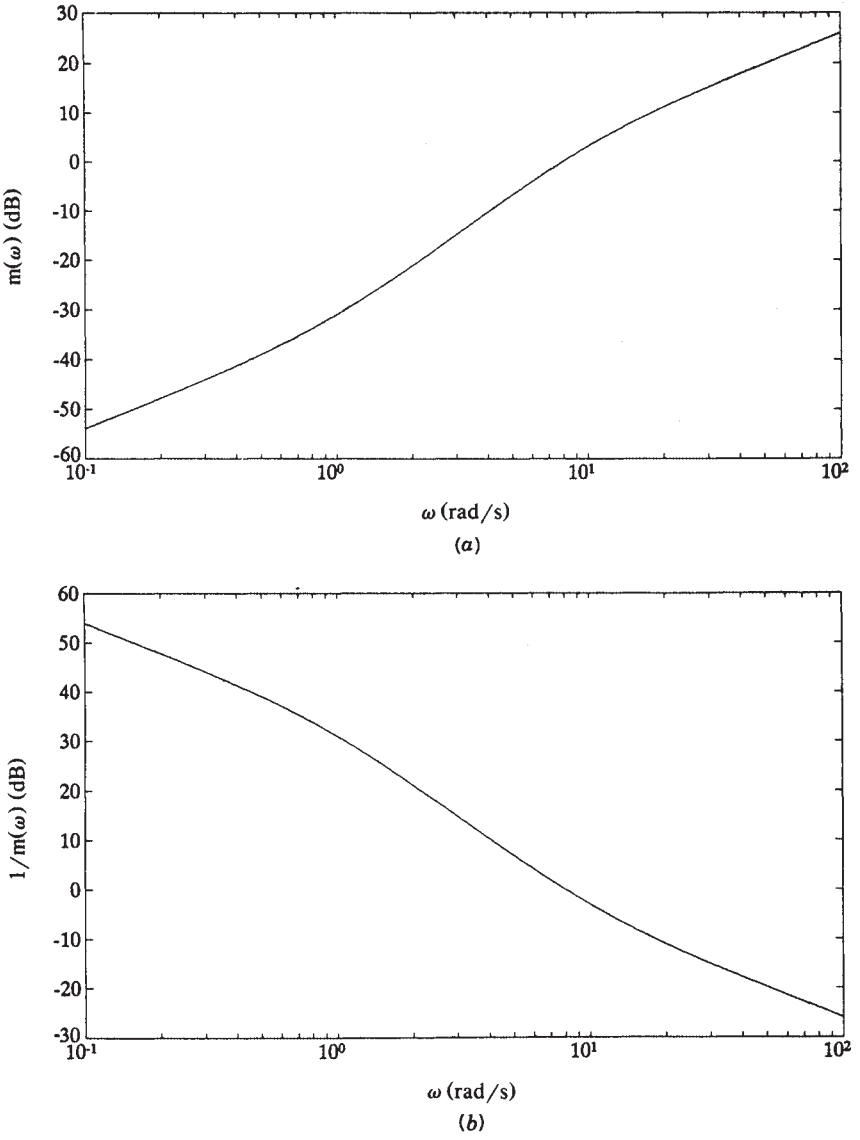

Figure 6.2-11 High-frequency stability robustness bound: (*a*) $\boldsymbol{m}(\omega)$; (*b*) $1/m(\omega)$.

and compute the approximate system

$$\dot{w} = \begin{bmatrix} -1 & 0 \\ 0 & -2 \end{bmatrix} w + \begin{bmatrix} 1 & 0 \\ 0 & 1 \end{bmatrix} u = Fw + Gu \tag{23a}$$

$$z = \begin{bmatrix} 1 & 0 \\ 0 & 1 \end{bmatrix} w + \begin{bmatrix} 0 & 0 \\ 0.2 & 0 \end{bmatrix} u = Jw + Du \tag{23b}$$

This has a transfer function of

$$G(s) = \frac{R_1}{s+1} + \frac{R_2}{s+2} + D \tag{24}$$

Singular-value plots of the actual plant (19) and the reduced-order approximation (23) are shown in Figure 6.2-10.

The multiplicative error is given by

$$M = (G' - G)G^{-1} = \begin{bmatrix} 0 & 0 \\ -\frac{0.2s(s+1)}{s+10} & 0 \end{bmatrix}, \tag{25}$$

whence

$$m(\omega) = \overline{\sigma}(M(j(\omega)) = \frac{0.2\omega\sqrt{\omega^2+1}}{\sqrt{\omega^2+100}}, \tag{26}$$

and the high-frequency bound on the loop gain $GK(j\omega)$ is given by

$$\frac{1}{m(j\omega)} = \frac{5\sqrt{\omega^2+100}}{\omega\sqrt{\omega^2+1}} \tag{28}$$

This bound is plotted in Figure 6.2-11. Note that the modeling errors become appreciable (i.e., of magnitude 1) at a frequency of 8.0 rad/s. Above this frequency, we should ensure that constraint (6.2-50) on the loop gain magnitude holds to guarantee stability robustness. This will be a restriction on any compensator $K(s)$ designed using the reduced-order plant (23). ■

Robustness Bounds for Plant Parameter Variations

The aircraft is nonlinear, but for controller design we use linearized models obtained at some operating point. In practice, it is necessary to determine linear models at several design operating points over a specified flight envelope and determine optimal control gains for each one. Then these design control gains are tabulated and scheduled using microprocessors, so that the gains most appropriate for the actual operating point of the aircraft are used in the controller. It is usual to determine which of the design operating points are closest to the actual operating point and use some sort of linear combination of the control gains corresponding to these design points.

It is important for the control gains to stabilize the aircraft at all points near the design operating point for this gain-scheduling procedure to be effective. In passing

from operating point to operating point, the parameters of the state-variable model vary. Using (6.2-49), we may design controllers that guarantee robust stability despite plant parameter variations.

Suppose that the nominal perturbed model used for design is

$$\begin{aligned} \dot{x} &= Ax + Bu \\ y &= Cx \end{aligned} \tag{6.2-51}$$

which has the transfer function

$$G(s) = C(sI - A)^{-1}B \tag{6.2-52}$$

However, due to operating point changes the actual aircraft perturbed motion is described by

$$\begin{aligned} \dot{x} &= (A + \Delta A)x + (B + \Delta B)u \\ y &= (C + \Delta C)x, \end{aligned} \tag{6.2-53}$$

where the plant parameter variation matrices are ΔA, ΔB, ΔC. It is not difficult to show [see Stevens et al. (1987) and the problems at the end of this chapter] that this results in the transfer function

$$G'(s) = G(s) + \Delta G(s),$$

with

$$\begin{aligned} \Delta G(s) = {} & C(sI - A)^{-1}\Delta B + \Delta C\ (sI - A^{-1})B \\ & + C(sI - A)^{-1}\,\Delta A(sI - A)^{-1}B, \end{aligned} \tag{6.2-54}$$

where second-order effects have been neglected. Hence (6.2-48) may be used to determine the multiplicative uncertainty bound $m(\omega)$. The cosensitivity $T(j\omega)$ should then satisfy the upper bound (6.2-49) for guaranteed stability in the face of the parameter variations ΔA, ΔB, ΔC.

Since $(sI - A)^{-1}$ has a relative degree of at least 1, the high-frequency roll-off of $\Delta G(j\omega)$ is at least -20 dB/decade. Thus, plant parameter variations yield an upper bound for the cosensitivity at low frequencies.

Using (6.2-54) it is possible to design robust controllers over a range of operating points that do not require gain scheduling. Compare with Minto et al. (1990).

6.3 ROBUST OUTPUT FEEDBACK DESIGN

We should now like to incorporate the robustness concepts introduced in Section 6.2 into the LQ output feedback design procedure for aircraft control systems. This may be accomplished using the following steps:

1. If necessary, augment the plant with added dynamics to achieve the required steady-state error behavior or to achieve balanced SVs at dc. Use the techniques of Example 6.2-3.
2. Select a performance index, the PI weighting matrices Q and R, and, if applicable, the time weighting factor k in t^k.
3. Determine the optimal output feedback again K using, for instance, Table 5.4-1 or 5.5-1.
4. Simulate the time responses of the closed-loop system to verify that they are satisfactory. If not, select different Q, R, and k and return to step 3.
5. Determine the low-frequency and high-frequency bounds required for performance robustness and stability robustness. Plot the loop gain SVs to verify that the bounds are satisfied. If they are not, select new Q, R, and k and return to step 3.

An example will illustrate the robust output feedback design procedure.

Example 6.3-1: Pitch-Rate Control System Robust to Wind Gusts and Unmodeled Flexible Mode Here we will illustrate the design of a pitch-rate control system that is robust in the presence of vertical wind gusts and the unmodeled dynamics associated with a flexible mode. It would be worthwhile first to review the pitch-rate CAS designed in Examples 4.5-1 and 5.5-3.

(a) *Control System Structure*. The pitch-rate CAS system is described in Example 5.5-3. The state and measured outputs are

$$x = \begin{bmatrix} \alpha \\ q \\ \delta_e \\ \alpha_F \\ \epsilon \end{bmatrix}, \qquad y = \begin{bmatrix} \alpha_F \\ q \\ \epsilon \end{bmatrix}, \tag{1}$$

with α_F the filtered angle of attack and ϵ the output of the integrator added to ensure zero steady-state error. The performance output $z(t)$ that should track the reference input $r(t)$ is $q(t)$.

Linearizing the F-16 dynamics about the nominal flight condition in Table 3.6-3 (502 ft/s, level flight, $x_{cg} = 0.35\ \bar{c}$) yields

$$\dot{x} = Ax + Bu + Gr \tag{2}$$

$$y = Cx + Fr \tag{3}$$

$$z = Hx, \tag{4}$$

with the system matrices given in Example 5.5-3.

The control input is

$$u = -Ky = -\begin{bmatrix} k_\alpha & k_q & k_1 \end{bmatrix} y = -k_\alpha \alpha_F - k_q q - k_I \epsilon \tag{5}$$

It is desired to select the control gains to guarantee a good response to a step command r in the presence of vertical wind gusts and the unmodeled dynamics of the first flexible mode.

(b) *Frequency-Domain Robustness Bounds*. According to *Mil. Spec. 1797* (1987), the vertical wind gust noise has a spectral density given in Dryden form as

$$\Phi_w(\omega) = 2L\sigma^2 \frac{1 + 3L^2\omega^2}{(1 + L^2\omega^2)^2}, \tag{6}$$

with ω the frequency in rad/s, σ the turbulence intensity, and L the turbulence scale length divided by true airspeed. Assuming that the vertical gust velocity is a disturbance input that changes the angle of attack, the software described in Chapter 3 can be used to find a control input matrix from gust velocity to x. Then, using stochastic techniques like those in Example 6.4-2, the magnitude of the gust disturbance versus frequency can be found. It is shown in Figure 6.3-1. We took $\sigma = 10$ ft/s and $L = (1700\,\text{ft})/(502\,\text{ft/s}) = 3.49$ s.

Let the transfer function of the rigid dynamics from $u(t)$ to $z(t)$ be denoted by $G(s)$. Then the transfer function including the first flexible mode is given by Blakelock (1965):

$$G'(s) = G(s)F(s), \tag{7}$$

where

$$F(s) = \frac{\omega_n^2}{s^2 + 2\zeta\omega_n s + \omega_n^2}, \tag{8}$$

with $\omega_n = 40$ rad/s and $\zeta = 0.3$. According to Section 6.2, therefore, the multiplicative uncertainty is given by

$$M(s) = F(s) - I = \frac{-s(s + 2\zeta\omega_n)}{s^2 + 2\zeta\omega_n s + \omega_n^2} \tag{9}$$

The magnitude of $1/M(j\omega)$ is shown in Figure 6.3-1.

We should like to perform our control design using only the rigid dynamics $G(s)$. Then, for performance robustness in the face of the gust disturbance and stability robustness in the face of the first flexible mode, the loop gain SVs should lie within the bounds implied by the gust disturbance magnitude and $1/|M(j\omega)|$.

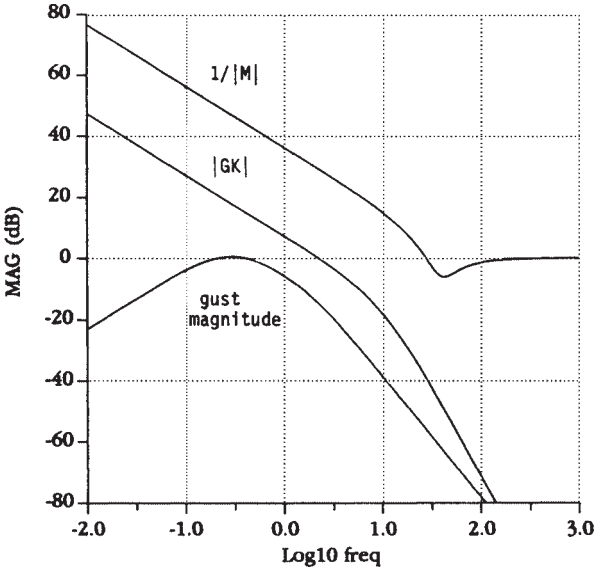

Figure 6.3-1 Frequency-domain magnitude plots and robustness bounds.

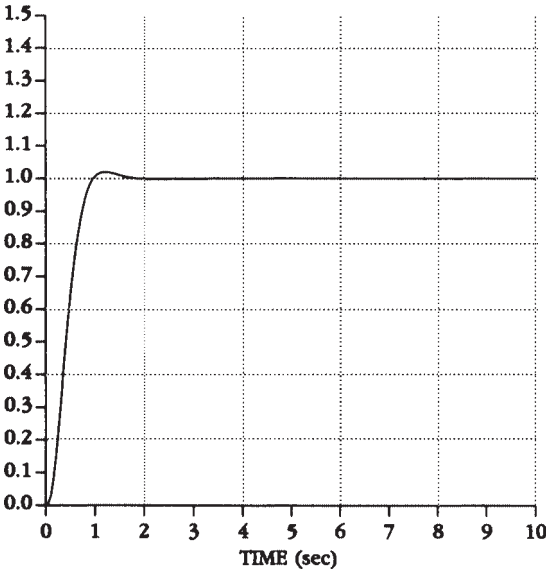

Figure 6.3-2 Optimal pitch-rate step response.

(c) *Controls Design and Robustness Verification*. In Example 5.5-3(c) we performed a derivative-weighting design and obtained the control gains

$$K = \begin{bmatrix} -0.0807 & -0.475 & 1.361 \end{bmatrix} \tag{10}$$

The resulting step response is reproduced in Figure 6.3-2, and the closed-loop poles were

$$\begin{aligned} s = &-3.26 \pm j2.83 \\ &-1.02 \\ &-10.67, -14.09 \end{aligned} \tag{11}$$

To verify that the robustness bounds hold for this design, it is necessary to find the loop gain $GK(s)$ of the closed-loop system. Thus, in the figure of Example 5.5-3 it is necessary to find the loop transfer function from $e(t)$ around to $e(t)$ [i.e., from $e(t)$ to $-z(t)$]. With respect to this loop gain, note that some of the elements in (10) are feedforward gains while some are feedback gains.

The magnitude of $GK(j\omega)$ is plotted in Figure 6.3-1. Note that the robustness bounds are satisfied. Therefore, this design is robust in the presence of vertical turbulence velocities up to 10 ft/s as well as the first flexible mode. ■

6.4 OBSERVERS AND THE KALMAN FILTER

The central theme in Chapter 5 was control design using partial state or output feedback. We saw in Section 5.4 that by using output feedback a compensator of any desired structure may be used, with the feedback gains being selected by modern LQ techniques. Thus, output feedback design is very suitable for aircraft control. In Section 6.3 we saw how to verify the robustness of the closed-loop system using multivariable Bode plots.

On the other hand, in Section 5.7 we saw that the design equations for full-state-variable feedback were simpler than those for output feedback. In fact, in state-variable design it is only necessary to solve the matrix Riccati equation, for which there are many good techniques [ORACLS (Armstrong, 1980), PC-MATLAB (Moler et al., 1987), and MATRIX$_x$ (1989)]. By contrast, in output feedback design it is necessary to solve three coupled nonlinear equations (see Table 5.3-1), which must generally be done using iterative techniques (Moerder and Calise, 1985; Press et al., 1986).

Moreover, in the case of full state feedback, if the system (A, B) is reachable and $(\sqrt{Q}, A)$ is observable (with Q the state weighting in the PI), the Kalman gain is guaranteed to stabilize the plant and yield a global minimum value for the PI. This is a fundamental result of modern control theory, and no such result yet exists for output feedback. The best that may be said is that if the plant is output stabilizable, the algorithm of Table 5.3-2 yields a local minimum for the PI and a stable plant.

Another issue is that the LQ regulator with full state feedback enjoys some important robustness properties that are not guaranteed using output feedback. Specifically, as we will see in Section 6.5, it has an infinite gain margin and 60% of phase margin.

Thus, state feedback design offers some advantages over output feedback if the structure of the compensator is of no concern. Although this is rarely the case in aircraft controls, it is nevertheless instructive to pursue a compensator design technique based on state feedback.

Since all the states are seldom available, the first order of business is to estimate the full state $x(t)$ given only partial information in the form of the measured outputs $y(t)$. This is the *observer design* problem. Having estimated the state, we may then use the *estimate* of the state for feedback purposes, designing a feedback gain *as if* all the states were measurable. The combination of the observer and the state feedback gain is then a dynamic regulator similar to those used in classical control, as we will show in the last portion of this section. In the modern approach, however, it is straightforward to design multivariable regulators with desirable properties by solving matrix equations due to the fundamental *separation principle,* which states that the feedback gain and observer may be designed separately and then concatenated.

One of our prime objectives in this section and the next is to discuss the LQG/LTR technique for control design. This is an important modern technique for the design of robust aircraft control systems. It relies on full-state-feedback design, followed by the design of an observer that allows full recovery of the guaranteed robustness properties of the LQ regulator with state feedback.

Of course, observers and filters have important applications in aircraft in their own right. For instance, the angle of attack is difficult to measure accurately; however, using an observer or Kalman filter, it is not difficult to estimate the angle of attack very precisely by measuring pitch rate and normal acceleration (see Example 6.4-2).

Observer Design

In aircraft control, all of the states are rarely available for feedback purposes. Instead, only the measured outputs are available. Using modern control theory, if the measured outputs capture enough information about the dynamics of the system, it is possible to use them to *estimate* or *observe* all the states. Then these state estimates may be used for feedback purposes.

To see how a state observer can be constructed, consider the aircraft equations in state-space form

$$\dot{x} = Ax + Bu \tag{6.4-1}$$

$$y = Cx, \tag{6.4-2}$$

with $x(t) \in \mathbf{R}^n$ the state, $u(t) \in \mathbf{R}^m$ the control input, and $y(t) \in \mathbf{R}^p$ the available measured outputs.

Let the estimate of $x(t)$ be $\hat{x}(t)$. We claim that the state observer is a dynamical system described by

$$\dot{\hat{x}} = A\hat{x} + Bu + L(y - C\hat{x}) \tag{6.4-3}$$

or

$$\dot{\hat{x}} = (A - LC)\hat{x} + Bu + Ly \equiv A_0\hat{x} + Bu + Ly \tag{6.4-4}$$

That is, the observer is a system with two inputs, namely, $u(t)$ and $y(t)$, both of which are known.

Since $\hat{x}(t)$ is the state estimate, we could call

$$\hat{y} = C\hat{x} \tag{6.4-5}$$

the estimated output. It is desired that $\hat{x}(t)$ be close to $x(t)$. Thus, if the observer is working properly, the quantity $y - \hat{y}$ that appears in (6.4-3) should be small. In fact,

$$\tilde{y} = y - \hat{y} \tag{6.4-6}$$

is the *output estimation error*.

It is worth examining Figure 6.4-1, which depicts the state observer. Note that the observer consists of two parts: a *model of the system* involving (A, B, C) and an *error-correcting portion* that involves the output error multiplied by L. We call matrix L the *observer gain*.

To demonstrate that the proposed dynamical system is indeed an observer, it is necessary to show that it manufactures an estimate $\hat{x}(t)$ that is close to the actual state $x(t)$. For this purpose, define the (*state*) *estimation error* as

$$\tilde{x} = x - \hat{x} \tag{6.4-7}$$

By differentiating (6.4-7) and using (6.4-1) and (6.4-4), it is seen that the estimation error has dynamics given by

$$\dot{\tilde{x}} = (A - LC)\tilde{x} = A_0\tilde{x} \tag{6.4-8}$$

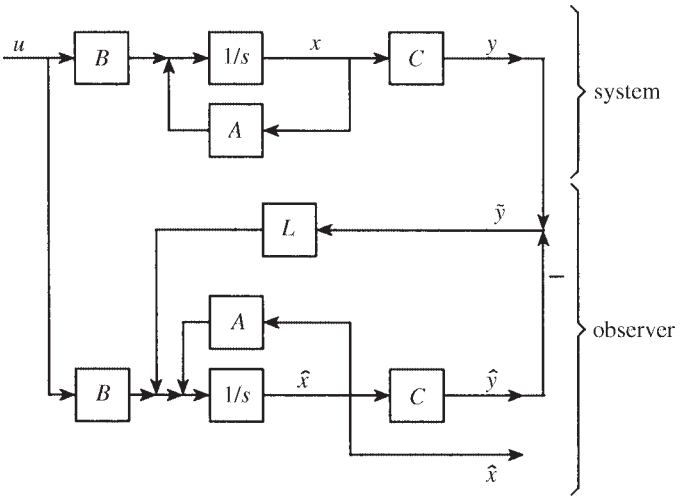

Figure 6.4-1 State observer.

The initial estimation error is $\tilde{x}(0) = x(0) - \hat{x}(0)$, with $\hat{x}(0)$ the initial estimate, which is generally taken as zero.

It is required that the estimation error vanish with time for any $\tilde{x}(0)$, for then $\hat{x}(t)$ will approach $x(t)$. This will occur if $A_0 = (A - LC)$ is asymptotically stable. Therefore, as long as we select the observer gain L so that $(A - LC)$ is stable, (6.4-3) is indeed an observer for the state in (6.4-1). The observer design problem is to select L so that the error vanishes suitably quickly. It is a well-known result of modern control theory that the poles of $(A - LC)$ may be arbitrarily assigned to desired locations if and only if (C, A) is observable.

Since, according to Figure 6.4-1, we are injecting the output into the state derivative, L is called an *output injection*. Observers of the sort we are mentioning here are called *output injection observers,* and their design could be called output injection design.

It is important to discuss the output injection problem of selecting L so that $(A - LC)$ is stable, for it is a problem we have already solved under a different guise. The state feedback control law for system (6.4-1) is

$$u = -Kx, \tag{6.4-9}$$

which results in the closed-loop system

$$\dot{x} = (A - BK)x \tag{6.4-10}$$

The state feedback design problem is to select K for desired closed-loop properties. We have shown how this may be accomplished in Section 5.7. Thus, if we select the feedback gain as the Kalman gain

$$K = R^{-1}B^{\mathrm{T}}P, \tag{6.4-11}$$

with P the positive-definite solution to the algebraic Riccati equation (ARE)

$$0 = A^{\mathrm{T}}P + PA + Q - PBR^{-1}B^{\mathrm{T}}P, \tag{6.4-12}$$

then if (A, B) is reachable and $(\sqrt{Q}, A)$ is observable, the closed-loop system is guaranteed to be stable. The matrices Q and R are design parameters that will determine the closed-loop dynamics, as we have seen in the examples of Chapter 5.

Now, compare (6.4-8) and (6.4-10). They are very similar. In fact,

$$(A - LC)^{\mathrm{T}} = A^{\mathrm{T}} - C^{\mathrm{T}}L^{\mathrm{T}}, \tag{6.4-13}$$

which has the free matrix L^{T} to the right, exactly as in the state feedback problem involving $(A - BK)$. This important fact is called *duality,* that is, state feedback and output injection are duals. [Note that $A - LC$ and $(A - LC)^{\mathrm{T}}$ have the same poles.]

The important result of duality for us is that *the same theory we have developed for selecting the state feedback gain may be used to select the output injection gain L.*

In fact, compare (6.4-13) to $(A - BK)$. Now, in the design equations (6.4-11) and (6.4-12) let us replace A, B, and K everywhere they occur by A^{T}, C^{T}, and L^{T}, respectively. The result is

$$\begin{aligned} L^{\mathrm{T}} &= R^{-1}CP \\ 0 &= AP + PA^{\mathrm{T}} + Q - PC^{\mathrm{T}}R^{-1}CP \end{aligned} \tag{6.4-14}$$

The first of these may be rewritten as

$$L = P\,C^{\mathrm{T}}R^{-1} \tag{6.4-15}$$

We call (6.4-14) the *observer ARE*.

Let us note the following connection between reachability and observability. Taking the transpose of the reachability matrix yields

$$\begin{aligned} U^{\mathrm{T}} &= \begin{bmatrix} B & AB & A^2B & \cdots & A^{n-1}B \end{bmatrix}^{\mathrm{T}} \\ &= \begin{bmatrix} B^{\mathrm{T}} \\ B^{\mathrm{T}}A \\ \vdots \\ B^{\mathrm{T}}\left(A^{\mathrm{T}}\right)^{n-1} \end{bmatrix} \end{aligned} \tag{6.4-16}$$

However, the observability matrix is

$$V = \begin{bmatrix} C \\ CA \\ \vdots \\ CA^{n-1} \end{bmatrix} \tag{6.4-17}$$

Comparing U^{T} and V, it is apparent that they have the same form. In fact, since U and U^{T} have the same rank, it is evident that (A, B) is reachable if and only if $(B^{\mathrm{T}}, A^{\mathrm{T}})$ is observable. This is another aspect of duality.

Taking into account these notions, an essential result of output injection is the following. It is the dual of the guaranteed stability using the Kalman gain discussed in Section 5.7. Due to its importance, we formulate it as a theorem.

Theorem. *Let (C, A) be observable and $(A, \sqrt{Q})$ be reachable. Then the error system (6.4-8) using the gain L given by (6.4-15), with P the unique positive-definite solution to (6.4-14), is asymptotically stable.* ■

Stability of the error system guarantees that the state estimate $\hat{x}(t)$ will approach the actual state $x(t)$. By selecting L to place the poles of $(A - LC)$ far enough to the left in the s-plane, the estimation error $\tilde{x}(t)$ can be made to vanish as quickly as desired.

The power of this theorem is that we may treat Q and R as design parameters that may be turned until suitable observer behavior results for the gain computed from the

observer ARE. As long as we select Q and R to satisfy the theorem, observer stability is assured. An additional factor, of course, is that software for solving the observer ARE is readily available [e.g., ORACLS (Armstrong, 1980), PC-MATLAB (Moler et al., 1987), and MATRIX$_x$ (1989)].

We have assumed that the system matrices (A, B, C) are exactly known. Unfortunately, in reality this is rarely the case. In aircraft control, for instance, (6.4-1) and (6.4-2) represent a model of a nonlinear system at an equilibrium point. Variations in the operating point will result in variations in the elements of A, B, and C. However, if the poles of $(A - LC)$ are selected far enough to the left in the s -plane (i.e., fast enough), the estimation error will be small despite uncertainties in the system matrices. That is, the observer has some robustness to modeling inaccuracies.

It is worth mentioning that there are many other techniques for the selection of the observer gain L. In the single-output case the observability matrix V is square. Then Ackermann's formula (Franklin et al., 1986) may be used to compute L. If

$$\Delta_{(0)}(s) = |sI - (A - LC)| \tag{6.4-18}$$

is the desired observer characteristic polynomial, the required observer gain is given by

$$L = \Delta_0(A)V^{-1}e_n, \tag{6.4-19}$$

with $e_n = [0 \cdots 0 \;\; 1]^{\mathrm{T}}$ the last column of the $n \times n$ identity matrix.

A general rule of thumb is that for suitable accuracy in the state estimate $\hat{x}(t)$, the slowest observer pole should have a real part 5 to 10 times larger than the real part of the fastest system pole. That is, the observer time constants should be 5 to 10 times larger than the system time constants.

Example 6.4-1: Observer Design for Double Integrator System In Example 5.7-1 we discussed state feedback design for systems obeying Newton's laws,

$$\dot{x} = \begin{bmatrix} 0 & 1 \\ 0 & 0 \end{bmatrix} x + \begin{bmatrix} 0 \\ 1 \end{bmatrix} u = Ax + Bu, \tag{1}$$

where the state is $x = [d \;\; v]^{\mathrm{T}}$, with $d(t)$ the position and $v(t)$ the velocity, and the control $u(t)$ is an acceleration input. Let us take position measurements so that the measured output is

$$y = [1 \quad 0]x = Cx \tag{2}$$

We should like to design an observer that will reconstruct the full state $x(t)$ given only position measurements. Let us note that simple differentiation of $y(t) = d(t)$ to obtain $v(t)$ is unsatisfactory, since differentiation increases sensor noise. In fact, the observer is a *low-pass* filter that provides estimates while rejecting high-frequency noise. We will discuss two techniques for observer design.

(a) *Riccati Equation Design*. There is good software available in standard design packages for solving the observer ARE [e.g., ORACLS (Armstrong, 1980) and PCMATLAB (Moler et al., 1987)]. However, in this example we want to solve the ARE analytically to show the relation between the design parameters Q and R and the observer poles.

Selecting $R = 1$ and $Q = \text{diag}\{q_d, q_v^2\}$ with q_d and q_v nonnegative, we may assume that

$$P = \begin{bmatrix} p_1 & p_2 \\ p_2 & p_3 \end{bmatrix} \tag{3}$$

for some scalars p_1, p_2, and p_3 to be determined. The observer ARE (6.4-14) becomes

$$\begin{aligned} 0 = &\begin{bmatrix} 0 & 1 \\ 0 & 0 \end{bmatrix} \begin{bmatrix} p_1 & p_2 \\ p_2 & p_3 \end{bmatrix} + \begin{bmatrix} p_1 & p_2 \\ p_2 & p_3 \end{bmatrix} \begin{bmatrix} 0 & 0 \\ 1 & 0 \end{bmatrix} + \begin{bmatrix} q_d & 0 \\ 0 & q_v^2 \end{bmatrix} \\ &- \begin{bmatrix} p_1 & p_2 \\ p_2 & p_3 \end{bmatrix} \begin{bmatrix} 1 & 0 \\ 0 & 0 \end{bmatrix} \begin{bmatrix} p_1 & p_2 \\ p_2 & p_3 \end{bmatrix}, \end{aligned} \tag{4}$$

which may be multiplied out to obtain the three scalar equations

$$0 = 2p_2 - p_1^2 + q_d \tag{5a}$$

$$0 = p_3 - p_1 p_2 \tag{5b}$$

$$0 = p_2^2 + q_v^2 \tag{5c}$$

Solving these equations gives

$$p_2 = q_v \tag{6a}$$

$$p_1 = \sqrt{2}\sqrt{q_v + \frac{q_d}{2}} \tag{6b}$$

$$p_3 = q_v\sqrt{2}\sqrt{q_v + \frac{q_d}{2}}, \tag{6c}$$

where we have selected the signs that make P positive definite.

According to (6.4-15), the observer gain is equal to

$$L = \begin{bmatrix} p_1 & p_2 \\ p_2 & p_3 \end{bmatrix} \begin{bmatrix} 1 \\ 0 \end{bmatrix} = \begin{bmatrix} p_1 \\ p_2 \end{bmatrix} \tag{7}$$

Therefore,

$$L = \begin{bmatrix} \sqrt{2}\sqrt{q_v + \frac{q_d}{2}} \\ q_v \end{bmatrix} \tag{8}$$

Using (8), the error system matrix is found to be

$$A_0 = (A - LC) = \begin{bmatrix} -\sqrt{2}\sqrt{q_v + \frac{q_d}{2}} & 1 \\ -q_v & 0 \end{bmatrix} \tag{9}$$

Therefore, the observer characteristic polynomial is

$$\Delta_0(s) = |sI - A_0| = s^2 + 2\zeta\omega s + \omega^2, \tag{10}$$

with the observer natural frequency ω and damping ratio ζ given by

$$\omega = \sqrt{q_v}, \quad \zeta = \frac{1}{\sqrt{2}}\sqrt{1 + \frac{q_d}{2q_v}} \tag{11}$$

It is now clear how selection of Q affects the observer behavior. Note that if $q_d = 0$, the damping ratio becomes the familiar $1/\sqrt{2}$.

The reader should verify that the system is observable and that $(A, \sqrt{Q})$ is reachable as long as $q_v \neq 0$. A comparison with Example 5.7-1, where a state feedback was designed for Newton's system, reveals some interesting aspects of duality.

(b) *Ackermann's Formula Design*. Riccati equation observer design is useful whether the plant has only one or multiple outputs. If there is only one output, we may use Ackermann's formula (6.4-19).

Let the desired observer polynomial be

$$\Delta_0(s) = s^2 + 2\zeta\omega s + \omega^2 \tag{12}$$

for some specified damping ratio ζ and natural frequency ω. Then

$$\Delta_0(A) = A^2 + 2\zeta\omega A + \omega^2 I = \begin{bmatrix} \omega_2 & 2\zeta\omega \\ 0 & \omega^2 \end{bmatrix} \tag{13}$$

$$V = \begin{bmatrix} C \\ CA \end{bmatrix} = I, \tag{14}$$

so that the observer gain is

$$L = \begin{bmatrix} 2\zeta\omega \\ \omega_2 \end{bmatrix} \tag{15}$$

One may verify that the characteristic polynomial of $A_0 = A - LC$ is indeed (12).

(c) *Simulation*. To design an observer with a complex pole pair having damping ratio of $\zeta = 1/\sqrt{2}$ and natural frequency of $\omega = 1$ rad/s, the observer gain was selected as

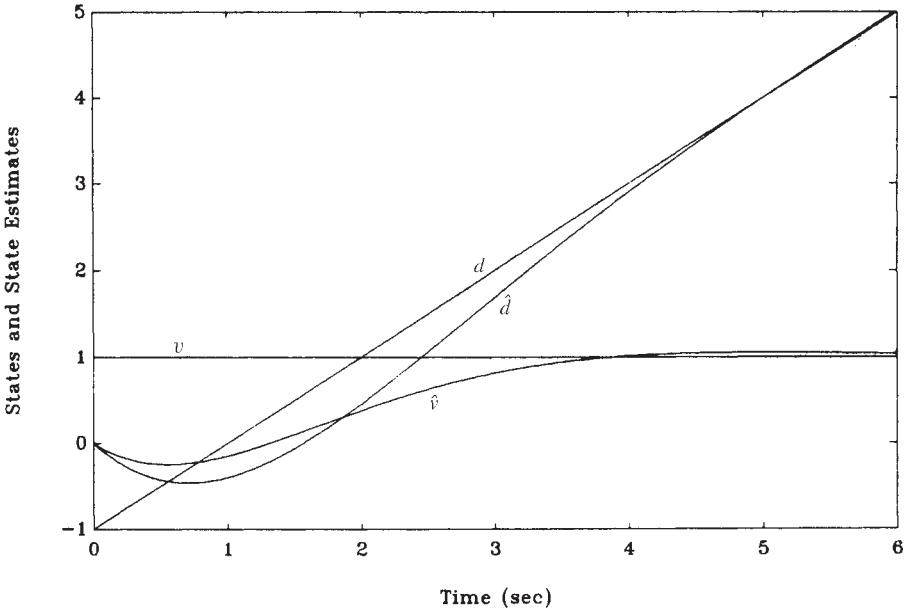

Figure 6.4-2 Actual and estimated states.

$$L = \begin{bmatrix} \sqrt{2} \\ 1 \end{bmatrix} \tag{16}$$

A simulation was performed. The time histories of the actual states and their estimates are shown in Figure 6.4-2. The initial conditions were $d(0) = -1$, $v(0) = 1$ and the input was $u(t) = 0$. The observer was started with initial states of $\hat{d}(0) = 0, \hat{v}(0) = 0$. ■

The Kalman Filter

Throughout Chapter 5 we assumed that the system is exactly known and that no modeling inaccuracies, disturbances, or noises are present. In fact, nature is seldom so cooperative. In Sections 6.2 and 6.3 we showed how to take account of uncertainties in the model and the environment using a robust frequency-domain approach. An alternative is to treat uncertainties using *probability theory*.

In this subsection we develop the Kalman filter, which is based on a probabilistic treatment of process and measurement noises. The Kalman filter is an observer that is used for navigation and other applications that require the reconstruction of the state from noisy measurements. Since it is fundamentally a low-pass filter, it has good noise rejection capabilities. In Example 6.4-2 we show how to use the Kalman filter to estimate the angle of attack in the face of gust disturbances. In Section 6.5 we show how to use a state-variable feedback and a Kalman filter to design robust aircraft controllers by using the LQG/LTR technique.

We begin with a brief review of probability theory. It is not necessary to follow the derivation to use the Kalman filter: It Is only necessary to solve the design equations in Table 6.4-1 below. Thus, one could skip the review that follows. However, an understanding of the theory will result in more sensible application of the filter. Supplemental references are Gelb (1974) and Lewis (1986*b*).

A Brief Review of Probability Theory Suppose that the plant is described by the stochastic dynamical equation

$$\dot{x} = Ax + Bu + Gw \tag{6.4-20}$$

$$y = Cx + v, \tag{6.4-21}$$

with state $x(t) = \in \mathbf{R}^n$, control input $u(t) \in \mathbf{R}^m$, and measured output $y(t) \in \mathbf{R}^p$. Signal $w(t)$ is an unknown *process noise* that acts to disturb the plant. It could represent the effects of wind gusts, for instance, or unmodeled high-frequency plant dynamics. Signal $v(t)$ is an unknown *measurement noise* that acts to impair the measurements; it could represent sensor noise.

Since (6.4-20) is driven by process noise, the state $x(t)$ is now also a random process, as is $y(t)$. To investigate average properties of random processes, we will require several concepts from probability theory (Papoulis, 1984). The point is that although $w(t)$ and $v(t)$ represent unknown random processes, we do in fact know something about them which can help us in control design. For instance, we may know their average values or total energy content. The concepts we will now define allow us to incorporate this general sort of knowledge into our theory.

Given a random vector $z \in \mathbf{R}^n$, we denote by $f_z(\zeta)$ the *probability density function* (*PDF*) of z. The PDF represents the probability that z takes on a value within the differential region $d\zeta$ centered at ζ. Although the value of z may be unknown, it is quite common in many situations to have a good feel for its PDF.

The *expected value* of a function $g(z)$ of a random vector z is defined as

$$E\{g(z)\} = \int_{-\infty}^{\infty} g(\zeta) f_z(\zeta) d\zeta \tag{6.4-22}$$

The *mean* or *expected value* of z is defined by

$$E\{z\} = \int_{-\infty}^{\infty} \zeta f_z(\zeta) d\zeta, \tag{6.4-23}$$

which we will symbolize by $\overline{z}$ to economize on notation. Note that $\overline{z} \in \mathbf{R}^n$.

The covariance of z is given by

$$P_z = E\{(z - \overline{z})(z - \overline{z})^{\mathrm{T}}\} \tag{6.4-24}$$

Note that P_z is an $n \times n$ constant matrix.

An important class of random vectors is characterized by the *Gaussian* or *normal* PDF

$$f_z(\zeta) = \frac{1}{\sqrt{(2\pi)^n |P_z|}} e^{-(\zeta-\bar{z})^{\mathrm{T}} P_z^{-1} (\zeta-\bar{z})/2} \tag{6.4-25}$$

In the scalar case $n = 1$ this reduces to the more familiar

$$f_z(\zeta) = \frac{1}{\sqrt{2\pi P_z}} e^{-(\zeta-\bar{z})^2/2P_z}, \tag{6.4-26}$$

which is illustrated in Figure 6.4-3. Such random vectors take on values near the mean $\bar{z}$ with greatest probability and have a decreasing probability of taking on values farther away from $\bar{z}$. Many naturally occurring random variables are Gaussian.

If the random vector is a time function, it is called a *random process,* symbolized as $z(t)$. Then the PDF may also be time varying and we write $f_z(\zeta, t)$. One can imagine the PDF in Figure 6.4-3 changing with time. In this situation, the expected value and covariance matrix are also functions of time, so we write $\bar{z}(t)$ and $P_z(t)$.

Many random processes $z(t)$ of interest to us have a time-invariant PDF. These are *stationary* processes and, even though they are random time functions, they have a constant mean and covariance.

To characterize the relation between two random processes $z(t)$ and $x(t)$, we employ the *joint PDF* $f_{zx}(\zeta, \xi, t_1, t_2)$, which represents the probability that $(z(t_1), x(t_2))$ is within the differential area $d\zeta \times d\xi$ centered at (ζ, ξ). For our purposes, we will assume that the processes $z(t)$ and $x(t)$ are *jointly stationary,* that is, the joint PDF is not a function of both times t_1 and t_2 but depends only on the difference $(t_1 - t_2)$.

In the stationary case, the expected value of the function of two variables $g(z, x)$ is defined as

$$E\{q(z(t_1), x(t_2))\} = \int_{-\infty}^{\infty} g(\zeta, \xi) f_{z,x}(\zeta, \xi,\ t_1 - t_2) d\zeta d\xi \tag{6.4-27}$$

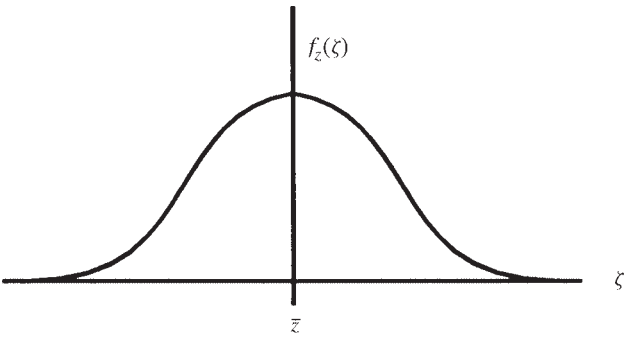

Figure 6.4-3 Gaussian PDF.

In particular, the *cross-correlation matrix* is defined by

$$R_{zx}(\tau) = E\{z(t+\tau)x^{\mathrm{T}}(t)\} \tag{6.4-28}$$

In the sequel, we will briefly require the cross-correlation matrix of two nonstationary processes, which is defined as

$$R_{zx}(t,\tau) = E\{z(t)x^{\mathrm{T}}(\tau)\} \tag{6.4-29}$$

Considering $z(t_1)$ and $z(t_2)$ as two jointly distributed random stationary processes, we may define the *autocorrelation function* of $z(t)$ as

$$R_z(\tau) = E\{z(t+\tau)z^{\mathrm{T}}(t)\} \tag{6.4-30}$$

The autocorrelation function gives us some important information about the random process $z(t)$. For instance,

$$\mathrm{tr}\left[R_z(0)\right] = \mathrm{tr}\left[E\left\{z(t)\,z^{\mathrm{T}}(t)\right\}\right] = E\left\{\|z(t)\|^2\right\}$$

is equal to the total energy in the process $z(t)$. (In writing this equation recall that, for any compatible matrices M and N, $\mathrm{tr}(MN) = \mathrm{tr}(NM)$.)

If

$$R_{zx}(\tau) = 0, \tag{6.4-31}$$

we call $z(t)$ and $x(t)$ *orthogonal*. If

$$R_z(\tau) = P\delta(\tau), \tag{6.4-32}$$

where P is a constant matrix and $\delta(t)$ is the Dirac delta, then $z(t)$ is orthogonal to $z(t+\tau)$ for any $\tau \neq 0$. What this means is that the value of the process $z(t)$ at one time t is unrelated to its value at another time $\tau \neq t$. Such a process is called *white noise*. An example is the thermal noise in an electric circuit, which is due to the thermal agitation of the electrons in the resistors.

Note that $P\delta(0)$ is the covariance of $z(t)$, which is unbounded. We call P a *spectral density matrix*. It is sometimes loosely referred to as a covariance matrix.

Derivation of the Kalman Filter We may now return to system (6.4-20)/(6.4-21). Neither the initial state $x(0)$, the process noise $w(t)$, nor the measurement noise $v(t)$ is exactly known. However, in practice we may have some feeling for their general characteristics. Using the concepts we have just discussed, we may formalize this general knowledge so that it may be used in control design.

The process noise is due to some sort of system disturbance, such as wind gusts; the measurement noise is due to sensor inaccuracies; and the initial state is uncertain

because of our ignorance. Since these are all unrelated, it is reasonable to assume that $x(0)$, $w(t)$, and $v(t)$ are mutually orthogonal. Some feeling for $x(0)$ may be present in that we may know its mean $\overline{x}_0$ and covariance P_0. We symbolize this as

$$x(0) \sim (\overline{x}_0, P_0) \tag{6.4-33}$$

It is not unreasonable to assume that $w(t)$ and $v(t)$ have means of zero, since, for instance, there should be no bias on the measuring instruments. We will also assume that the process noise and measurement noise are white noise processes, so that

$$R_w(\tau) = E\{w(t+\tau)w^{\mathrm{T}}(t)\} = Q\delta(\tau) \tag{6.4-34}$$

$$R_v(\tau) = E\{v(t+\tau)v^{\mathrm{T}}(t)\} = R\delta(\tau) \tag{6.4-35}$$

Spectral density matrices Q and R will be assumed known. [Often, we have a good feeling for the standard deviations of $w(t)$ and $v(t)$.] According to (6.4-30), Q and R are positive semidefinite. We will assume in addition that R is nonsingular. In summary, we will assume that

$$w(t) \sim (0,\ Q), \quad Q \geq 0 \tag{6.4-36}$$

$$v(t) \sim (0,\ R), \quad R > 0 \tag{6.4-37}$$

The assumption that $w(t)$ and $v(t)$ are white may in some applications be a bad one. For instance, wind gust noise is generally of low frequency. However, suppose that $w(t)$ is not white. Then we can determine a system description

$$\dot{x}_w = A_w x_w + B_w n \tag{6.4-38}$$

$$w = C_w x_w + D_w n, \tag{6.4-39}$$

which has a white noise input $n(t)$ and output $w(t)$. This is called a *noise-shaping filter*. These dynamics may be combined with the plant equations (6.4-20) and (6.4-21) to obtain the augmented dynamics

$$\begin{bmatrix} \dot{x} \\ \dot{x}_w \end{bmatrix} = \begin{bmatrix} A & GC_w \\ 0 & A_w \end{bmatrix} \begin{bmatrix} x \\ x_w \end{bmatrix} + \begin{bmatrix} B \\ 0 \end{bmatrix} u + \begin{bmatrix} CD_w \\ B_w \end{bmatrix} n \tag{6.4-40}$$

$$y = \begin{bmatrix} C & 0 \end{bmatrix} \begin{bmatrix} x \\ x_w \end{bmatrix} + v \tag{6.4-41}$$

This augmented system does have a white process noise $n(t)$. A similar procedure may be followed if $v(t)$ is nonwhite. Thus, we can generally describe a plant with nonwhite noises in terms of an augmented system with white process and measurement noises.

The determination of a system (6.4-38)/(6.4-39) that describes nonwhite noise $w(t)$ [or $v(t)$] is based on factoring the spectral density of the noise $w(t)$. For details, see Lewis (1986*b*). We will illustrate the procedure in Example 6.4-2.

We should now like to design an estimator for the stochastic system (6.4-20)/(6.4-21) under the assumptions just listed. We will propose the output injection observer, which has the form

$$\dot{\hat{x}} = A\hat{x} + Bu + L(y - \hat{y}) \tag{6.4-42}$$

or

$$\dot{\hat{x}} = (A - LC)\hat{x} + Bu + Ly \tag{6.4-43}$$

The time function $\hat{x}(t)$ is the state estimate and

$$\hat{y} = E\{Cx + v\} = C\hat{x} \tag{6.4-44}$$

is the estimate of the output $y(t)$. [This expected value is actually the *conditional* mean given the previous measurements; see Lewis (1986*b*).]

The estimator gain L must be selected to provide an optimal estimate in the presence of the noises $w(t)$ and $v(t)$. To select L, we will need to define the estimation error

$$\tilde{x}(t) = x(t) - \hat{x}(t) \tag{6.4-45}$$

Using (6.4-20) and (6.4-42), we may derive the error dynamics to be

$$\begin{aligned} \dot{\tilde{x}} &= (A - LC)\tilde{x} + Gw - Lv \\ &\equiv A_0\tilde{x} + Gw - Lv \end{aligned} \tag{6.4-46}$$

Note that the error system is driven by both the process and measurement noise. The output of the error system may be taken as $\tilde{y} = y - \hat{y}$ so that

$$\tilde{y} = C\tilde{x} + v \tag{6.4-47}$$

The *error covariance* is given by

$$P(t) = E\{\tilde{x}\tilde{x}^{\mathrm{T}}\}, \tag{6.4-48}$$

which is time varying. Thus, $\tilde{x}(t)$ is a nonstationary random process. The error covariance is a measure of the *uncertainty* in the estimate. Smaller values for $P(t)$ mean that the estimate is better, since the error is more closely distributed about its mean value of zero if $P(t)$ is smaller.

If the observer is asymptotically stable and $w(t)$ and $v(t)$ are stationary processes, the error $\tilde{x}(t)$ will eventually reach a *steady state* in which it is also stationary with constant mean and covariance. The gain L will be chosen to minimize the *steady-state error covariance* P. Thus, the optimal gain L will be a constant matrix of observer gains.

Before determining the optimal gain L, let us compute the mean and covariance of the estimation error $\tilde{x}(t)$. Using (6.4-46) and the linearity of the expectation operator,

$$E\{\dot{\tilde{x}}\} = A_0 E\{\tilde{x}\} + GE\{w\} - LE\{v\}, \tag{6.4-49}$$

so that

$$\frac{d}{dt}E\{\tilde{x}\} = A_0 E\{\tilde{x}\} \tag{6.4-50}$$

Thus, $E\{\tilde{x}\}$ is a deterministic time-varying quantity that obeys a differential equation with system matrix A_0. If $A_0 = A - LC$ is stable, then $E\{\tilde{x}\}$ eventually stabilizes at a steady-state value of zero, since the process and measurement noises are of zero mean. Since

$$E\{\hat{x}\} = E\{x\} - E\{\hat{x}\} = E\{x\} - \hat{x}, \tag{6.4-51}$$

it follows that in this case the estimate $\hat{x}(t)$ approaches $E\{x(t)\}$. Then the estimate is said to be *unbiased*. According also to (6.4-51), the mean of the initial error $\hat{x}(0)$ is equal to zero if the observer (6.4-43) is initialized to $\hat{x}(0) = x_0$, with $\overline{x}_0$ the mean of $x(0)$.

If the process noise $w(t)$ and/or measurement noise $v(t)$ have means that are not zero, then according to (6.4-49), the steady-state value of $E\{\tilde{x}\}$ is not equal to zero. In this case, $\hat{x}(t)$ does not tend asymptotically to the true state $x(t)$ but is offset from it by the constant value $-E\{\tilde{x}\}$. Then the estimates are said to be biased (see the problems).

To determine the error covariance, note that the solution of (6.4-46) is given by

$$\tilde{x}(t) = e^{A_0 t}\tilde{x}(0) - \int_0^t e^{A_0(t-\tau)}Lv(\tau)d\tau + \int_0^t e^{A_0(t-\tau)}Gw(\tau)d\tau \tag{6.4-52}$$

We will soon require the cross-correlation matrices $R_{v\tilde{x}}(t,t)$ and $R_{w\tilde{x}}(t,t)$. To find them, use (6.4-52) and the assumption that $x(0)$ [and hence $\tilde{x}(0)$], $w(t)$, and $v(t)$ are orthogonal. Thus,

$$\begin{aligned} R_{v\tilde{x}}(t,t) &= E\{v(t)\tilde{x}^{\mathrm{T}}(t)\} \\ &= -\int_0^t E\{v(t)v^{\mathrm{T}}(\tau)\}L^{\mathrm{T}}e^{A_0^{\mathrm{T}}(t-\tau)}\ d\tau \end{aligned} \tag{6.4-53}$$

Note that

$$R_v(t,\tau) = R\delta(t-\tau) \tag{6.4-54}$$

but the integral in (6.4-53) has an upper limit of t. Recall that the unit impulse can be expressed as

$$\delta(t) = \lim_{T\to 0}\frac{1}{T}\prod\left(\frac{t}{T}\right), \tag{6.4-55}$$

where the rectangle function

$$\frac{1}{T}\prod\left(\frac{t}{T}\right)=\begin{cases}\frac{1}{T}, & |t|<\frac{T}{2}\\ 0 & \text{otherwise}\end{cases} \tag{6.4-56}$$

is centered at $t=0$. Therefore, only half the area of $\delta(t-\tau)$ should be considered as being to the left of $\tau=t$. Hence, (6.4-53) is

$$R_{v\tilde{x}}(t,t)=-\tfrac{1}{2}RL^{\mathrm{T}} \tag{6.4-57}$$

Similarly,

$$\begin{aligned}R_{w\tilde{x}}(t,t)&=E\{w(t)\tilde{x}^{\mathrm{T}}(t)\}\\ &=\int_0^t E\{w(t)w^{\mathrm{T}}(\tau)\}G^{\mathrm{T}}e^{A_0^{\mathrm{T}}(t-\tau)}\,d\tau\end{aligned} \tag{6.4-58}$$

or

$$R_{w\tilde{x}}(t,t)=\tfrac{1}{2}QG^{\mathrm{T}} \tag{6.4-59}$$

To find a differential equation for $P(t)=E\{\tilde{x}\tilde{x}^{\mathrm{T}}\}$, write

$$\dot{P}(t)=E\left\{\frac{d\tilde{x}}{dt}\tilde{x}^{\mathrm{T}}\right\}+E\left\{\tilde{x}\frac{d\tilde{x}^{\mathrm{T}}}{dt}\right\} \tag{6.4-60}$$

According to the error dynamics (6.4-46) the first term is equal to

$$E\left\{\frac{d\tilde{x}}{dt}\tilde{x}^{\mathrm{T}}\right\}=(A-LC)P+\tfrac{1}{2}LRL^{\mathrm{T}}+\tfrac{1}{2}GQG^{\mathrm{T}}, \tag{6.4-61}$$

where we have used (6.4-57) and (6.4-59). To this equation add its transpose to obtain

$$\dot{P}=A_0P+PA_0^{\mathrm{T}}+LRL^{\mathrm{T}}+GQG^{\mathrm{T}} \tag{6.4-62}$$

What we have derived in (6.4-62) is an expression for the error covariance when the observer (6.4-43) is used with a specific gain L. Given any L such that $(A-LC)$ is stable, we may solve (6.4-62) for $P(t)$ using as initial condition $P(0)=P_0$, with P_0 the covariance of the initial state, which represents the uncertainty in the initial estimate $\hat{x}(0)=\overline{x}_0$.

Clearly, gains that result in smaller error covariances $P(t)$ are better, for then the error $\tilde{x}(t)$ is generally closer to its mean of zero. That is, the error covariance is a measure of the performance of the observer, and smaller covariance matrices are

indicative of better observers. We say that P is a measure of the uncertainty in the estimate. [Given symmetric positive-semidefinite matrices P_1 and P_2, P_1 is less than P_2 if $(P_2 - P_1) \geq 0$.]

The error covariance $P(t)$ reaches a bounded steady-state value P as $t \to \infty$ as long as A_0 is asymptotically stable. At steady state, $\dot{P} = 0$ so that (6.4-62) becomes the algebraic equation

$$0 = A_0 P + P A_0^{\mathrm{T}} + LRL^{\mathrm{T}} + GQG^{\mathrm{T}} \tag{6.4-63}$$

The steady-state error covariance is the positive-(semi)definite solution to (6.4-63). To obtain a constant observer gain, we may select *L to minimize the steady-state error covariance P*. Necessary conditions for L are now easily obtained after the same fashion that the output feedback gain K was obtained in Section 5.3.

Thus, define a performance index (PI)

$$J = \tfrac{1}{2}\mathrm{tr}(P) \tag{6.4-64}$$

[Note that $\mathrm{tr}(P)$ is the sum of the eigenvalues of P. Thus, a small J corresponds to a small P.] To select L so that J is minimized subject to the constraint (6.4-63), define the Hamiltonian

$$\mathscr{H} = \tfrac{1}{2}\mathrm{tr}(P) + \tfrac{1}{2}\mathrm{tr}(gS), \tag{6.4-65}$$

where

$$g = A_0 P + P A_0^{\mathrm{T}} + LRL^{\mathrm{T}} + GQG^{\mathrm{T}} \tag{6.4-66}$$

and S is an $n \times n$ undetermined (Lagrange) multiplier.

To minimize J subject to the constraint $g = 0$, we may equivalently minimize $\mathscr{H}$ with no constraints. Necessary conditions for a minimum are therefore given by

$$\frac{\partial \mathscr{H}}{\partial S} = A_0 P + P A_0^{\mathrm{T}} + LRL^{\mathrm{T}} + GQG^{\mathrm{T}} = 0 \tag{6.4-67}$$

$$\frac{\partial \mathscr{H}}{\partial P} = A_0^{\mathrm{T}} S + S A_0 + I = 0 \tag{6.4-68}$$

$$\frac{1}{2}\frac{\partial \mathscr{H}}{\partial L} = SLR - SPC^{\mathrm{T}} = 0 \tag{6.4-69}$$

If A_0 is stable, the solution S to (6.4-68) is positive definite. Then, according to (6.4-69),

$$L = PC^{\mathrm{T}} R^{-1} \tag{6.4-70}$$

Substituting this value for L into (6.4-67) yields

$$(A - PC^{\mathrm{T}} R^{-1} C)P + P(A - PC^{\mathrm{T}} R^{-1} C)^{\mathrm{T}} + PC^{\mathrm{T}} R^{-1} CP + GQG^{\mathrm{T}} = 0 \tag{6.4-71}$$

or

$$AP + PA^T + GQG^T - PC^T R^{-1} CP = 0 \tag{6.4-72}$$

To determine the optimal observer gain L, we may therefore proceed by solving (6.4-72) for the error covariance P and then using (6.4-70) to compute L. The matrix quadratic equation (6.4-72) is called the *algebraic* (*filter*) Riccati equation (ARE). There are several efficient techniques for solving the ARE for P [e.g., Armstrong, 1980; IMSL, 1980; MATRIX$_x$, 1989; MATLAB (Moler et al., 1987)].

The optimal gain L determined using (6.4-70) is called the *steady-state Kalman gain,* and the observer so constructed is called the *steady-state Kalman filter*. The term *steady state* refers to the fact that although the optimal gain that minimizes $P(t)$ is generally time varying, we have selected the optimal gain that minimizes the *steady-state* error covariance in order to obtain a constant observer gain. Since the gain must eventually be gain scheduled in actual flight control applications, we require a constant gain to keep the number of parameters to be scheduled within reason.

The design equations for the Kalman filter are collected in Table 6.4-1. A block diagram appears in Figure 6.4-1. The steady-state Kalman filter is the best estimator with constant gains that has the dynamics of the form in the table. Such a filter is said to be *linear*. It can be shown (Lewis, 1986*b*) that if the process noise $w(t)$ and measurement noise $v(t)$ are *Gaussian,* this is also *the optimal* steady-state estimator of any form.

The quantity

$$\tilde{y}(t) = y(t) - \hat{y}(t) = y(t) - C\hat{x}(t) \tag{6.4-73}$$

TABLE 6.4-1 The Kalman Filter

System Model

$\dot{x} = Ax + Bu + Gw$

$y = Cx + v$

$x(0) \sim (\bar{x}_0, P_0), \quad w(t) \sim (0, Q), \quad v(t) \sim (0, R)$

Assumptions

$w(t)$ and $v(t)$ are white noise processes orthogonal to each other and to $x(0)$.

Initialization

$\hat{x}(0) = \bar{x}_0$

Error Covariance ARE

$AP + PA^{\mathrm{T}} + GQG^{\mathrm{T}} - PC^{\mathrm{T}} R^{-1} CP = 0$

Kalman Gain

$L = PC^{\mathrm{T}} R^{-1}$

Estimate Dynamics (Filter Dynamics)

$\dot{\hat{x}} = A\hat{x} + Bu + L(y - C\hat{x})$

that drives the filter dynamics in the table is called the residual. For more information on the Kalman filter, see the work of Bryson and Ho (1975), Kwakernaak and Sivan (1972), and Lewis (1986*b*).

The filter ARE should be compared to the ARE we discussed at the beginning of this section in connection with output injection design. There, no particular meaning was given to the auxiliary matrix P. In this stochastic setting, we have discovered that it is nothing but the error covariance. Small values of P generally indicate a filter with good estimation performance.

The theorem offered in connection with output injection observer design also holds here. Thus, suppose that (C, A) is observable and $(A, G\sqrt{Q})$ is reachable. Then the ARE has a unique positive-definite solution P. Moreover, error system (6.4-46) using the gain Kalman gain L given by (6.4-70), with P the unique positive-definite solution to the ARE, is asymptotically stable.

One might be inclined to believe that the less noise in the system, the better. However, the actual situation is quite surprising. For the existence of the Kalman filter it was necessary to assume that $R > 0$, that is, that *the measurement noise corrupts all the measurements*. If there are some noise-free measurements, a more complicated filter known as the *Deyst filter* must be used. Moreover, the assumption that $(A, G\sqrt{Q})$ is reachable means that *the process noise should excite all the states*.

Example 6.4-2: Kalman Filter Estimation of Angle of Attack in Gust Noise The short-period approximation to the F-16 longitudinal dynamics is

$$\dot{x} = Ax + B\delta_e + Gw_g, \tag{1}$$

with $x = \begin{bmatrix}\alpha & q\end{bmatrix}^{\mathrm{T}}$, α the angle of attack, q the pitch rate, control input δ_e the elevator deflection, and w_g the vertical wind gust disturbance velocity. Using the software described in Chapter 3 to linearize the F-16 dynamics about the nominal flight condition in Table 3.6-3 (true airspeed of 502 ft/s, dynamic pressure of 300 psf, and cg at $0.35\,\overline{c}$), the plant matrices are found to be

$$A = \begin{bmatrix} -1.01887 & 0.90506 \\ 0.82225 & -1.07741 \end{bmatrix}, \quad B = \begin{bmatrix} -0.00215 \\ -0.17555 \end{bmatrix}, \quad G = \begin{bmatrix} 0.00203 \\ -0.00164 \end{bmatrix} \tag{2}$$

The vertical wind gust noise is not white but according to *Mil. Spec. 1797* (1987) has a spectral density given in Dryden form as

$$\Phi_w(\omega) = 2L\sigma^2 \frac{1 + 3L^2\omega^2}{(1 + L^2\omega^2)^2}, \tag{3}$$

with ω the frequency in rad/s, σ the turbulence intensity, and L the turbulence scale length divided by true airspeed. Taking $\sigma = 10$ ft/s and $L = (1750\,\text{ft})/(502\,\text{ft/s}) = 3.49$ s (see *Mil. Spec. 1797*, 1987) the gust spectral density is shown in Figure 6.4-4.

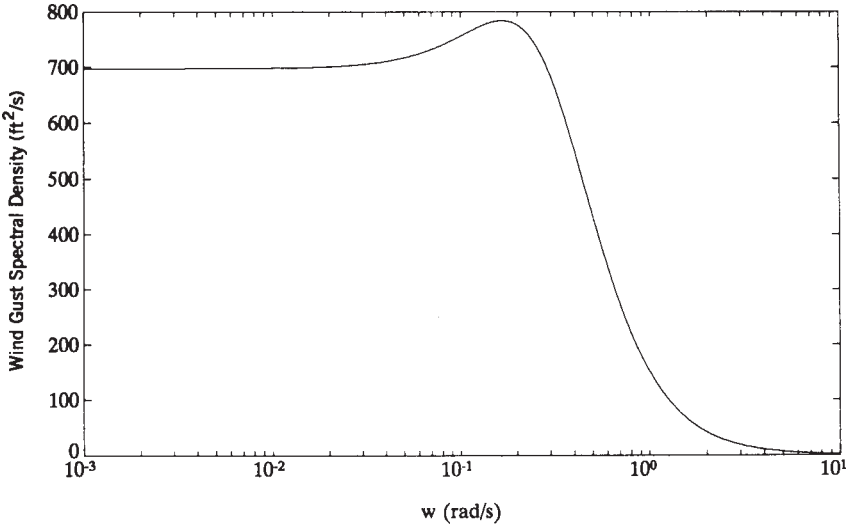

Figure 6.4-4 Vertical wind gust spectral density.

(a) *Determination of Gust-Shaping Filter.* Since w_g is not white, a noise-*shaping filter* of the form of (6.4-38), (6.4-39) must be determined by factoring $\Phi_w(s)$ (Lewis, 1986*b*). Note that

$$\Phi_w(\omega) = 2L\sigma^2 \frac{\left(1 + \sqrt{3}Lj\omega\right)\left(1 - \sqrt{3}Lj\omega\right)}{(1 + Lj\omega)^2(1 - Lj\omega)^2}, \tag{4}$$

so that

$$\Phi_w(s) = H_w(s)H_w(-s) \tag{5}$$

with

$$H_w(s) = \sigma\sqrt{\frac{6}{L}}\frac{s + 1/L\sqrt{3}}{L(s + 1/L)^2} \tag{6}$$

$$H_w(s) = \sigma\sqrt{\frac{6}{L}}\frac{s + 1/L\sqrt{3}}{s^2 + 2s/L + 1/L^2} \tag{7}$$

Now a reachable canonical form realization of $H_w(s)$ (Kailath, 1980) is given by

$$\dot{z} = \begin{bmatrix} 0 & 1 \\ -\frac{1}{L^2} & -\frac{2}{L} \end{bmatrix} z + \begin{bmatrix} 0 \\ 1 \end{bmatrix} w \tag{8}$$

$$w_g = \gamma \begin{bmatrix} \frac{1}{L\sqrt{3}} & 1 \end{bmatrix} z, \tag{9}$$

where the gain is $\gamma = \sigma\sqrt{g/L}$ Using $\sigma = 10$, $L = 3.49$ yields

$$\dot{z} = \begin{bmatrix} 0 & 1 \\ -0.0823 & -0.5737 \end{bmatrix} z + \begin{bmatrix} 0 \\ 1 \end{bmatrix} w \approx A_w z + B_w w \tag{10}$$

$$w_g = \begin{bmatrix} 2.1728 & 13.1192 \end{bmatrix} z \equiv C_w z \tag{11}$$

The shaping filter (10)/(11) is a system driven by the *white* noise input $w(t) \sim (0, 1)$ that generates the gust noise $w_g(t)$ with spectral density given by (3).

(b) *Augmented Plant Dynamics*. The overall system, driven by the white noise input $w(t) \sim (0, 1)$ and including an elevator actuator with transfer function $20.2/(s + 20.2)$, is given by [see (6.4-40)]

$$\frac{d}{dt}\left[\begin{array}{c} \alpha \\ q \\ \hline z_1 \\ z_2 \\ \hline \delta_e \end{array}\right] = \left[\begin{array}{cc|cc|c} -1.01887 & 0.90506 & 0.00441 & 0.02663 & -0.00215 \\ 0.82225 & -1.07741 & -0.00356 & -0.02152 & -0.17555 \\ \hline 0 & 0 & 0 & 1 & 0 \\ 0 & 0 & -0.0823 & -0.5737 & 0 \\ \hline 0 & 0 & 0 & 0 & -20.2 \end{array}\right] \left[\begin{array}{c} \alpha \\ q \\ \hline z_1 \\ z_2 \\ \hline \delta_e \end{array}\right]$$

$$+ \left[\begin{array}{c} 0 \\ 0 \\ \hline 0 \\ 0 \\ \hline 20.2 \end{array}\right] u + \left[\begin{array}{c} 0 \\ 0 \\ \hline 0 \\ 1 \\ \hline 0 \end{array}\right] w \tag{12}$$

with $u(t)$ the elevator actuator input. To economize on notation, let us symbolize this augmented system as

$$\dot{x} = Ax + Bu + Gw \tag{13}$$

(c) *Estimating Angle of Attack*. Direct measurements of angle of attack α are noisy and biased. However, pitch rate q and normal acceleration n_z are convenient to measure. Using the software in Chapter 3 it is determined that

$$n_z = 15.87875\alpha + 1.48113q \tag{14}$$

Therefore, let us select the measured output as

$$y = \begin{bmatrix} n_z \\ q \end{bmatrix} = \begin{bmatrix} 15.87875 & 1.48113 & 0 & 0 & 0 \\ 0 & 1 & 0 & 0 & 0 \end{bmatrix} x + v \equiv Cx + v, \tag{15}$$

where $v(t)$ is measurement noise. A reasonable measurement noise covariance is

$$R = \begin{bmatrix} \frac{1}{20} & 0 \\ 0 & \frac{1}{60} \end{bmatrix} \tag{16}$$

Now the algebraic Riccati equation in Table 6.4-1 may be solved using standard available software [e.g., ORACLS (Armstrong, 1980; IMSL, 1980), PC-MATLAB (Moler et al., 1987), and MATRIX$_x$ (1989)] to obtain the Kalman gain

$$L = \begin{bmatrix} 0.0375 & -0.0041 \\ -0.0202 & 0.0029 \\ 3.5981 & -0.2426 \\ 1.9061 & -0.2872 \\ 0 & 0 \end{bmatrix}, \tag{17}$$

whence the Kalman filter is given by

$$\dot{\hat{x}} = (A - LC)\hat{x} + Bu + Ly \tag{18}$$

Note that the Kalman gain corresponding to the fifth state δ_e is zero. This is due to the fact that, according to (12), the gust noise $w(t)$ does not excite the actuator motor.

To implement the estimator we could use the state formulation (18) in a subroutine or compute the transfer function to the angle-of-attack estimate given by

$$H_\alpha(s) = \begin{bmatrix} 1 & 0 & \cdots & 0 \end{bmatrix} [sI - (A - LC)]^{-1} \begin{bmatrix} B & L \end{bmatrix} \tag{19}$$

(Note that α is the first component of x.) Then the angle-of-attack estimate is given by

$$\hat{\alpha}(s) = H(s) \begin{bmatrix} U(s) \\ Y(s) \end{bmatrix}, \tag{20}$$

so that $\alpha(t)$ may be estimated using $u(t)$ and $y(t)$, both of which are known.

Similarly, the estimate of the wind gust velocity $w_g(t)$ may be recovered. ■

Dynamic Regulator Design Using the Separation Principle

The fundamental approach to regulator and compensator design in this book involves selecting the compensator dynamics using the intuition of classical control and traditional aircraft design. Then the adjustable compensator gains are computed using the output feedback design equations in Table 5.3-1, 5.4-1, or 5.5-1. The advantages of this approach include:

1. Good software for solving the design equations is available [e.g., the Davidon-Fletcher-Powell algorithm (Press et al., 1986)]. See Appendix B.
2. General multi-input/multi-output control design is straightforward.

3. All the intuition in classical control design in the aircraft industry can be used to select the compensator structure.
4. Complicated compensator structures are avoided, which is important from the point of view of the pilot's feel for the aircraft and also simplifies the gain-scheduling problem.

However, in complicated modern systems (e.g., aircraft engines) there may be no a priori guidelines for selecting the compensator structure. In this case, a combination of LQ state feedback and observer/filter design proves very useful for controller design. This combination is known as linear quadratic Gaussian (LQG) design and is explored next. In Section 6.5 we discuss the LQG/LTR technique for robust design, which has become popular in some aspects of aircraft control.

Linear Quadratic Gaussian Design The linear quadratic regulator (LQR) and the Kalman filter can be used together to design a dynamic regulator. This procedure is called linear quadratic Gaussian (LQG) design and will now be described. An important advantage of LQG design is that the compensator structure is given by the procedure, so that it need not be known beforehand. This makes LQG design useful in the control of complicated modern-day systems (e.g., space structures, aircraft engines), where an appropriate compensator structure may not be known.

Suppose that the plant and measured outputs are given by

$$\dot{x} = Ax + Bu + Gw \tag{6.4-74}$$

$$y = Cx + v, \tag{6.4-75}$$

with $x(t) \in \mathbf{R}^n$, $u(t)$ the control input, $w(t)$ the process noise, and $v(t)$ the measurement noise. Suppose that the full-state-feedback control

$$u = -Kx + r \tag{6.4-76}$$

has been designed, with $r(t)$ the pilot's input command. That is, the state feedback gain K has been selected by some technique, such as the LQR technique in Section 5.7. If the control (6.4-76) is substituted into (6.4-74), the closed-loop system is found to be

$$\dot{x} = (A - BK)x + Br + Gw \tag{6.4-77}$$

Full-state-feedback design is attractive because if the conditions in Section 5.7 hold, the closed-loop system is guaranteed stable. Such a strong result has not yet been shown for output feedback. Moreover, using full state feedback all the poles of $(A - BK)$ may be placed arbitrarily as desired. Finally, the state feedback design equations are simpler than those for output feedback and may be solved using standard available routines [e.g., ORACLS (Armstrong, 1980; IMSL, 1980), PCMATLAB (Moler et al., 1987), and MATRIX$_x$ (1989)]. However, the control law (6.4-76) cannot be implemented since all the states are usually not available as measurements.

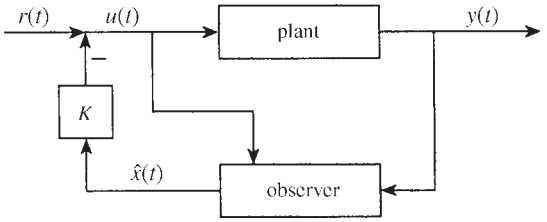

Figure 6.4-5 Regulator design using observer and full state feedback.

Now, suppose that an observer or Kalman filter

$$\dot{\hat{x}} = (A - LC)\hat{x} + Bu + Ly \tag{6.4-78}$$

has been designed. That is, the filter gain L has been selected by any of the techniques discussed in this section to provide state estimates. Then, since all the states are not measurable and the control (6.4-76) cannot be implemented in practice, we propose to feed back the *estimate* $x(t)$ instead of the actual state $x(t)$. That is, let us examine the feedback law

$$u = -K\hat{x} + r \tag{6.4-79}$$

The closed-loop structure using this controller is shown in Figure 6.4-5. Due to the fact that the observer is a dynamical system, the proposed controller is nothing but a dynamical regulator of the sort seen in classical control theory. However, in contrast to classical design, the theory makes it easy to design *multivariable regulators with guaranteed stability even for complicated MIMO systems*.

If K is selected using the LQR Riccati equation in Section 5.7 and L is selected using the Kalman filter Riccati equation in Table 6.4-1, this procedure is called LQG design.

We propose to show that using this control:

1. The closed-loop poles are the same as if the full state feedback (6.4-76) had been used.
2. The transfer function from $r(t)$ to $y(t)$ is the same as if (6.4-76) had been used.

The importance of these results is that the state feedback K and the observer gain L may be designed *separately* to yield desired closed-loop plant behavior and observer behavior. This is the *separation principle,* which is at the heart of modern control design. Two important ramifications of the separation principle are that closed-loop stability is guaranteed and good software is available to solve the matrix design equations that yield K and L.

The Separation Principle To show the two important results just mentioned, define the estimation error (6.4-45) and examine the error dynamics (6.4-46). In terms of

$\widetilde{x}(t)$, we may write (6.4-79) as

$$u = -Kx + K\widetilde{x} + r, \tag{6.4-80}$$

which, when used in (6.4-74), yields

$$\dot{x} = (A - BK)x + BK\widetilde{x} + Br + Gw \tag{6.4-81}$$

Now, write (6.4-81) and (6.4-46) as the augmented system

$$\frac{d}{dt}\begin{bmatrix} x \\ \widetilde{x} \end{bmatrix} = \begin{bmatrix} A - BK & BK \\ 0 & A - LC \end{bmatrix}\begin{bmatrix} x \\ \widetilde{x} \end{bmatrix} + \begin{bmatrix} B \\ 0 \end{bmatrix} r + \begin{bmatrix} G \\ G \end{bmatrix} w - \begin{bmatrix} 0 \\ L \end{bmatrix} v \tag{6.4-82}$$

$$y = \begin{bmatrix} C & 0 \end{bmatrix}\begin{bmatrix} x \\ \widetilde{x} \end{bmatrix} + v \tag{6.4-83}$$

This represents the complete dynamics of Figure 6.4-5.

Since the augmented system is block triangular, the closed-loop characteristic equation is

$$\Delta(s) = |sI - (A - BK)\ |\cdot\ |sI - (A - LC)| = 0 \tag{6.4-84}$$

That is, the closed-loop poles are nothing but the plant poles that result by choosing K and the desired observer poles that result by choosing L. Thus, the state feedback gain K and observer gain L may be selected separately for desirable closed-loop behavior.

The closed-loop transfer function from $r(t)$ to $y(t)$ is given by

$$H_c(s) = \begin{bmatrix} C & 0 \end{bmatrix}\begin{bmatrix} A - BK & BK \\ 0 & A - LC \end{bmatrix}^{-1}\begin{bmatrix} B \\ 0 \end{bmatrix},$$

and the triangular form of the system matrix makes it easy to see that

$$H_c(s) = C\ [sI - (A - BK)]^{-1}\ B \tag{6.4-85}$$

This, however, is exactly what results if the full state feedback (6.4-76) is used.

Of course, the initial conditions also affect the output $y(t)$. However, since the observer is stable, the effects of the initial error $\widetilde{x}(0)$ will vanish with time. The observer poles [i.e., those of $(A - LC)$] should be chosen 5 to 10 times faster than the desired closed-loop plant poles [i.e., those of $(A - BK)$] for good closed-loop behavior.

Discussion From our point of view, when possible it is usually better to design compensators using output feedback as we have demonstrated in the previous chapters than to use separation principle design. To see why, let us examine the structure of the dynamic compensator in Figure 6.4-5 in more detail.

The control input $u(t)$ may be expressed as

$$U(s) = H_y(s)Y(s) + H_u(s)U(s) + R(s), \tag{6.4-86}$$

where, according to (6.4-79) and (6.4-78), the transfer function from $y(t)$ to $u(t)$ is

$$H_y(s) = -K[sI - (A - LC)]^{-1} \; L \tag{6.4-87}$$

and the transfer function from $u(t)$ to $u(t)$ is

$$H_u(s) = -K[sI - (A - LC)]^{-1} \; B \tag{6.4-88}$$

Now, note that the compensator designed by this technique has order equal to the order n of the plant. This means that it has too many parameters to be conveniently gain scheduled. Moreover, it has no special structure. This means that none of the classical control intuition available in the aircraft industry has been used in its design.

It is possible to design *reduced-order* compensators using the separation principle. Three possible approaches are:

1. Find a reduced-order model of the plant, then design a compensator for this reduced-order model.
2. Design a compensator for the full plant, then reduce the order of the compensator.
3. Design the reduced-order compensator directly from the full-order plant.

One technique for order reduction is the partial fraction expansion technique in Example 6.2-3. Other techniques include principal-component analysis (Moore, 1982) and the frequency-weighted technique by Anderson and Liu (1989). A very convenient approach is given by Ly et al. (1985).

It is important to realize that although the plant is minimal (i.e., reachable and observable), the LQ regulator may not be. That is, it may have unreachable or unobservable states. A technique for reducing the regulator to minimal form is given by Yousuff and Skelton (1984).

In Section 6.5 we illustrate the design of a LQ regulator in robust design using the LQG/LTR approach.

6.5 LINEAR QUADRATIC GAUSSIAN/LOOP TRANSFER RECOVERY

We saw in Sections 6.2 and 6.3 how to use the multivariable Bode plot to design controllers guaranteeing performance robustness and stability robustness using output feedback. In Section 6.4 we discussed the Kalman filter. In this section we propose to cover the LQG/LTR design technique for robust controllers. This approach is quite popular in the current literature and has been used extensively by Honeywell and others to design multivariable aircraft flight control systems (Doyle and Stein, 1981; Athans, 1986). It is based on the fact that the linear quadratic regulator (LQR) using state-variable feedback has certain *guaranteed robustness properties*.

Thus, suppose that a state feedback gain K has been computed using the ARE as in Section 5.7. This state feedback cannot be implemented since all of the states are not available as measurements; however, it can be used as the basis for the design of a dynamic LQR by using a Kalman filter to provide state estimates for feedback purposes. We would like to discuss two issues. First, we will show that, in contrast to output feedback, state feedback has certain guaranteed robustness properties in terms of gain and phase margins. Then we will see that the Kalman filter may be designed so that the dynamic regulator recovers the desirable robustness properties of full state feedback.

Guaranteed Robustness of the LQR

We have discussed conditions for performance robustness and stability robustness for the general feedback configuration of the form shown in Figure 6.2-1, where $G(s)$ is the plant and $K(s)$ is the compensator. The LQR using *state feedback* has many important properties, as we have seen in Section 5.7. In this subsection we should like to return to the LQR to show that it has certain *guaranteed robustness properties* that make it even more useful (Safonov and Athans, 1977).

Thus, suppose that in Figure 6.2-1, $K(s) = K$, the constant optimal LQ state feedback gain determined using the ARE as in Table 5.7-1. Suppose, moreover, that

$$G(s) = (sI - A)^{-1}B \tag{6.5-1}$$

is a plant in state-variable formulation.

For this subsection, it will be necessary to consider the loop gain *referred to the control input* $u(t)$ in Figure 6.2-1. This is in contrast to the work in Section 6.2, where we referred the loop gain to the output $z(t)$, or equivalently to the signal $s(t)$ in the figure. Breaking the loop at $u(t)$ yields the loop gain

$$KG(s) = K(sI - A)^{-1}B \tag{6.5-2}$$

Our discussion will be based on the *optimal return difference relation* that holds for the LQR with state feedback (Lewis, 1986*a*; Grimble and Johnson, 1988; Kwakernaak and Sivan, 1972), namely,

$$\begin{aligned}&[I + K(-sI - A)^{-1}B]^{\mathrm{T}}[I + K(sI - A)^{-1}B]\\ &\quad = I + \frac{1}{\rho}B^{\mathrm{T}}(-sI - A)^{-\mathrm{T}}Q(sI - A)^{-1}B,\end{aligned} \tag{6.5-3}$$

where "$-\mathrm{T}$" means the inverse transposal. We have selected $R = P_I$.

Denoting the ith SV of a matrix M as $\sigma_i(M)$, we note that, by definition

$$\sigma_i(M) = \sqrt{\lambda_i(M^*M)}, \tag{6.5-4}$$

with $\lambda_i(M^*M)$ the ith eigenvalue of matrix M^*M and M^* the complex conjugate transpose of M. Therefore, according to (6.5-3), there results (Doyle and Stein, 1981)

$$\sigma_i[I + KG(j\omega)] = \left[\lambda_i \left[I + \frac{1}{\rho}B^{\mathrm{T}}(-j\omega I - A)^{-\mathrm{T}}Q(j\omega I - A)^{-1}B\right]\right]^{1/2}$$
$$= \left[1 + \frac{1}{\rho}\lambda_i \left[B^{\mathrm{T}}(-j\omega I - A)^{-\mathrm{T}}Q(j\omega I - A)^{-1}B\right]\right]^{1/2}$$

or

$$\sigma_i[I + KG(j\omega)] = \left[1 + \frac{1}{\rho}\sigma_i^2\left[H(j\omega)\right]\right]^{1/2}, \tag{6.5-5}$$

with

$$H(s) = H(sI - A)^{-1}B \tag{6.5-6}$$

and $Q = H^{\mathrm{T}}H$.

We could call (6.5-5) the *optimal SV relation* of the LQR. It is important due to the fact that the right-hand side is known in terms of open-loop quantities *before the optimal feedback gain is found* by solution of the ARE, while the left-hand side is the closed-loop return difference. Thus, exactly as in classical control, we are able to derive properties of the closed-loop system in terms of properties of the open-loop system.

According to this relation, for all ω the minimum SV satisfies the *LQ optimal SV constraint*

$$\underline{\sigma}[I + KG(j\omega)] \geq 1 \tag{6.5-7}$$

Thus, the LQ regulator always results in a *decreased sensitivity*.

Some important conclusions on the guaranteed robustness of the LQR may now be discovered using the *multivariable Nyquist criterion* (Postlethwaite et al., 1981), which we will refer to as the polar plot of the return difference $I + KG(s)$, where the origin is the critical point (Grimble and Johnson, 1988). [Usual usage is to refer the criterion to the polar plot of the loop gain $KG(s)$ where -1 is the critical point.]

A typical polar plot of $\underline{\sigma}(I + KG(j\omega))$ is shown in Figure 6.5-1, where the optimal SV constraint appears as the condition that *all the SVs remain outside the unit disc*. To see how the end points of the plots were discovered, note that since $K(sI - A)^{-1}B$ has relative degree of at least 1, its limiting value for $s = j\omega$ as $\omega \to \infty$ is zero. Thus, in this limit, $I + KG(j\omega)$ tends to I. On the other hand, as $\omega \to 0$, the limiting value of $I + KG(j\omega)$ is determined by the dc loop gain, which should be large.

The multivariable Nyquist criterion says that the closed-loop system is stable if none of the SV plots of $I + KG(j\omega)$ encircle the origin in the figure. Clearly, due to the optimal SV constraint, no encirclements are possible. This constitutes a proof of the *guaranteed stability* of the LQR.

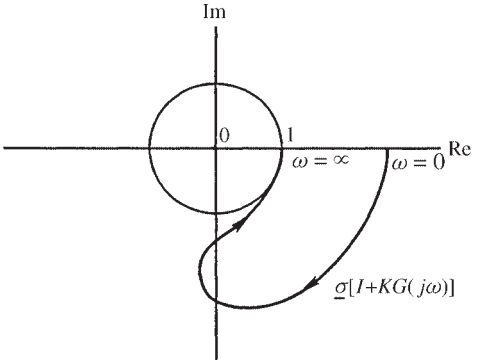

Figure 6.5-1 Typical polar plot for optimal LQ return difference (referred to the plant input).

Multiplying the optimal feedback K by any positive scalar gain k results in a loop gain of $kKG(s)$, which has a minimum SV plot identical to the one in Figure 6.5-1 except that it is scaled outward. That is, the $\omega \to 0$ limit (i.e., the dc gain) will be larger, but the $\omega \to \infty$ limit will still be 1. Thus, the closed-loop system will still be stable. In classical terms, the LQR has *an infinite gain margin*.

The *phase margin* may be defined for multivariable systems as the angle marked "PM" in Figure 6.5-2. As in the classical case, it is the angle through which the polar plot of $\sigma[I + KG(j\omega)]$ must be rotated (about the point 1) clockwise to make the plot go through the critical point.

Figure 6.5-3 combines Figures 6.5-1 and 6.5-2. By using some simple geometry, we may find the value of the angle indicated as 60°. Therefore, due to the LQ SV constraint, the plot of $\sigma[I + KG(j\omega)]$ must be rotated through at least 60° to make it pass through the origin. The LQR thus has a *guaranteed phase margin of at least 60°*.

This means that a phase shift of up to 60° may be introduced in any of the m paths in Figure 6.2-1 or in all paths simultaneously as long as the paths are not coupled to each other in the process.

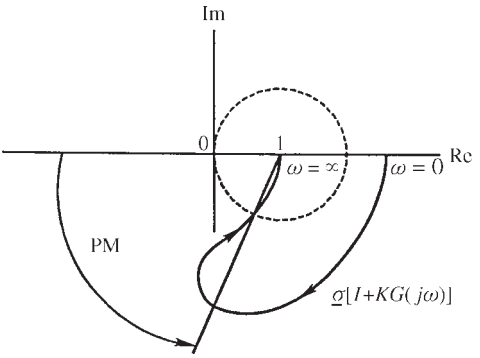

Figure 6.5-2 Definition of multivariable phase margin.

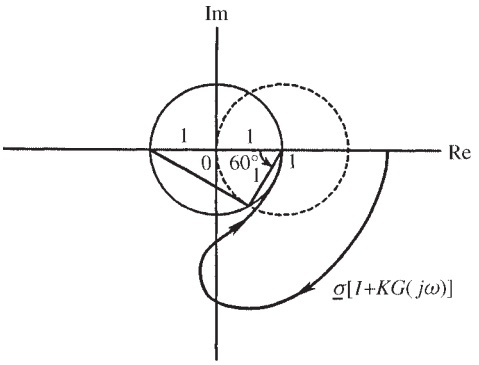

Figure 6.5-3 Guaranteed phase margin of the LQR.

This phase margin is excessive; it is higher than that normally required in classical control system design. This overdesign means that in other performance aspects the LQR may have some deficiencies. One of these turns out to be that at the crossover frequency (loop gain = 1), the slope of the multivariable. The Bode plot is -20 dB/decade, which is a relatively slow attenuation rate (Doyle and Stein, 1981). By allowing a Q weighting matrix in the PI that is not positive semidefinite, it is possible to obtain better LQ designs that have higher roll-off rates at high frequencies (Shin and Chen, 1974; Ohta et al., 1990; Al-Sunni et al., 1992).

A stability robustness bound like (6.2-49) may be obtained for the loop gain referred to the input $u(t)$. It is

$$\overline{\sigma}[KG(I+KG)^{-1}] < \frac{1}{m(\omega)} \tag{6.5-8}$$

The inverse of this is

$$m(\omega) < \frac{1}{\overline{\sigma}[KG(I+KG)^{-1}]} = \underline{\sigma}[I+(KG)^{-1}] \tag{6.5-9}$$

It can be shown (see the problems) that (6.5-7) implies that

$$\underline{\sigma}[I+(KG(j\omega))^{-1}] \geq \tfrac{1}{2} \tag{6.5-10}$$

Therefore, *the LQR remains stable for all multiplicative uncertainties in the plant transfer function which satisfy* $m(\omega) < \frac{1}{2}$.

Loop Transfer Recovery

The control design techniques we discussed in Chapter 5 involve selecting a desirable compensator structure using classical aircraft control intuition. Then the compensator

gains are adjusted using output feedback design for suitable performance. Robustness may be guaranteed using the multivariable Bode plot as shown in Sections 6.2 and 6.3.

However, in some cases, the plant may be so complex that there is little intuition available for selecting the compensator structure. This can be the case, for instance, for a jet engine (Athans et al., 1986). In this event, the technique to be presented in this section may be useful for controller design, since it yields a suitable compensator structure automatically.

Let us examine here the plant

$$\dot{x} = Ax + Bu + Gw \tag{6.5-11}$$

$$y = Cx + v, \tag{6.5-12}$$

with process noise $w(t) \sim (0, M)$ and measurement $n(t) \sim (0, v^2N)$ both white, $M > 0$, $N > 0$, and v a scalar parameter.

We have seen that the full-state-feedback control

$$u = -Kx \tag{6.5-13}$$

has some extremely attractive features, including simplified design equations (Section 5.7) and some important guaranteed robustness properties. Unfortunately, *these are not shared by an output feedback control law,* where the robustness must be checked independently. However, state feedback is usually impossible to use since all the states are seldom available for feedback in any practical application.

According to Figure 6.5-4*a*, where the plant transfer function is

$$\Phi(s)B = (sI - A)^{-1}B, \tag{6.5-14}$$

the loop gain, breaking the loop at the input $u(t)$, is

$$L_s(s) = K\Phi B \tag{6.5-15}$$

According to Section 6.4, if an observer or Kalman filter is used to produce a state estimate $\hat{x}(t)$, which is then used in the control law

$$u = -K\hat{x}, \tag{6.5-16}$$

the result is a regulator which, due to the separation principle, has the same transfer function as the state feedback controller. However, it is known that the guaranteed robustness properties of the full-state-feedback controller are generally lost (Doyle, 1978).

In this section we will assume that a state feedback gain K has already been determined using, for instance, the ARE design technique in Section 5.7. This K yields suitable robustness properties of $K\Phi B$. We should like to present a technique for

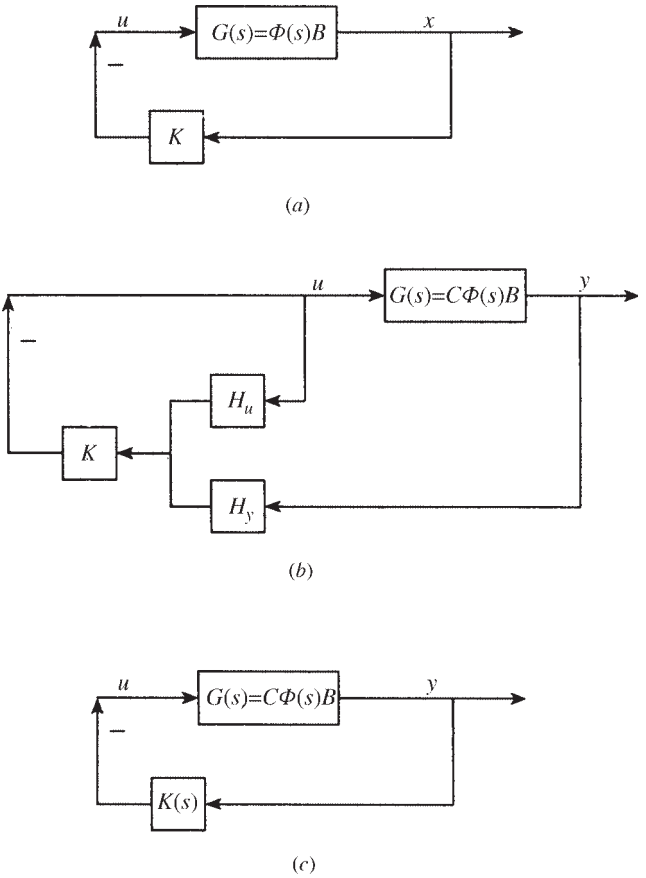

Figure 6.5-4 (*a*) Loop gain with full state feedback; (*b*) regulator using observer and estimate feedback; (*c*) regulator loop gain.

designing a Kalman filter that results in a regulator that *recovers* the guaranteed robustness properties of the full-state-feedback control law as the design parameter ν goes to zero. The technique is called linear quadratic Gaussian/loop transfer recovery (LQG/LTR), since the loop gain (i.e., loop transfer function) $K\Phi B$ of full state feedback is recovered in the regulator as $\nu \to 0$. As we will see, the key to robustness using a stochastic regulator is in the selection of the noise spectral densities M and N.

Regulator Loop Gain Using an observer or Kalman filter, the closed-loop system appears in Figure 6.5-4*b*, where the regulator is given by (Section 6.4)

$$\begin{aligned} U(s) &= -K[sI-(A-LC)]^{-1}BU(s) - K[sI-(A-LC)]^{-1}\ LY(\mathrm{s}) \\ &= -H_u(s)U(s) - H_y(s)Y(s) \end{aligned} \tag{6.5-17}$$

and L is the observer or Kalman gain. Denoting the observer resolvent matrix as

$$\Phi_0(s) = [sI - (A - LC)]^{-1} \tag{6.5-18}$$

we write

$$H_u = K\Phi_0 B, \qquad H_y = K\Phi_0 L \tag{6.5-19}$$

To find an expression for $K(s)$ in Figure 6.5-4*c* using the regulator, note that $(I + H_u)U = -H_y Y$, so that

$$U = -(I + H_w)^{-1} H_y Y = -K(s)Y \tag{6.5-20}$$

However,

$$\begin{aligned}
&(I + H_u)^{-1} K \\
&\quad = [I + K(sI - (A - LC))^{-1} B]^{-1} K \\
&\quad = [I - K(sI - (A - BK - LC))^{-1} B] \\
&\quad = K(sI - (A - BK - LC))^{-1} [(sI - (A - BK - LC)) - BK] \\
&\quad = K(sI - (A - BK - LC))^{-1} \Phi_0^{-1},
\end{aligned}$$

where the matrix inversion lemma was used in the second step. Therefore,

$$\begin{aligned}
K(s) &= (I + H_u)^{-1} H_y \\
&= K[sI - (A - BK - LC)]^{-1} \Phi_0^{-1} \Phi_0 L
\end{aligned}$$

or

$$K(s) = K[sI - (A - BK - LC)]^{-1} L \equiv K\Phi_r L, \tag{6.5-21}$$

with $\Phi_r(s)$ the regulator resolvent matrix.

We will now show how to make the loop gain (at the input) using the regulator

$$L_r(s) = K(s)G(s) = K\Phi_r LC\Phi B \tag{6.5-22}$$

approach the loop gain $L_s(s) = K\Phi B$ using full state feedback, which is guaranteed to be robust.

Recovery of State Feedback Loop Gain at the Input To design the Kalman filter so that the regulator loop gain at the input $L_r(s)$ is the same as the state feedback loop gain $L_s(s)$, we will need to assume that the plant $C\Phi B$ is *minimum phase* (i.e., with stable zeros), with B and C of full rank and $\dim(u) = \dim(y)$. The references for this subsection are Doyle and Stein (1979, 1981), Athans (1986), Stein and Athans (1987), and Birdwell (1989).

Let us propose $G = I$ and the process noise spectral density matrix

$$M = \nu^2 M_0 + BB^{\mathrm{T}}, \tag{6.5-23}$$

with $M_0 > 0$. Then, according to Table 6.4-1,

$$L = PC^{\mathrm{T}}(\nu^2 N)^{-1} \tag{6.5-24}$$

and the Kalman filter ARE becomes

$$0 = AP + PA^{\mathrm{T}} + (\nu^2 M_0 + BB^{\mathrm{T}}) - PC^{\mathrm{T}}(\nu^2 N)^{-1} CP \tag{6.5-25}$$

According to Kwakernaak and Sivan (1972), if the aforementioned assumptions hold, then $P \to 0$ as $\nu \to 0$, so that

$$L(\nu^2 N)L^{\mathrm{T}} = PC^{\mathrm{T}}(\nu^2 N)^{-1} CP \to B B^{\mathrm{T}}$$

The general solution of this equation is

$$L \to \frac{1}{\nu} BU N^{-1/2}, \tag{6.5-26}$$

with U any unitary matrix.

We claim that in this situation $L_r(s) \to L_s(s)$ as $\nu \to 0$. Indeed, defining the full-state-feedback resolvent as

$$\Phi_c(s) = (sI - (A - BK))^{-1} \tag{6.5-27}$$

we may write

$$\begin{aligned}
L_r(s) = K(s)G(s) &= K[sI - (A - BK - LC)^{-1}]LC\Phi B \\
&= K[\Phi_c^{-1} + LC]^{-1} LC\,\Phi\, B \\
&= K[\Phi_c - \Phi_c L(I + C\,\Phi_c L)^{-1} C\Phi_C]LC\Phi B \\
&= K\Phi_c L[I - (I + C\Phi_c L)^{-1} C\Phi_C L]C\Phi B \\
&= K\Phi_c L[(I + C\Phi_c L) - C\Phi_c L](I + C\Phi_c L)^{-1} C\Phi B \\
&= K\Phi_c L(I + C\Phi_c L)^{-1} C\Phi B \\
&\to K\Phi_c B(C\Phi_c B)^{-1} C\Phi B \\
&= K\Phi B(1 + K\Phi B)^{-1}[C\Phi B(I + K\Phi B)^{-1}]^{-1} C\Phi B \\
&= [K\Phi B(C\Phi B)^{-1}]C\Phi B = K\Phi B
\end{aligned} \tag{6.5-28}$$

The matrix inversion lemma was used in going from line 2 to line 3 and from line 7 to line 8. The limiting value (6.5-26) for L was used at the arrow.

What we have shown is that using $G = I$ and the process noise given by (6.5-23), as $\nu \to 0$, the regulator loop gain using a Kalman filter approaches the loop gain using full state feedback. This means that as $\nu \to 0$, all the robustness properties of the full-state-feedback control law are recovered in the stochastic regulator.

The *LQG/LTR design procedure* is thus as follows:

1. Use the control ARE in Table 5.7-1 to design a state feedback gain K with desirable properties. This may involve iterative design varying the PI weighting matrices Q and R.
2. Select $G = I$, process noise spectral density $M = \nu^2 M_0 + BB^{\mathrm{T}}$ and noise spectral density $\nu^2 N$ for some $M_0 > 0$ and $N > 0$. Fix the design parameter ν and use the Kalman filter ARE to solve for the Kalman gain L.
3. Plot the maximum and minimum SVs of the regulator loop gain $L_r(s)$ and verify that the robustness bounds are satisfied. If they are not, decrease ν and return to 2.

A *reduced-order* regulator with suitable robustness properties may be designed by the LQG/LTR approach using the notions at the end of Section 6.4. That is, either a regulator may be designed for a reduced-order model of the plant or the regulator designed for the full-order plant may then have its order reduced. In using the first approach, a high-frequency bound characterizing the unmodeled dynamics should be used to guarantee stability robustness.

An interesting aspect of the LQR/LTR approach is that the recovery process may be viewed as a *frequency-domain linear quadratic* technique that trades off the smallness of the sensitivity $S(j\omega)$ and the cosensitivity $T(j\omega)$ at various frequencies. These notions are explored by Stein and Athans (1987) and Safonov et al. (1981).

Non-Minimum-Phase Plants and Parameter Variations The limiting value of $K(s)$ is given by the bracketed term in (6.5-28). Clearly, as $\nu \to 0$ the regulator *inverts the plant transfer function* $C\phi B$. If the plant is of minimum phase, with very stable zeros, the LQG/LTR approach generally gives good results. On the other hand, if the plant is non-minimum-phase or has stable zeros with large time constants, the approach can be unsuitable.

In some applications, however, even if the plant is non-minimum-phase, the LQG/LTR technique can produce satisfactory results (Athans, 1986). In this situation, better performance may result if the design parameter ν is not nearly zero. If the right-half-plane zeros occur at high frequencies where the loop gain is small, the LQG/LTR approach works quite well.

An additional defect of the LQG/LTR approach appears when there are plant parameter variations. As seen in Section 6.2, stability in the presence of parameter variations requires that the loop gain SVs be below some upper bound at low frequencies. However, this bound is not taken into account in the LQG/LTR derivation. Thus, LQG/LTR can yield problems for aircraft control design, where gain scheduling

is required. The H-infinity design approach (Francis et al., 1984; Doyle et al., 1989) has been used with success to overcome this problem.

Recovery of Robust Loop Gain at the Output We have shown that, by designing the state feedback first and then computing the Kalman filter gain using a specific choice of noise spectral densities, the stochastic regulator recovers the robustness of the loop gain $K(s)G(s)$ referred to the input $u(t)$ in Figure 6.5-4. However, in Section 6.2 we saw that for a small tracking error the robustness should be studied in terms of the loop gain $G(s)K(s)$ referred to the error or equivalently to the system *output*.

Here we should like to show how to design a stochastic regulator that recovers a robust loop gain $G(s)K(s)$. This yields a second LQG/LTR design algorithm.

Thus, suppose that we *first design a Kalman filter* with gain L using Table 6.4-1. By duality theory, one may see that the Kalman filter loop gain

$$L_k(s) = C\Phi L \tag{6.5-29}$$

enjoys exactly the same guaranteed robustness properties as the state feedback loop gain $K\Phi B$ that were described earlier in this section:

$$L_r^o(s) = G(s)K(s) = C\Phi BK\Phi_r L \tag{6.5-30}$$

Thus, we should like to determine how to design a state feedback gain K so that $L_r^o(s)$ approaches $C\Phi L$. As we will see, the key to this is in the selection of the PI weighting matrices Q and R in Table 5.7-1.

To determine K, let us propose the PI

$$J = \tfrac{1}{2}\int_0^\infty (x^{\mathrm{T}}Qx + \rho^2 u^{\mathrm{T}}Ru)dt \tag{6.5-31}$$

where

$$Q = \rho^2 Q_0 + C^{\mathrm{T}}C, \tag{6.5-32}$$

with $Q_0 > 0$. By using techniques dual to those above, we may demonstrate that as $\rho \to 0$ the state feedback gain determined using Table 5.7-1 approaches

$$K \to \frac{1}{\rho}R^{-1/2}WC, \tag{6.5-33}$$

with W a unitary matrix. Using this fact, it may be shown that

$$L_r^o(s) = G(s)K(s) \to C\Phi L \tag{6.5-34}$$

The LQR/LTR design technique for loop gain recovery at the output is therefore exactly dual to that for recovery at the input. Specifically, the Kalman gain L is first

determined using Table 6.4-1 for desired robustness properties. Then Q and R are selected, with Q of the special form (6.5-32). For a small value of ρ, the state feedback gain K is determined using Table 5.7-1. If the SV Bode plots of $L_r^o(s)$ do not show acceptable robustness, ρ is decreased and a new K is determined.

If the plant $C\Phi B$ is minimum phase, all is well as ρ is decreased. However, if there are zeros in the right-half plane, there could be problems as ρ becomes too small, although with care the LQG/LTR technique often still produces good results for suitable ρ.

Example 6.5-1: LQG/LTR Design of Aircraft Lateral Control System We will illustrate the loop transfer recovery technique on a lateral aircraft CAS design. This example should be compared with examples in Chapter 4 and Example 5.5-4. All computations, including solving for the state feedback gains and Kalman filter gains, were carried out very easily using MATLAB (Moler et al., 1987).

(a) *Control Objective*. The tracking control system shown in Figure 6.5-5 is meant to provide coordinated turns by causing the bank angle $\phi(t)$ to follow a desired command while maintaining the sideslip angle $\beta(t)$ at zero. It is a two-channel system with control input $u = [u_\phi \;\; u_\beta]^{\mathrm{T}}$.

The reference command is $r = [r_\phi \;\; r_\beta]^{\mathrm{T}}$. The control system should hold ϕ at the commanded value of r_ϕ and $\beta(t)$ at the commanded value of r_β, which is equal to zero. The tracking error is $e = [e_\phi \;\; e_\beta]^{\mathrm{T}}$ with

$$\begin{aligned} e_\phi &= r_\phi - \phi \\ e_\beta &= r_\beta - \beta \end{aligned} \tag{1}$$

The negatives of the errors appear in the figure since a minus sign appears in $u = -K\hat{x}$ as is standard for LQG design.

(b) *State Equations of Aircraft and Basic Compensator Dynamics*. To obtain the basic aircraft dynamics, the nonlinear F-16 model was linearized at the nominal flight

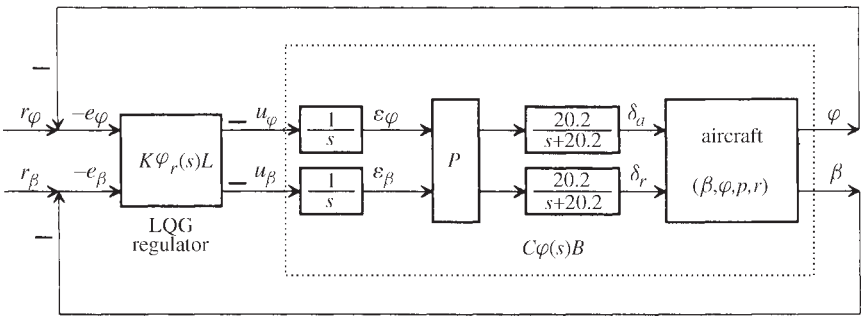

Figure 6.5-5 Aircraft turn coordinator control system.

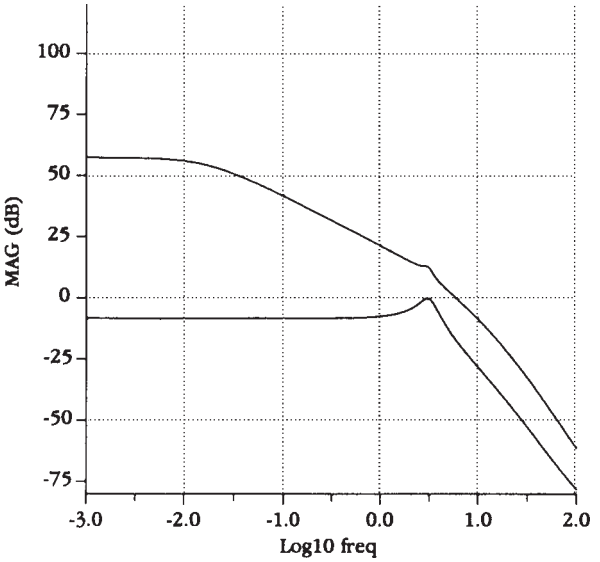

Figure 6.5-6 Singular values of the basic aircraft dynamics.

condition in Table 3.6-3 ($V_T = 502\,\text{ft/s}$, 0 ft altitude, 300 psf dynamic pressure, cg at $0.35\bar{c}$) retaining the state sideslip β, bank angle ϕ, roll rate p, and yaw rate r. Additional states δ_a and δ_r are introduced by the aileron and rudder actuators, both of which are modeled as having approximate transfer functions of $20.2/(s + 20.2)$. The aileron deflection is δ_a and the rudder deflection is δ_r.

The SVs versus frequency of the basic aircraft with actuators are shown in Figure 6.5-6. Clearly, the steady-state error will be large in the closed loop since the loop gain has neither integrator behavior nor large SVs at dc. Moreover, the SVs are widely separated at dc, so that they are not balanced.

To correct these deficiencies we may use the techniques of Example 6.2-3. The dc gain of the system is given by

$$H(0) = \begin{bmatrix} -727.37 & -76.94 \\ -2.36 & 0.14 \end{bmatrix} \tag{2}$$

First, the dynamics are augmented by integrators in each control channel. We denote the integrator outputs by ϵ_ϕ and ϵ_β. The SV plots including the integrators are shown in Figure 6.5-7. The dc slope is now -20 dB/decade, so that the closed-loop steady-state error will be zero. Next, the system was augmented by $P = H^{-1}(0)$ to balance the SVs at dc. The net result is shown in Figure 6.5-8, which is very suitable.

The entire state vector, including aircraft states and integrator states, is

$$x = [\beta \;\; \phi \;\; p \;\; r \;\; \delta_a \;\; \delta_r \;\; \epsilon_\phi \; \epsilon_\beta]^{\mathrm{T}} \tag{3}$$

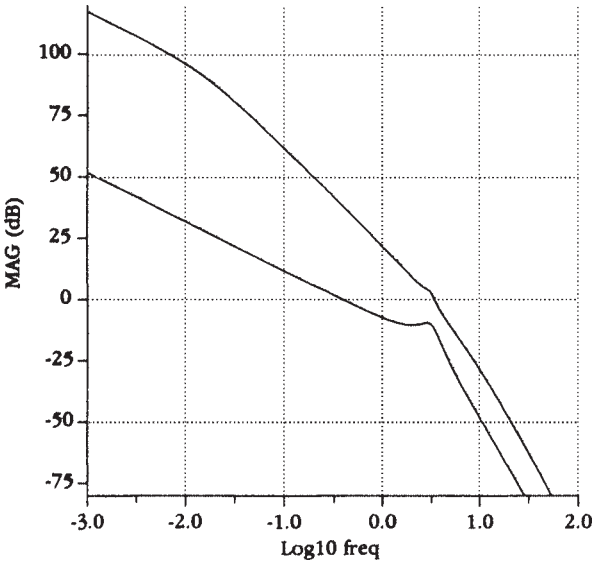

Figure 6.5-7 Singular values of aircraft augmented by integrators.

The full-state-variable model of the aircraft plus actuators and integrators is of the form

$$\dot{x} = Ax + Bu \tag{4}$$

with

$$A = \begin{bmatrix} -0.3220 & 0.0640 & 0.0364 & -0.9917 & 0.0003 & 0.0008 & 0 & 0 \\ 0 & 0 & 1 & 0.0037 & 0 & 0 & 0 & 0 \\ -30.6492 & 0 & -3.6784 & 0.6646 & -0.7333 & 0.1315 & 0 & 0 \\ 8.5395 & 0 & -0.0254 & -0.4764 & -0.0319 & -0.0620 & 0 & 0 \\ 0 & 0 & 0 & 0 & -20.2 & 0 & -0.01 & -5.47 \\ 0 & 0 & 0 & 0 & 0 & -20.2 & -0.168 & 51.71 \\ 0 & 0 & 0 & 0 & 0 & 0 & 0 & 0 \\ 0 & 0 & 0 & 0 & 0 & 0 & 0 & 0 \end{bmatrix} \tag{5}$$

$$B = \begin{bmatrix} 0 & 0 \\ 0 & 0 \\ 0 & 0 \\ 0 & 0 \\ 0 & 0 \\ 0 & 0 \\ 1 & 0 \\ 0 & 1 \end{bmatrix} \tag{6}$$

The output is given by $y = [\phi \quad \beta]^{\mathrm{T}}$, or

$$y = \begin{bmatrix} 0 & 57.2958 & 0 & 0 & 0 & 0 & 0 & 0 \\ 57.2958 & 0 & 0 & 0 & 0 & 0 & 0 & 0 \end{bmatrix} x = Cx, \tag{7}$$

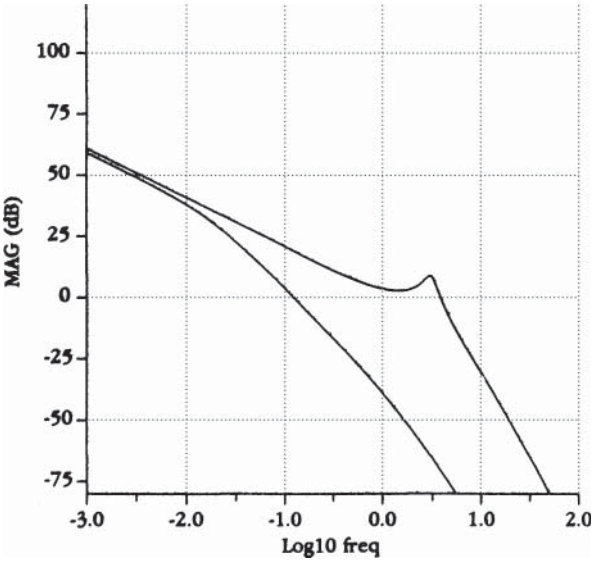

Figure 6.5-8 Singular values of aircraft augmented by integrators and inverse dc gain matrix P.

where the factor of 57.2958 converts radians to degrees. Then

$$e = r - y \tag{8}$$

(c) *Frequency-Domain Robustness Bounds*. We now derive the bounds on the loop gain MIMO Bode magnitude plot that guarantee robustness of the closed-loop system. Consider first the high-frequency bound. Let us assume that the aircraft model is accurate to within 10% up to a frequency of 2 rad/s, after which the uncertainty grows without bound at the rate of 20 dB/decade. The uncertainty could be due to actuator modeling inaccuracies, aircraft flexible modes, and so on. This behavior is modeled by

$$m(\omega) = \frac{s+2}{20} \tag{9}$$

We assume $m(\omega)$ to be a bound on the multiplicative uncertainty in the aircraft transfer function (Section 6.2).

For stability robustness, despite the modeling errors, we saw in Section 6.2 that the loop gain referred to the output should satisfy

$$\overline{\sigma}(GK(j\omega)) < \frac{1}{m(\omega)} = \left|\frac{20}{s+2}\right| \tag{10}$$

when $1/m(\omega) \ll 1$. The function $1/m(\omega)$ is plotted in Figure 6.5-9.

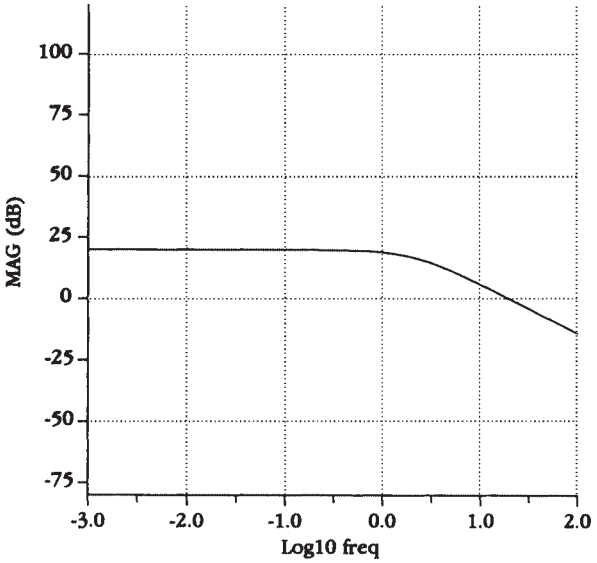

Figure 6.5-9 Multiplicative uncertainty bound 1/m(ω) for the aircraft dynamical model.

Turning to the low-frequency bound on the closed-loop gain, the closed-loop system should be robust to wind gust disturbances. Using techniques like those in Examples 6.3-1, the gust magnitude plot shown in Figure 6.5-10*a* may be obtained. According to Section 6.2, for robust performance despite wind gusts, the minimum loop gain SV $\underline{\sigma}(GK(j\omega))$ should be above this bound.

(d) *Target Feedback Loop Design*. The robustness bounds just derived are expressed in terms of the SV plots referred to $e(t)$. To recover the loop gain $GK(j\omega)$ at $e(t)$, or equivalently at the output, the Kalman filter should be designed first, so that we should employ LQG/LTR algorithm 2. Then $C\Phi(s)L$ is the target feedback loop which should be recovered in the state feedback design phase.

In standard applications of the LQG/LTR technique, the regulator is designed for robustness, but the time responses are not even examined until the design has been completed. It is difficult to obtain decent time responses using this approach. In this example we should like to emphasize the fact that *it is not difficult to obtain good time responses as well as robustness using LQG/LTR*. It is only necessary to select the Kalman gain L in Table 6.4-1 for good robustness properties as well as *suitable step responses* of the target feedback loop $C\Phi(s)L$, where $\Phi(s) = (sI - A)^{-1}$.

Using MATLAB, the Kalman filter design equations in Table 6.4-1 were solved using

$$Q = \text{diag}\{0.01, 0.01, 0.01, 0.01, 0, 0, 1, 1\}, \tag{11}$$

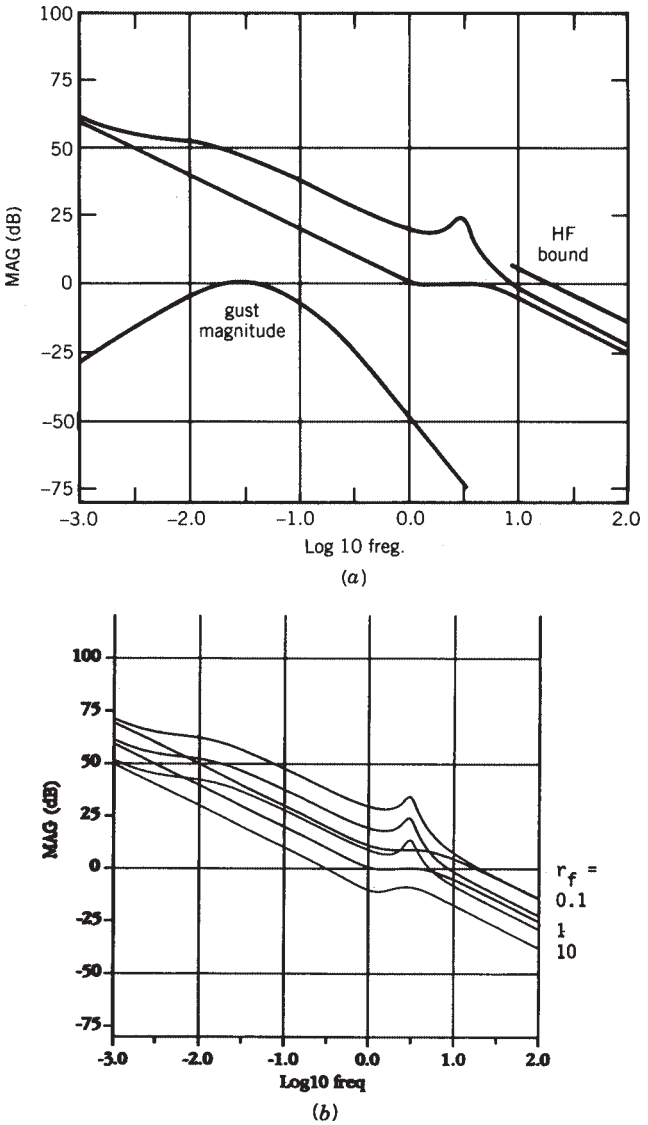

Figure 6.5-10 Singular values of Kalman filter open-loop gain $C\Phi(s)L$: (*a*) for $r_f = 1$, including robustness bounds; (*b*) for various values of r_f.

$R = r_f I$, and various values of r_f. The maximum and minimum SVs of the filter open-loop gain $C = \Phi(s)L$ for $r_f = 1$ are shown in Figure. 6.5-10*a*, which also depicts the robustness bounds. The SVs for several values of r_f are shown in Figure 6.5-10*b*. Note how the SV magnitudes increase as r_f decreases, reflecting improved rejection of low-frequency disturbances. The figures show that the robustness bounds are

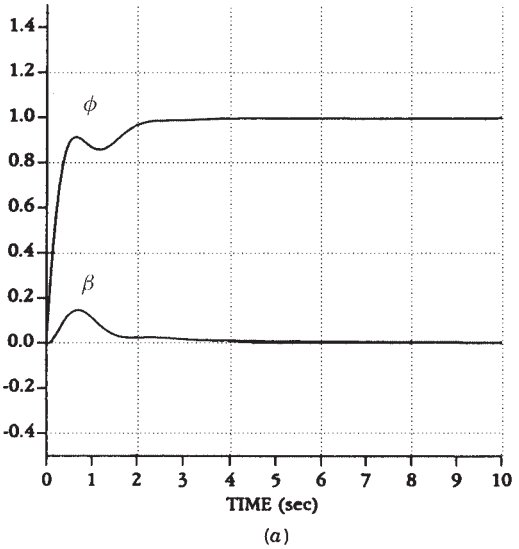

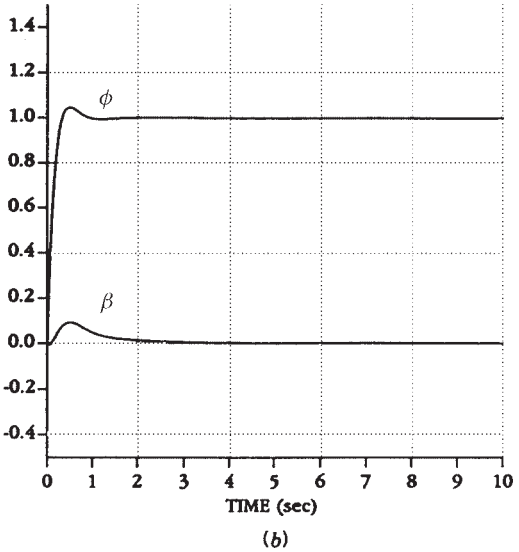

Figure 6.5-11 Step responses of target feedback loop $C\Phi(s)L$: (*a*) $r_f = 10$; (*b*) $r_f = 1$; (*c*) $r_f = 0.1$.

satisfied for $r_f = 1$ and $r_f = 10$ but the high-frequency bound is violated for $r_f = 0.1$.

The associated step responses of $C = \Phi(s)L$ with reference commands of $r_\phi = 1$, $r_\beta = 0$ are shown in Figure 6.5-11. The response for $r_f = 10$ is unsuitable, while the response for $r_f = 0.1$ is too fast and would not be appreciated by the pilot.

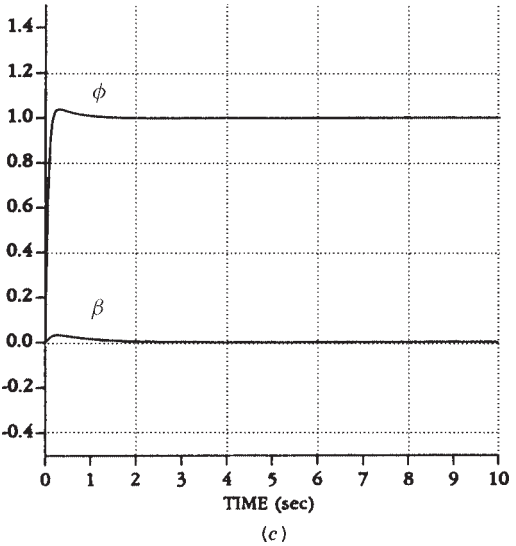

Figure 6.5-11 (*continued*)

On the other hand, the response for $r_f = 1$ shows suitable time of response and overshoot characteristics as well as good decoupling between the bank angle $\phi(t)$ and the sideslip $\beta(t)$.

Therefore, the target feedback loop was selected as $C = \Phi(s)L$ with $r_f = 1$, since this results in a design that has suitable robustness properties and step responses. The corresponding Kalman gain is given by

$$L = \begin{bmatrix} -0.007 & 0.097 \\ 0.130 & -0.007 \\ 0.199 & -0.198 \\ -0.093 & -0.020 \\ -0.197 & -0.185 \\ 1.858 & 1.757 \\ 0.685 & -0.729 \\ 0.729 & 0.684 \end{bmatrix} \tag{12}$$

The Kalman filter poles (e.g., those of $A - LC$) are given by

$$\begin{aligned} s = &-0.002, -0.879, -1.470, \\ &-3.952 \pm j3.589, \\ &-7.205, -20.2, -20.2 \end{aligned} \tag{13}$$

Although there is a slow pole, the step response is good, so this pole evidently has a small residue.

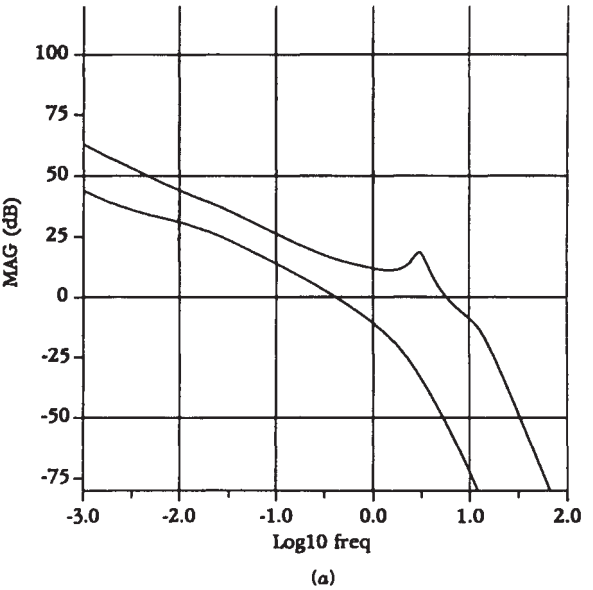

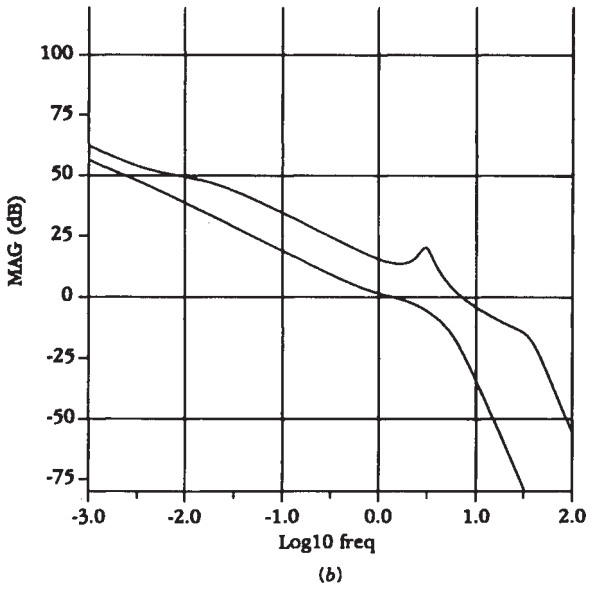

Figure 6.5-12 Singular-value plots for the LQG regulator: (*a*) LQG with $r_c = 10^{-3}$; (*b*) LQG with $r_c = 10^{-7}$; (*c*) LQG with $r_c = 10^{-11}$, including robustness bounds.

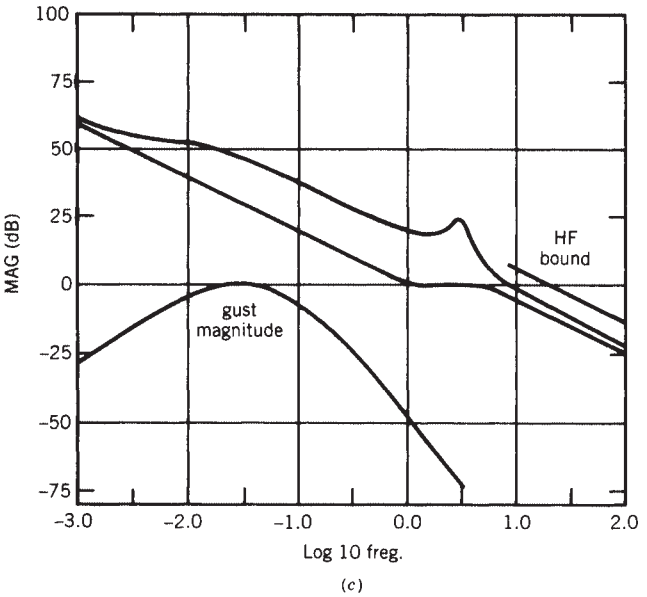

Figure 6.5-12 (*continued*)

It is of interest to discuss how the frequency and time responses were plotted. For the frequency response, we used the open-loop system

$$\begin{aligned} \dot{\hat{x}} &= A\hat{x} + Le \\ \hat{y} &= C\hat{x}, \end{aligned} \tag{14}$$

which has a transfer function of $C\Phi(s)L = C(sI - A)^{-1}L$. A program was written which plots the SVs versus frequency for a system given in state-space form. This yielded Figure 6.5-10.

For the step response, it is necessary to examine the closed-loop system. In this case, the loop is closed by using $e = r - \hat{y}$ in (14), obtaining

$$\begin{aligned} \dot{\hat{x}} &= (A - LC)\hat{x} + Lr \\ \hat{y} &= C\hat{x} \end{aligned} \tag{15}$$

Using these dynamics in program TRESP (Appendix B) with $r = \begin{bmatrix} 1 & 0 \end{bmatrix}^{\mathrm{T}}$ produces the step-response plot.

A word on the choice for Q is in order. The design parameters Q and R should be selected so that the target feedback loop $C = \Phi(s)L$ has good robustness and time-response properties. It is traditional to select $Q = BB^{\mathrm{T}}$, which accounts for the last two diagonal entries of (11). However, in this example it was impossible to obtain good step responses using this selection for Q. Motivated by the fact that the process

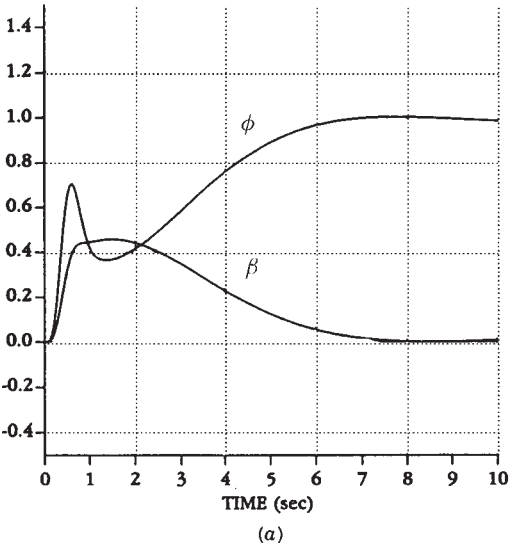

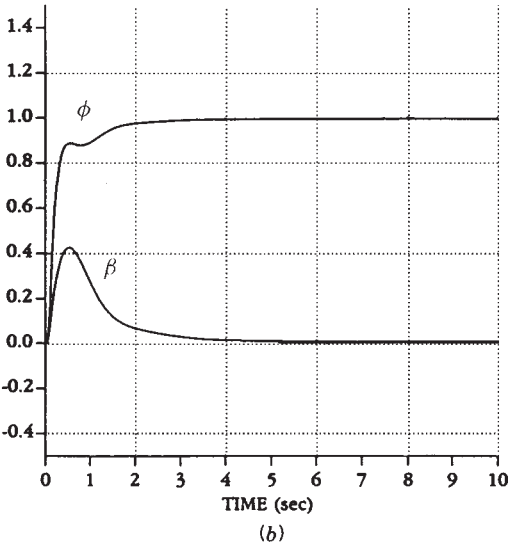

Figure 6.5-13 Closed-loop step responses of the LQG regulator: (*a*) LQG with $r_c = 10^{-3}$; (*b*) LQG with $r_c = 10^{-7}$; (*c*) LQG with $r_c = 1-^{-11}$.

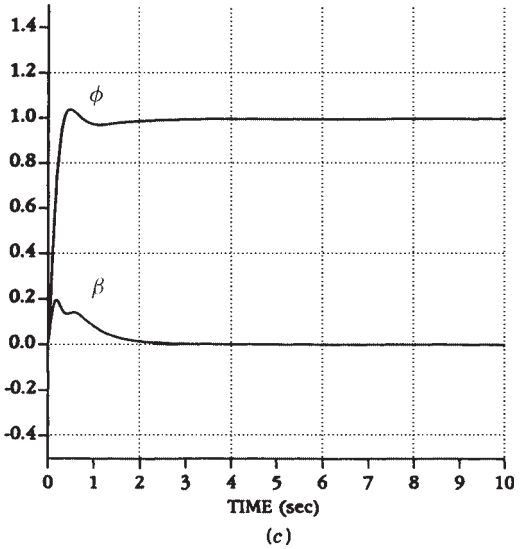

Figure 6.5-13 (*continued*)

noise in the aircraft excites the first four states as well, we experimented with different values for Q, plotting in each case the SVs and step responses. After a few iterations, the final choice (11) was made.

(e) *Loop Transfer Recovery at the Output*. The target feedback loop $C\Phi(s)L$ using $r_f = 1$ has good properties in both the frequency and time domains. Unfortunately, the closed-loop system with the LQG regulator has a loop gain referred to the output of $C\Phi(s)BK\Phi_r(s)L$, with the regulator resolvent given by

$$\Phi_r(s) = [sI - (A - LC - BK)]^{-1} \tag{16}$$

On the other hand, LQG/LTR algorithm 2 shows how to select a state feedback gain K so that the LQG regulator loop gain approaches the ideal loop gain $C\Phi(s)L$. Let us now select such a feedback gain matrix.

Using MATLAB, the LQR design problem in Table 5.7-1 was solved with $Q = C^{\mathrm{T}}C, R = \rho^2 I$, and various values of $r_c \equiv \rho^2$ to obtain different feedback gains K. Some representative SVs of the LQG loop gain $C\Phi(s)BK\Phi_r(s)L$ are plotted in Figure 6.5-12, where L is the target loop Kalman gain (12). Note how the actual SVs approach the target SVs in Figure 6.5-10*a* as r_c decreases. A good match is obtained for $r_c = 10^{-11}$.

Figure 6.5-12*c* also depicts the robustness bounds, which are satisfied for this choice of $r_c = 10^{-11}$. The corresponding step responses are given in Figure 6.5-13. A suitable step response that matches well the target response of Figure 6.5-11*b* results when $r_c = 10^{-11}$.

It is of interest to discuss how these plots were obtained. For the LQG SV plots, the complete dynamics are given by

$$\begin{aligned}\dot{x} &= Ax + Bu \\ \dot{\hat{x}} &= (A - LC)\hat{x} + Bu + Lw \\ u &= -K\hat{x},\end{aligned} \tag{17}$$

where $w(t) = -e(t)$. These may be combined into the augmented system

$$\begin{bmatrix}\dot{x} \\ \dot{\hat{x}}\end{bmatrix} = \begin{bmatrix}A & -BK \\ 0 & A - LC - BK\end{bmatrix}\begin{bmatrix}x \\ \hat{x}\end{bmatrix} + \begin{bmatrix}0 \\ L\end{bmatrix} w \tag{18}$$

$$y = \begin{bmatrix}C & 0\end{bmatrix}\begin{bmatrix}x \\ \hat{x}\end{bmatrix}, \tag{19}$$

which has transfer function $C\Phi(s)BK\Phi_r(s)L$. The SVs are now easily plotted.

For the step responses, the closed-loop system must be studied. To close the loop, set $w = y - r$ in (18) to obtain the closed-loop dynamics

$$\begin{bmatrix}\dot{x} \\ \dot{\hat{x}}\end{bmatrix} = \begin{bmatrix}A & -BK \\ LC & A - LC - BK\end{bmatrix}\begin{bmatrix}x \\ \hat{x}\end{bmatrix} + \begin{bmatrix}0 \\ -L\end{bmatrix} r \tag{20}$$

$$y = \begin{bmatrix}C & 0\end{bmatrix}\begin{bmatrix}x \\ \hat{x}\end{bmatrix} \tag{21}$$

These are used with program TRESP in Appendix B to obtain Figure 6.5-13.

The final LQG regulator is given by the Kalman gain L in (12) and the feedback gain K corresponding to $r_c = 10^{-11}$.

(f) *Reduced-Order Regulator.* The LQG regulator just designed has order $n = 8$, the same as the plant. This is excessive for an aircraft lateral control system. A reduced-order regulator that produces very good results may easily be determined using the partial-fraction-expansion approach in Example 6.2-4, principal-component analysis (Moore, 1982), or other techniques. This is easily accomplished using MATLAB. The SV plots and step response using the reduced-order regulator should be examined to verify robustness and suitable performance. ■

6.6 SUMMARY

In Section 6.2 we extended some classical frequency-domain analysis techniques to multivariable systems using the notion of the SV. We defined the multivariable loop gain, return difference, and sensitivity and showed that the multivariable Bode magnitude plot is just the plot of the maximum and minimum SVs of the loop gain versus frequency. To guarantee stability robustness to unmodeled high-frequency dynamics

and plant parameter variations, as well as performance robustness in the presence of disturbances, we derived various frequency-domain bounds that the SVs of the loop gain must satisfy.

A convenient robust output feedback design approach was presented in Section 6.3 that results in acceptable time-domain performance with guaranteed robustness.

In Section 6.4 we covered the design of multivariable observers for estimating the full state of the aircraft model from the measured outputs. We discussed the Kalman filter, showing an example of its use by reconstructing the angle of attack from normal acceleration and pitch-rate measurements in the presence of wind gust noise. We showed how to use full state feedback and an observer to design a dynamic regulator.

Finally, in Section 6.5 we covered the popular LQG/LTR robust design technique, illustrating with the design of a multivariable lateral control system.

REFERENCES

Al-Sunni, F. M., B. L. Stevens, and F. L. Lewis. "Negative State Weighting in the Linear Quadratic Regulator for Aircraft Control," *Journal of Guidance, Control, and Dynamics*, 15, no. 5 (September–October, 1992): 1279–1281.

Anderson, B.D.O., and Y. Liu. "Controller Reduction: Concepts and Approaches," *IEEE Transactions on Automatic Control* AC-34, no. 8 (August 1989): 802–812.

Armstrong, E. S. *ORACLS: A Design System for Linear Multivariable Control*. New York: Marcel Dekker, 1980.

Athans, M. "A Tutorial on the LQG/LTR Method." *Proceedings of the American Control Conference,* June 1986, pp. 1289–1296.

Athans, M., P. Kapsouris, E. Kappos, and H. A. Spang III. "Linear-Quadratic Gaussian with Loop-Transfer Recovery Methodology for the F-100 Engine." *Journal of Guidance, Control, and Dynamics* 9, no. 1 (January–February 1986): 45–52.

Birdwell, J. D. "Evolution of a Design Methodology for LQG/LTR." *IEEE Control Systems Magazine* 9(3) (April 1989): 73–77.

Blakelock, J. H. *Automatic Control of Aircraft and Missiles*. New York: Wiley, 1965.

Bryson, A. E., Jr., and Y.-C. Ho. *Applied Optimal Control*. New York: Hemisphere, 1975.

Doyle, J. C. "Guaranteed Margins for LQG Regulators." *IEEE Transactions on Automatic Control* (August 1978): 756–757.

Doyle, J. C., and G. Stein. "Robustness with Observers." *IEEE Transactions on Automatic Control* AC-24, no. 4 (August 1979): 607–611.

———. "Multivariable Feedback Design: Concepts for a Classical/Modern Synthesis." *IEEE Transactions on Automatic Control* AC-26, no. 1 (February 1981): 4–16.

Doyle, J. C., K. Glover, P. P. Khargonekar, and B. Francis. "State-Space Solutions to Standard H_2 and H_∞ Control Problems." *IEEE Transactions on Automatic Control* AC-34, no. 8 (August 1989): 831–847.

Francis, B., J. W. Helton, and G. Zames. "H_∞ Optimal Feedback Controllers for Linear Multivariable Systems." *IEEE Transactions on Automatic Control* AC-29, no. 10 (October 1984): 888–900.

Franklin, G. F., J. D. Powell, and A. Emami-Naeini. *Feedback Control of Dynamic Systems*. Reading, Mass.: Addison-Wesley, 1986.

Gelb, A., ed. *Applied Optimal Estimation*. Cambridge, Mass.: MIT Press, 1974.

Grimble, M. J., and M. A. Johnson. *Optimal Control and Stochastic Estimation: Theory and Applications*, vol. 1. New York: Wiley, 1988.

IMSL. *Library Contents Document*. 8th ed. Houston, Tex.: International Mathematical and Statistical Libraries, Inc., 1980.

Kailath, T. *Linear Systems*. Englewood Cliffs, N.J.: Prentice Hall, 1980.

Kaminer, I., P. P. Khargonekar, and G. Robel. "Design of Localizer Capture and Track Modes for a Lateral Autopilot Using H-infinity Synthesis." *IEEE Control Systems Magazine* 10, no. 4 (June 1990): 13–21.

Kwakernaak, H., and R. Sivan. *Linear Optimal Control Systems*. New York: Wiley, 1972.

Laub, A. J. "An Inequality and Some Computations Related to the Robust Stability of Linear Dynamic Systems." *IEEE Transactions on Automatic Control* AC-24, no. 2 (April 1979): 318–320.

——— "Efficient Multivariable Frequency Response Computations." *IEEE Transactions on Automatic Control* AC-26, no. 2 (April 1981): 407–408.

Lewis, F. L. *Optimal Control*. New York: Wiley, 1986*a*.

——— *Optimal Estimation*. New York: Wiley, 1986*b*.

Ly, U.-L., A. E. Bryson, and R. H. Cannon. "Design of Low-Order Compensators Using Parameter Optimization." *Automatica* 21, no. 3 (1985): 315–318.

MacFarlane, A.G.J. "Return-Difference and Return-Ratio Matrices and Their Use in the Analysis and Design of Multivariable Feedback Control Systems." *Proceedings of the Institute of Electrical Engineering* 117, no. 10 (October 1970): 2037–2049.

MacFarlane, A.G.J., and B. Kouvaritakis. "A Design Technique for Linear Multivariable Feedback Systems." *International Journal of Control* 25 (1977): 837–874.

MATRIX_x. Santa Clara, Calif.: Integrated Systems, Inc., 1989.

Mil. Spec. 1797. "Flying Qualities of Piloted Vehicles." 1987.

Minto, K. D., J. H. Chow, and J. W. Beseler. "An Explicit Model-Matching Approach to Lateral-Axis Autopilot Design." *IEEE Control Systems Magazine* 10, no. 4 (June 1990): 22–28.

Moerder, D. D., and A. J. Calise. "Convergence of a Numerical Algorithm for Calculating Optimal Output Feedback Gains." *IEEE Transactions on Automatic Control* AC-30, no. 9 (September 1985): 900–903.

Moler, C., J. Little, and S. Bangert. *PC-Matlab*. Sherborn, Mass.: The Mathworks, Inc., 1987.

Moore, B. C. "Principal Component Analysis in Linear Systems: Controllability, Observability, and Model Reduction." *IEEE Transactions on Automatic Control* AC-26, no. 1 (1982): 17–32.

Morari, M., and E. Zafiriou. *Robust Process Control*. Englewood Cliffs, N.J.: Prentice Hall, 1989.

Ohta, H., P. N. Nikiforuk, and M. Kakinuma. "Use of negative weights in linear quadratic regulator synthesis." *Journal of Guidance, Control, and Dynamics* 14.4 (1991): 791–796

Papoulis, A. *Probability, Random Variables, and Stochastic Processes*. 2d ed. New York: McGraw-Hill, 1984.

Postlethwaite, I., J. M. Edmunds, and A.G.J. MacFarlane. "Principal Gains and Principal Phases in the Analysis of Linear Multivariable Systems." *IEEE Transactions on Automatic Control* AC-26, no. 1 (February 1981): 32–46.

Press, W. H., B. P. Flannery, S. A. Teukolsky, and W. T. Vetterling. *Numerical Recipes: The Art of Scientific Computing*. New York: Cambridge University Press, 1986.

Rosenbrock, H. H. *Computer-Aided Control System Design*. New York: Academic, 1974.

Safonov, M. G., and M. Athans. "Gain and Phase Margin for Multiloop LQG Regulators." *IEEE Transactions on Automatic Control* AC-22, no. 2 (April 1977): 173–178.

Safonov, M. G., A. J. Laub, and G. L. Hartmann. "Feedback Properties of Multivariable Systems: The Role and Use of the Return Difference Matrix." *IEEE Transactions on Automatic Control* AC-26, no. 1 (February 1981): 47–65.

Shin, V., and C. Chen. "On the Weighting Factors of the Quadratic Criterion in Optimal Control." *International Journal of Control* 19 (May 1974): 947–955.

Stein, G., and M. Athans. "The LQG/LTR Procedure for Multivariable Feedback Control Design." *IEEE Transactions on Automatic Control* AC-32, no. 2 (February 1987): 105–114.

Stevens, B. L., P. Vesty, B. S. Heck, and F. L. Lewis. "Loop Shaping with Output Feedback." *Proceedings of the American Control Conference* (June 1987): 146–149.

Strang, G. *Linear Algebra and Its Applications*. 2d ed. New York: Academic, 1980.

Yousuff, A., and R. E. Skelton. "A Note on Balanced Controller Reduction." *IEEE Transactions on Automatic Control* AC-29, no. 3 (March 1984): 254–257.

PROBLEMS

Section 6.2

6.2-1 Derive in detail the multivariable expressions (6.2-16) and (6.2-17) for the performance output and the tracking error.

6.2-2 Prove (6.2-54). You will need to neglect any terms that contain second-order terms in the parameter variation matrices and use the fact that, for small X, $(I - X)^{-1} \approx (I + X)$.

6.2-3 Multivariable Closed-Loop Transfer Relations. In Figure 6.2-1, let the plant $G(s)$ be described by

$$\dot{x} = \begin{bmatrix} 0 & 1 & 0 \\ 0 & -3 & 0 \\ 0 & 0 & 0 \end{bmatrix} x + \begin{bmatrix} 0 & 0 \\ 1 & 0 \\ 0 & 1 \end{bmatrix} u, \qquad z = \begin{bmatrix} 1 & 0 & 0 \\ 0 & 0 & 1 \end{bmatrix} x$$

and the compensator is $K(s) = 2I_2$.

(a) Find the multivariable loop gain and return difference.

(b) Find the sensitivity and cosensitivity.

(c) Find the closed-loop transfer function from $r(t)$ to $z(t)$ and hence the closed-loop poles.

6.2-4 For the continuous-time system in Example 6.2-1, plot the individual SISO Bode magnitude plots from input 1 to outputs 1 and 2 and from input 2 to outputs 1 and 2. Compare them to the MIMO Bode plot to see that there is no obvious relation. Thus, the robustness bounds cannot be given in terms of the individual SISO Bode plots.

6.2-5 Software for MIMO Bode Magnitude Plot. Write a computer program to plot the Bode magnitude plot for a multivariable system given in state-space form $\dot{x} = Ax + Bu, y = Cx + Du$. Your program should read in A, B, C, D. You may use a SVD routine [e.g., IMSL (1980) and Press et al. (1986)] or the technique by Laub (1979). Use the software to verify Examples 6.2-1 and 6.2-2.

6.2-6 Multivariable Bode Plot. For the system in Problem 6.2-3, plot the multivariable Bode magnitude plots for:

(a) The loop gain GK

(b) The sensitivity S and cosensitivity T. For which frequency ranges do the plots for $GK(j\omega)$ match those for $S(j\omega)$? For $T(j\omega)$?

6.2-7 Bode Plots for F-16 Lateral Regulator. Plot the loop gain multivariable Bode magnitude plot for the F-16 lateral regulator designed in Example 5.3-1.

6.2-8 Balancing and Zero Steady-State Error. Find a precompensator for balancing the SVs at low frequency and ensuring zero steady-state error for the system

$$\dot{x} = \begin{bmatrix} 0 & 1 & 0 \\ -2 & -3 & 0 \\ 0 & 0 & -3 \end{bmatrix} x + \begin{bmatrix} 0 & 0 \\ 1 & 0 \\ 0 & 1 \end{bmatrix} u, \qquad z = \begin{bmatrix} 1 & 0 & 0 \\ 0 & 0 & 1 \end{bmatrix} x$$

Plot the SVs of the original and precompensated system.

Section 6.3

6.3-1 Model Reduction and Neglected High-Frequency Modes. An unstable system influenced by high-frequency parasitics is given by

$$\dot{x} = \begin{bmatrix} 0 & 1 & 0 \\ 1 & 0 & 1 \\ 0 & 0 & -10 \end{bmatrix} x + \begin{bmatrix} 0 & 0 \\ 0 & 1 \\ 1 & 0 \end{bmatrix} u, \qquad z = \begin{bmatrix} 1 & 0 & 0 \end{bmatrix} x$$

(a) Use the technique of Example 6.2-4 to find a reduced-order model that neglects the high-frequency mode at $s = 10$ rad/s. Find the bound $m(j\omega)$ on the magnitude of the neglected portion.

(b) Using techniques like those in Sections 5.4 and 5.5, design a servo control system for the reduced-order model. Try a lead compensator whose gains are varied by the LQ algorithm, as used in Example 5.5-5. Verify the step response of the closed-loop system by performing a simulation on the reduced-order system.

(c) Find the loop gain of the closed-loop system and plot its SVs. Do they fall below the bound $1/m(j\omega)$, thus guaranteeing robustness to the neglected mode? If not, return to part (b) and find other gains that do guarantee stability robustness.

(d) Simulate your controller on the full system, including the high-frequency mode. How does the step response look?

(e) A better controller results if high-frequency dynamics are not neglected in the design stage. Design a servo control system for the full third-order system. It may be necessary to use a more complicated controller. Verify the step response of the closed-loop system by performing a simulation. Compare to the results of part (d).

6.3-2 Gain-Scheduling Robustness. In the problems for Section 5.4 a gain-scheduled normal acceleration CAS was designed for a transport aircraft using three equilibrium points. Using the results at the end of Section 6.2, we want to check the design for robustness to plant parameter variations. Call the systems at the three equilibrium points (A_i, B_i, C_i), $i = 1, 2, 3$.

(a) In Problem 6.2-5 you wrote a program to plot the MIMO Bode magnitude plots for a state-variable system. Note that a state-space realization of $\Delta G(s)$ in (6.2-54) is given by

$$\dot{x} = \begin{bmatrix} A & -\Delta A \\ 0 & A \end{bmatrix} x + \begin{bmatrix} \Delta B \\ b \end{bmatrix} u, \qquad y = \begin{bmatrix} C & \Delta C \end{bmatrix} x$$

That is, this system has transfer function of ΔG. Define $\Delta G_{ij}(s)$ as being computed using $\Delta A = A_i - A_j, \Delta B = B_i - B_j, \Delta C = C_i - C_j$. Use these facts combined with (6.2-48) to obtain low-frequency bounds for robustness to the gain-scheduling plant parameter variations.

(b) Find the loop gain SVs of your design for the gain-scheduled CAS. Do they fall below the robustness bounds? If not, select new PI weights and try to improve the design. If this fails, you will need to select more closely spaced equilibrium points for the gain-scheduled design.

Section 6.4

6.4-1 Nonzero-Mean Noise. Use (6.4-49) to write down the best estimate for $x(t)$ in terms of the filter state $\hat{x}(t)$ if the process noise $w(t)$ and measurement noise $v(t)$ have nonzero means of $\overline{w}$ and $\overline{v}$, respectively.

6.4-2 Observer for Angle of Attack. In Example 5.5-3 a low-pass filter of $10/(s + 10)$ was used to smooth out the angle-of-attack measurements to design a pitch-rate CAS. An alternative is to use an observer to reconstruct α. This completely avoids measurements of the angle of attack.

(a) Considering only the 2×2 short-period approximation, design an observer that uses measurements of $q(t)$ to provide estimates of $\alpha(t)$. The

observer should have $\zeta = 1\sqrt{2}$ and $\omega_n = 10$ rad/s. Use Ackermann's formula to find the output injection matrix L.

(b) Delete the α-filter in Example 5.5-3, replacing it by the dynamics of the second-order observer just designed. With the new augmented dynamics, perform the LQ design of Example 5.5-3. Compare the performance of this pitch-rate CAS to the one using the α-filter.

6.4-3 Dynamic LQ Regulator for Pitch-Rate CAS. In Example 5.5-3 and Problem 6.4-2, output feedback design was used to build a pitch-rate CAS. In this problem we would like to use LQG theory to perform the design.

(a) Design an observer for α using q measurements, as described in the previous problem.

(b) Neglect the elevator actuator, considering only the 2×2 short-period approximation in Example 5.5-3 plus the feedforward-path integrator. Find the state feedback gain K to place the poles at $\zeta = 1/\sqrt{2}, \omega_n = 3.5$ rad/s; this yields good flying qualities for the short-period mode. Use Ackermann's formula or the design software for Table 5.3-1 with $C = I$.

(c) Using the 2×2 observer and the state feedback K, construct a dynamic pitch-rate CAS. Verify its performance by plotting the step response.

6.4-4 Kalman Filter. Software for solving the Kalman filter ARE is available in Armstrong (1980) and IMSL (1980); also MATRIX_x (1989) and MATLAB (Moler et al., 1987). Alternatively, the Kalman filter gain L can be found using the software for Table 5.3-1 on the dual plant $(A^\text{T}, C^\text{T}, B^\text{T})$ with $B = I$. Repeat Example 6.4-2 if the wind gusts have a turbulence intensity of 20 ft/s.

Section 6.5

6.5-1 Show that (6.5-7) implies (6.5-10) (see Laub, 1979).

6.5-2 LQG/LTR Design. Note that the state feedback gain K can be found using the software for Table 5.3-1 with $C = I$. Likewise, the Kalman filter gain L can be found using the software for Table 5.3-1 on the dual plant $(A^\text{T}, C^\text{T}, B^\text{T})$, with $B = I$.

(a) In Problem 6.4-3(b), plot the loop gain SVs assuming full state feedback.

(b) Now angle-of-attack measurements are not allowed. Design a Kalman filter for various values of the design parameter ν. In each case, plot the closed-loop step response as well as the loop gain SVs. Compare the step response and the SVs to the case for full state feedback as ν becomes small.